

Received January 16, 2020, accepted February 3, 2020, date of publication February 7, 2020, date of current version February 18, 2020.

Digital Object Identifier 10.1109/ACCESS.2020.2972302

# Optimal Design and Model Predictive Control of Standalone HRES: A Real Case Study for Residential Demand Side Management

SHAFIQR REHMAN<sup>1,2</sup>, HABIB UR RAHMAN HABIB<sup>3,4</sup>, SHAORONG WANG<sup>3</sup>, MAHMUT SAMI BÜKER<sup>5</sup>, LUAI M. ALHEMS<sup>1,2</sup>, AND HASSAN ZUHAIR AL GARNI<sup>6</sup>

<sup>1</sup>Department of Mechanical Engineering, The Research Institute, King Fahd University of Petroleum and Minerals, Dhahran 31261, Saudi Arabia

<sup>2</sup>Center for Engineering Research, The Research Institute, King Fahd University of Petroleum and Minerals, Dhahran 31261, Saudi Arabia

<sup>3</sup>School of Electrical and Electronics Engineering, Huazhong University of Science and Technology, Wuhan 430074, China


<sup>4</sup>Department of Electrical Engineering, Faculty of Electrical and Electronics Engineering, University of Engineering and Technology Taxila, Taxila 47050, Pakistan

<sup>5</sup>Department of Aeronautical Engineering, NEU University, 42140 Konya, Turkey

<sup>6</sup>Jubail Industrial College, Al Jubail 31961, Saudi Arabia

Corresponding author: Habib Ur Rahman Habib (hr\_habib@hust.edu.cn)

**ABSTRACT** Conventional electricity generation is one of the greatest sources of CO<sub>2</sub> emissions. For a successful transformation of conventional energy systems into non-polluting and renewable energy systems, technology-focused traditional systems and economics must be combined for a more accurate holistic viewpoint with consideration of socio-political, technical, economic and environmental factors. Hybrid energy systems are considered the most feasible solution to the stochastic nature of renewable energy resources (RERs). Different renewable sources such as wind, solar, and hydrogen fuel cells can be integrated to form hybrid systems. An energy management strategy (EMS) is a strategy for power flow coordination among different components, by considering power demand and other constraints. The choice for an accurate EMS is the key element of a hybrid system as it is instrumental in providing an optimum solution of the hybrid system design and operation management. The objective of the optimization is to find suitable configurations for cost-effective solutions. Optimization and EMS must be treated as one entity to completely understand the system design. This study focuses on a techno-economic analysis with an optimized sizing of a hybrid renewable energy system (HRES) components to meet the residential load demand of a specific area in Pakistan. Nine different scenarios based on the PV-wind-diesel-BSS-converter system are investigated in terms of total net present cost (TNPC), Levelized cost of energy (LCOE), and greenhouse gas (GHG) emissions to find the optimal system design. HOMER Pro software is used to develop the HRES model and for simulation analysis, with optimal sizing of each component for an economical solution. Simulation studies established that PV-wind-BSS-converter is the best suitable choice for the given location, and the optimal component sizes were determined. The TNPC of this system is \$ 47,398 and the LCOE is \$ 0.309/kWh. This represents an 81.7 % decrease in overall cost, compared to the base case (diesel only) and a 100% reduction in harmful gases while satisfying 100 % of the energy requirement with a 63.9 % of the surplus. MATLAB/Simulink model is developed for the optimum HRES system design. Its validity is tested by maintaining bus voltages (dc and ac), the secure operation range of storage SOC and real power balance among different components of the hybrid renewable energy system (HRES), and an effective ac voltage, irrespective of external perturbations. Model predictive control (MPC) is regarded as a high-performing algorithm. Since power converters are largely applied in microgrids (MGs), the problem formulation with MPC for a reconfigurable bidirectional voltage source converter (VSC) is applied in this work for hybrid MG. The inevitable fluctuations due to the linear and non-linear loads and the nature of renewable sources are addressed. The regulation of ac voltage is implemented through a finite control set model predictive control (FCS-MPC) based active front end (AFE) rectifier, while direct power MPC (DPMPC) is used to control the power during grid-connected operation. The regulation of an ac load voltage is done through voltage based

The associate editor coordinating the review of this manuscript and approving it for publication was Bin Zhou .

MPC (MPVC) in the islanding operation of the MG. Moreover, the HRES transition from grid-tied to grid-isolated mode is comprehensively analyzed. MATLAB/Simulink<sup>®</sup> software certified the robustness and evaluated the performance of the proposed HRES model under different varying loads viz. balanced, unbalanced, and non-linear. The proposed strategy offers superior performance with low total harmonic distortion (THD), compared to previously developed strategies. The output waveform of voltage and current have THD of 0.28 % compared to 3.71 % with the conventional strategy. The contributions of this paper lie in the sequential use of HOMER as well as MATLAB tools and in the validation of the suggested HRES plan for the considered location; along with the implementation of FCS-MPC for a reconfigurable bidirectional VSC.

**INDEX TERMS** Distributed energy system, energy management, finite control set model predictive control, residential load, demand side management, net present value, cost of energy, techno-economic design optimization, reconfigurable bidirectional VSC, hybrid microgrid, voltage regulation.

## NOMENCLATURE

### Abbreviations:

AEDB	Alternative energy development board	LCC	Life cycle cost
APF	Active power filter	LPSP	Loss of power supply possibility
BGG	Biogas generator	LLP	Loss of load probability
BSS	Battery storage system	LCOE	Levelized cost of energy
BGG	Biogas generator	MRAS	Model reference adaptive system
BM	Biomass	MHT	Micro hydro turbine
CC	Continuous control set	MDA	Modified DA
CRF	Capital recovery factor	NTDC	National transmission and dispatch company
DFIG	Doubly-fed induction generator	NGG	Natural gas generator
DOD	Depth of discharge	NREL	National Renewable Energy Laboratory
DSS	Discrete state-space	NEPRA	National electric power regulatory authority
DISCO	Distribution company	$N$	Diode ideality factor
DG	Diesel generator	$N_S$	Series connected PV cells
ELF	Equivalent loss factor	$N_P$	Parallel connected PV cells
ESS	Energy storage system	$N_{day}$	Number of days
EMS	Energy management strategy	O&M	Operating and maintenance
$E_{NR}$	Non-renewable energy	PPIB	Private power and infrastructure board
$E_S$	Total energy supplied to the load	PE	Power electronic
FC	Fuel cell	PV	Photovoltaic
FW	Flywheel	PMSG	Permanent magnet synchronous generator
FC	Fuel cell	$P_{charge}^{max}$	maximum battery charging power
$F_{dirt}$	Dirt losses factor	$P_{discharge}^{max}$	Maximum discharge power
$f_{inf}$	Yearly inflation rate	$P_{PV}$	Output power of the $i^{th}$ PV unit
$Fuel_{C,DG}$	Fuel consumption rate (L/h)	$P_{WT}$	Output power of $i^{th}$ WT unit
$G_{irr}$	Irradiation over the tilted surface	$Q$	Battery capacity
GENCO	Generation company	$R_S$	Intrinsic series resistances
G2V	Grid to vehicle	$R$	Rotor blade radius
GCC	Gulf cooperation council	$R_{Sh}$	Intrinsic shunt resistances
$H_{ave}$	Solar radiations	SCIG	Squirrel-cage induction generator
$H_{o,ave}$	Top-of-atmosphere radiations	SC	Supercapacitor
HRES	Hybrid renewable energy system	SMES	Superconducting magnetic storage
$i_{nom}$	Nominal interest rate	RF	Renewable fraction
$I_O$	Reverse saturation current of PV	RES	Renewable energy source
$I_{PV}$	Photocurrent of PV cell	SFF	Sinking fund factor
$I_{SC}$	Short circuit current	TNPC	Total net present value
IC	Incremental conductance	TLBO	Teaching learning-based optimization
KESC	Karachi electric supply corporation	$T_{nom}$	Nominal insolation
$k_g$	Gear ratio of the gearbox	V2G	Vehicle to grid
$k_{temp}$	Temperature coefficient related	VSI	Voltage source inverter
LOA	Level of autonomy	$V$	No-load voltage
		$V_G$	Grid side load voltage vector
		$V_t$	Thermal voltage of PV cell

$v_w$	Wind speed
WT	Wind turbines
$\beta$	Pitch angle
$\eta_{conv}$	Converter efficiency
$\eta_{bat}$	Converter efficiency
$\lambda_{nom}$	Nominal temperature
$\lambda$	Blade tip speed ratio
$\rho$	Air density
$\varphi$	Longitudes
$\omega_t$	Wind turbine rotational speed
WRSG	Wound rotor synchronous generator
WAPDA	Water and power development authority

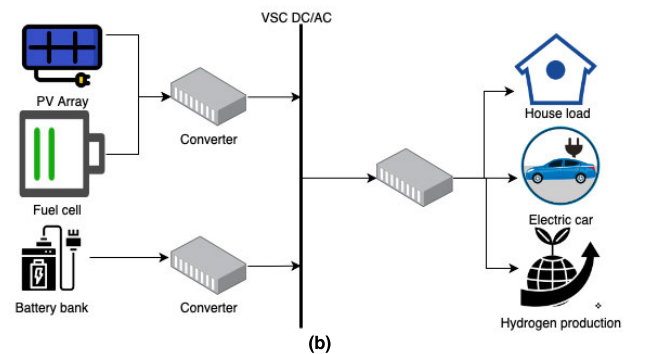
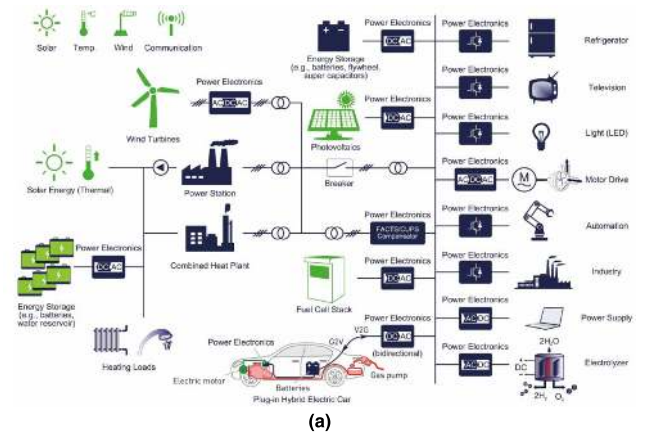


FIGURE 1. A general overview of energy production, distribution, utilization and control [11].

I. INTRODUCTION

With the growing demand for energy worldwide, caused by population growth and advancements in technology, the predictions of negative impacts of current energy systems are alarming. Most of the energy is being generated from fossil and nuclear fuels which create harmful emissions, greenhouse gases, and are proved to be dangerous to the environment. On the other hand, it is expected that a minimum or zero CO2 discharge could minimize global warming up to 2 °C annually [1].

In Pakistan, renewable energy has seen tremendous growth in recent years. According to IRENA “renewable energy capacity statistics”, the total renewable energy capacity installed in Pakistan was 13,049 MW in 2018, compared to 6,929 MW in 2009 [2], The solar and wind installed capacity was 1,568 MW in 2018, compared to 4 MW in 2009, and solar energy production was 889 GWh in 2017 compared to 5 GWh in 2009. The wind energy capacity has increased from 6 MW in 2009 to 1,186 MW in 2018 and wind energy production was 1,333 MW in 2017. The total renewable energy production was 29,643 GWh in 2009 and 37,439 GWh in 2017.

Wind may be available all day, but with large variations over short intervals and therefore wind generation is not reliable to supply the specific load. Solar energy is more predictable but it is not available at night. Aside from their intermittent nature, a high cost is also a major constraint on the use of renewable energy sources. To minimize these drawbacks, new energy systems need to combine several resources in a hybrid system with backup storage units for reliable and optimal power supply [3].

Currently, a large percentage of the global population is living in remote rural areas without access to the electricity grid. Two billion people worldwide have no access to grid-based electricity [4], while a total of 17% of the world population (1.2 billion people) have no electricity for their domestic use [5], [6]. For many remote areas, conventional energy generation units cannot fulfill the load demand due to the high cost of fuel and the infeasibility of grid extension because of geographical complexity. Moreover, conventional energy resources are the main sources of polluting GHG emissions. Access to electricity is related to economic, social,

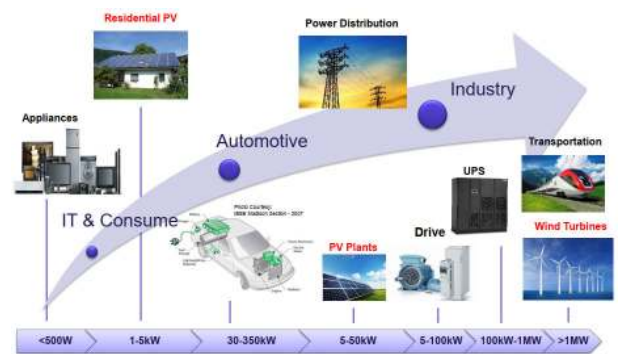
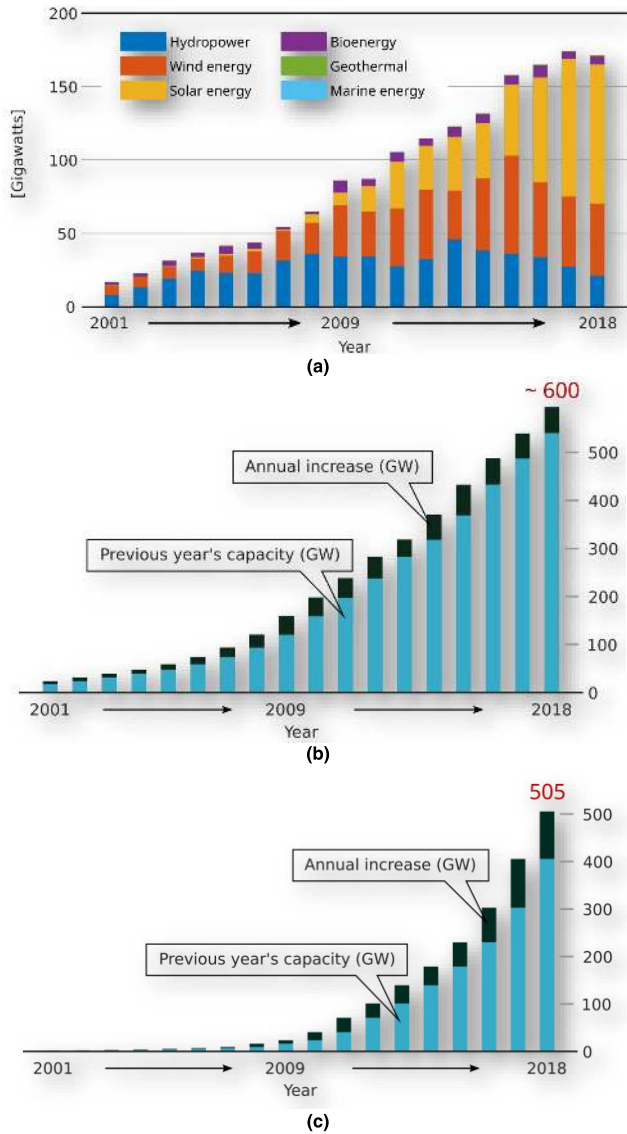


FIGURE 2. Power levels for the applications of renewable energy [11].

and environmental problems of remote communities especially in developing countries like Pakistan.

Distributed generation is considered as the safest and most viable approach to solving these decade-long problems. Due to the depletion of fossil fuels and the losses of transmission and distribution, standalone MG through distributed generations (DGs) [3] is seen as an attractive solution to fulfill the local energy demand of remote areas electrification, where access to the grid is obsolete or expensive. An increase in energy transfer among different countries is expected in the future due to globalization, distributed microgrid (MG) configurations and high penetration of distributed energy resources (DERs). The transformation from old centralized



**FIGURE 3. Global statistics of renewable energy [11] (a) Global renewable energy changes (b) Global installed wind capacity, total installed capacity in 2018 is 594GW with 53.9GW newly added capacity(c) Global installed PV capacity, total installed capacity in 2018 is 505GW with 100GW newly added capacity.**

systems into decentralized systems with the same fossil fuels makes the system more complex, without addressing its sustainability.

Incorporating renewable energy resources (like wind, and solar) offers a non-polluting solution as part of a distributed generation. The World is now looking for generation models with improved sustainable energy solutions, maximum system performance, and minimum resource usage. Such systems may integrate the wind, solar, hydro and hydrogen sourced through small and medium wind turbines (WT), photovoltaics (PV), micro-hydro turbines, and hydrogen cells (FC). Geothermal energy, ocean energy, biomass, and biogas are also primary energy resources, which can be incorporated with the common renewables. However, biomass and biogas

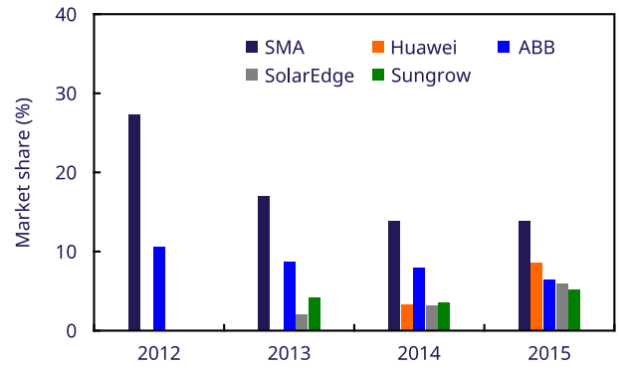


**FIGURE 4. Top five global suppliers of PV inverter.**

need constant fuel supply and therefore are not suitable for small residential or industrial loads. Also, incorporating FC into a system makes the system more complex and this component needs to be particularly considered during the design phase [3].

Modern diesel generators (DGs) and DC loads furnished with modern power electronics (PE) interface have unfolded the new interesting purview in DC energy systems which has led to hybrid MG modeling. The hybrid MG reduces the energy conversion stage, through a single-stage bidirectional converter, while offering the benefits of a hybrid system by including both AC & DC grids. The hybrid MG function is vital in the standalone mode - during main grid fault, and in supplying remote locations.

Energy storage systems (ESS) are necessary to handle the stochastic nature of the major RERs (wind and solar) and to supply the load profile while ensuring stability and reliability. In the short-term, ESS is used as a grid-supporting entity to fulfill the varying power demand and to maintain the system security and energy supply during load variations. In the long-term, ESS is used to meet the load demand during times of inadequate generation capacity. Currently, batteries are generally used for storage in medium and small-scale energy systems to overcome short-term energy shortage problems. High discharge and high load capacity of batteries make them suitable for coping with generation defects and deficiencies under variable load conditions. Moreover, the battery storage system (BSS) can be incorporated to handle the abrupt load or dynamic behavior of the HRES. Batteries have a high energy density, while supercapacitors (SC) and superconducting magnetic storage (SMES) can compensate for its low power density. The low storage capacity of SC restricts their use. Ultimately, batteries are superior in use to other ESS and are preferred worldwide [1]. Long-term ESS is based on non-renewable resources like diesel generators which have high maintenance costs and negative environmental effects [7].

MG operations are normally equipped with advanced control structure which needs modern control strategies as opposed to conventional control schemes used for

**TABLE 1. Top five wind manufacturer [11].**

Manufacturer	Country	Generator Type	Rotor Diameter Dimensions (m)	Power Rating (MW)
Vestas	Denmark	DFIG/PMSG	90-120/105-162	2.0-2.2/3.4-9.5
Siemens Gamesa	Spain	SCIG/PMSG/DFIG	154-167/120-142/114-145	6-8/3.5-4.3/2.1-4.5
Goldwind	China	PMSG	-	2-6
GE	USA	DFIG/PMSG	116-158/150	2-5/6
Enercon	Germany	WRSG	82-138	2-4.2

**TABLE 2. Top ten solar manufacturer [11].**

Manufacturer	Global installation (GW)	Specialized Focus
Canadian Solar	24.0	Large power rating
Trina Solar	11.0	Efficient panel operation
First Solar	17.0	Thin film technology
Jinko Solar	18.0	Monocrystalline technology
JA Solar	23.0	Supplies floating PV form
Sun Power Corp	18.0	Residential/commercial/utility
LG Energy	---	Bidirectional energy production
Winaico	---	Mono/polycrystalline
Hanwha Q Cells	---	Patented Q. ANTUM technology
Mitsubishi Electric	---	No soldering, recyclable, perishable materials

conventional DGs. An inner control loop is considered as the main control of DGs to regulate the voltage/frequency in MGs under varying load demand and intermittent DGs. The droop control is often used in this regard. This primary droop control is usually applied as voltage and current loops. The voltage control loop is simple, with the speedy reaction which includes few control loops, but it is not adequate to serve the need for DG protection under fault conditions and high fluctuating current. The current control loop with the additional property of current control resolves this problem. During the off-grid mode of the MG, the disturbances imposed on the DG may have dangerous effects on the DG functioning and can lead to unstable operation in terms of voltage and frequency. Thus, for reliable and economical operating conditions, there needs to be quick and precise control under variable loading conditions, during short time intervals [8].

Model predictive control (MPC) has shown superior performance for online optimization by handling problems with multiple variables through future prediction of control actions, and it is the most suitable and most developed method to address large and complex power system problems [9]. Finite control set model predictive control (FCS-MPC) is the most commonly used MPC due to its simplicity and accuracy. Predictive control for the control of power converters is a unique and powerful approach. Recently, MPC has seen growing applications in power electronics and industry. The quick dynamic reaction of MPC with its online receding horizon and its ability to handle uncertainties [10] make it a preferred method for the control of power converters.

The remainder of the paper is structured as follows. A literature review, as well as a comprehensive and

comparative investigation, are elaborated and discussed in section II, and the main objectives, scope, and implications of the proposed strategy are outlined. Section III includes a detailed description of the HRES including feasibility studies and components modeling. Techno-economic studies using HOMER are presented in section IV, including design optimization, objective formulation, and constraints description, with a detailed flow chart. Section V describes the employment of converters control in MATLAB/Simulink, to arrive at an optimal configuration model. Section VI depicts the simulation outcomes, with a detailed analysis of the proposed model. Section VII presents the verification of the key features of the proposed system and its comparison with other works in the literature. The conclusion is presented in section VIII.

## II. RESEARCH BACKGROUND SYNOPSIS

Many research studies are focused on standalone HRES. PV-battery based DC microgrid for Nigeria is studied in [12]. In [13], optimum sizing with hierarchical energy management of standalone PV-hydrogen-battery based DC grid is analyzed. PV-MPPT droop control is stabilizing the DC bus voltage while fuel cell (FC) output power fluctuations are handled by using sliding mode control (SMC) with current control mode with feedback linearization.

Application of MPC is found in current literature including FCS-MPC in [14] for primary control of voltage and frequency with large available bandwidth in off-grid systems, while FLC is applied as a secondary control to handle steady-state errors. Due to high cost, active power filter (APF) for unbalance and harmonics compensation, continuous control set MPC (CCS-MPC) with parameter tuning as the

TABLE 3. Summary of the Literature review.

Ref-Year-Authors	Achievements	Design/Analysis Strategy/tools	Demerits	Work Quality (10) *
[26]-2019-F. Fodhil, et al.	<ul style="list-style-type: none"> <li>• PV-diesel-battery for electrification of 20 Households (AC load) in Algeria with a daily load of 47 kWh.</li> <li>• Objectives: minimize [TSC, UL, CE]</li> <li>• PSO is more economical with more PV penetration.</li> <li>• DOD between 30-50% for higher battery (B) life.</li> <li>• High temp. reduces BSS life and vice versa.</li> </ul>	<ul style="list-style-type: none"> <li>• PSO and HOMER</li> <li>• Simulation only</li> </ul>	<ul style="list-style-type: none"> <li>• The optimal plan is inadequate due to it lacking the practical demonstration in terms of control and management.</li> <li>• No detailed sensitivity analysis is carried out on important parameters.</li> <li>• A load estimation analysis is not carried out.</li> </ul>	3.0
[27]-2019-M. Jahangiri et al.	<ul style="list-style-type: none"> <li>• Grid-PV-WT with vertical axis WTs in Iran.</li> <li>• The structure of the vertical axis WTs is a simple and easy installation for different speed ranges and directions.</li> </ul>	<ul style="list-style-type: none"> <li>• PSO and HOMER</li> <li>• Simulation only</li> </ul>	<ul style="list-style-type: none"> <li>• The objective function is not properly defined.</li> <li>• Mathematical analysis of vertical axis WTs is missing.</li> <li>• No sensitivity analysis is carried out.</li> <li>• No control strategy is used.</li> <li>• A load estimation analysis is not investigated.</li> </ul>	3.6
[28]-2019-A.S. Aziz et al.	<ul style="list-style-type: none"> <li>• Grid-isolated PV-hydro-diesel-battery for rural electrification in Iraq with a daily load of 19.846 kWh.</li> <li>• Multi-year criteria are applied for 20 years.</li> <li>• Seven sensitivity parameters are analyzed.</li> </ul>	<ul style="list-style-type: none"> <li>• HOMER</li> <li>• Simulation only</li> </ul>	<ul style="list-style-type: none"> <li>• The multi-year analysis shows a reduction in PV penetration, more diesel use, increased emission.</li> <li>• No adequate control strategy.is applied.</li> </ul>	5.7
[29]-2019-C.Y. Acevedo-Arenas et al.	<ul style="list-style-type: none"> <li>• PV-Wind-biomass for optimized dispatch is used for the residential load (5 houses) by using the demand response strategy and LabDER platform.</li> <li>• Objective: minimum cost and computation time with a maximum renewable fraction (RF).</li> <li>• Energy management with MPC is used for the selection of optimal controllers by incorporating two storages (battery and hydrogen).</li> </ul>	<ul style="list-style-type: none"> <li>• Evolutionary algorithms (MPC, GA)</li> <li>• MATLAB</li> <li>• Simulation and Experiment</li> </ul>	<ul style="list-style-type: none"> <li>• No sensitivity analysis is carried out.</li> <li>• No adequate control strategy.is applied.</li> <li>• Maximum power extraction from PV/wind is not considered.</li> <li>• Load voltage regulation is not analyzed.</li> <li>• No GHG emission analysis is elaborated.</li> </ul>	4.3
[30]-2019-Syed M. Shaahid et al.	<ul style="list-style-type: none"> <li>• PV-wind-battery model for 33.37 kWh/d load is proposed in Saudi Arabia.</li> <li>• Techno-economic investigation of 15 MW wind farm at two different locations are tested.</li> <li>• Objective: minimize COE</li> </ul>	<ul style="list-style-type: none"> <li>• HOMER</li> <li>• Simulation only</li> </ul>	<ul style="list-style-type: none"> <li>• No mathematical formulation is presented.</li> <li>• No mathematical details of the objective function are depicted.</li> <li>• No sensitivity analysis is carried out.</li> </ul>	4.3

TABLE 3. (Continued.) Summary of the Literature review.

[31]-2019- K. Murugaperumal <i>et al.</i>	<ul style="list-style-type: none"> <li>• PV-WT-MT-battery system for optimal energy management of microgrid with load prediction is analyzed for hourly on a daily and yearly basis.</li> <li>• Objective: minimize [fuel cost, operation/replacement cost]</li> <li>• The suggested technique outperformed three other algorithms.</li> <li>• A comparison is made in terms of power.</li> </ul>	<ul style="list-style-type: none"> <li>• ANFMDA,</li> <li>• HOMER,</li> <li>• MDA,</li> <li>• ABC</li> <li>• Simulation only</li> </ul>	<ul style="list-style-type: none"> <li>• Techno-economic observations based on NOC and COE are not analyzed.</li> <li>• NO HRES components modeling is considered.</li> <li>• No sensitivity analysis is carried out.</li> </ul>	4.3
[32]-2019- E.O. Diemuodeke <i>et al.</i>	<ul style="list-style-type: none"> <li>• PV-wind-diesel-battery for six residential areas in Nigeria is proposed.</li> <li>• TOPSIS multi-criteria is applied with consideration of economic, environmental and social aspects.</li> <li>• The most optimal plans are two viz. PV-wind-DG-BSS and PV-WT-BSS.</li> </ul>	<ul style="list-style-type: none"> <li>• TOPSIS Multi-criteria,</li> <li>• HOMER</li> </ul>	<ul style="list-style-type: none"> <li>• No sensitivity analysis is carried out.</li> <li>• No adequate control strategy.is applied.</li> <li>• Maximum power extraction from PV/wind is not considered.</li> <li>• Load voltage regulation is not analyzed.</li> </ul>	5.7
[33]-2019- Mehdi Bagheri <i>et al.</i>	<ul style="list-style-type: none"> <li>• PV-wind-BGG-battery is used for urban electrification in Canada and COE is reduced three times.</li> <li>• Three configurations are compared and COE is further reduced with NGG.</li> <li>• Three sensitivity parameters viz. capital cost (PV and battery) and discount rate are taken.</li> </ul>	<ul style="list-style-type: none"> <li>• HOMER</li> <li>• Simulation only</li> </ul>	<ul style="list-style-type: none"> <li>• Only three sensitivity parameters are used.</li> <li>• The load estimation is not elaborated in detail.</li> <li>• No adequate control strategy.is applied.</li> </ul>	3.7
[34]-2019- Habib Ur Rahman Habib <i>et al.</i>	<ul style="list-style-type: none"> <li>• WT-DG-BSS system is proposed for rural electrification in Pakistan.</li> <li>• Techno-economic observations with five possible configuration plans are compared and analyzed based on COE, NPC, and emission.</li> <li>• Adequate control and management strategy.is applied.</li> <li>• Maximum power extraction from wind is considered.</li> <li>• Load voltage regulation is analyzed.</li> <li>• GHG emission analysis is elaborated.</li> <li>• THD analysis is depicted for PI and MPC.</li> <li>• External disturbances from sources (wind) and load are analyzed.</li> </ul>	<ul style="list-style-type: none"> <li>• HOMER</li> <li>• MATLAB</li> <li>• Simulation only</li> </ul>	<ul style="list-style-type: none"> <li>• No sensitivity analysis is carried out.</li> <li>• The load estimation is not elaborated in detail.</li> <li>• PV is not considered for HRES.</li> </ul>	6.4
[35]-2019- Mohammed Guezgouz <i>et al.</i>	<ul style="list-style-type: none"> <li>• PV-wind-battery with 8.63 MWh load is examined for 8 residential consumers in Algeria.</li> <li>• Eight different configuration plans with two storage options (battery and pumped storage) are considered.</li> <li>• Bi-objectives: minimize cost, enhance reliability</li> </ul>	<ul style="list-style-type: none"> <li>• GWO</li> <li>• Simulation only</li> </ul>	<ul style="list-style-type: none"> <li>• Emission reduction is done without highlighting any optimal configuration.</li> <li>• No economic HRES is found during analysis.</li> <li>• No sensitivity analysis is applied.</li> </ul>	2.9
[36]-2019- A.S. Aziz <i>et al.</i>	<ul style="list-style-type: none"> <li>• PV-diesel-battery with 145 kWh daily load is implemented in Iraq.</li> <li>• Out of three dispatch schemes, a CD is the most optimal with least COE.</li> <li>• Five sensitivity parameters (SOC, time step, radiation, fuel, and load) are considered.</li> </ul>	<ul style="list-style-type: none"> <li>• HOMER</li> <li>• Simulation only</li> </ul>	<ul style="list-style-type: none"> <li>• A load estimation is not properly considered.</li> <li>• Sensitivity analysis is not carried out.</li> <li>• No adequate control and management strategy.is</li> </ul>	3.6

TABLE 3. (Continued.) Summary of the Literature review.

			applied.	
[37]-2019- Wenlong Jing <i>et al.</i>	<ul style="list-style-type: none"> <li>• PV-battery system with a smart scheme for enhancement of battery life is applied to feed rural load in Malaysia.</li> <li>• Battery stresses are analyzed with consideration of sudden charge/discharge, higher C-rate, and power surges.</li> <li>• These stresses are addressed by controlling current fluctuations and surges.</li> <li>• HES plug-in module comprises two batteries (Li-ion and lead-acid) that are used with a supercapacitor.</li> <li>• A scaled prototype experiment is used for results validation.</li> </ul>	<ul style="list-style-type: none"> <li>• HOMER</li> <li>• Simulation and prototype Experiment</li> </ul>	<ul style="list-style-type: none"> <li>• The strategy for voltage control of the dc bus is not implemented.</li> <li>• The control scheme for an interlinking inverter is not considered for regulated and efficient load voltage.</li> <li>• The techno-economic analysis is not implemented.</li> </ul>	4.4
[38]-2019- Partha Sarothi Sikder <i>et al.</i>	<ul style="list-style-type: none"> <li>• PV-wind-battery with an intelligent battery controller is applied.</li> <li>• The load voltage regulation is achieved through PI-based control of the inverter.</li> <li>• Maximum power extraction from PV is analyzed through the IC MPPT strategy.</li> <li>• Charge/discharge optimization is investigated with a battery management scheme.</li> </ul>	<ul style="list-style-type: none"> <li>• FLC</li> <li>• MATLAB</li> <li>• Simulation only</li> </ul>	<ul style="list-style-type: none"> <li>• The quality of load power is very low.</li> <li>• The mismatch of the load voltage is high.</li> <li>• The techno-economic analysis is not applied.</li> <li>• The dc bus control is not analyzed.</li> <li>• High transients of wind output.</li> <li>• No details of wind MPPT.</li> </ul>	4.3
[39]-2019-Eu- Tjin Chok <i>et al.</i>	<ul style="list-style-type: none"> <li>• PV-diesel-battery is implemented for the domestic load.</li> <li>• SOC management strategy is applied.</li> <li>• Out of three dispatch strategies, the FLC scheme is recommended for minimum COE.</li> </ul>	<ul style="list-style-type: none"> <li>• MATLAB</li> <li>• Simulation only</li> </ul>	<ul style="list-style-type: none"> <li>• No sensitivity analysis and adequate control strategy is applied.</li> <li>• Load estimation is not examined.</li> </ul>	2.1
[40]-2019- Javier Carroquino <i>et al.</i>	<ul style="list-style-type: none"> <li>• PV-battery system with no GHG emission is proposed for a vineyard in Spain.</li> <li>• FC based HEV is driven by hydrogen generated through surplus energy.</li> <li>• Site selection with proper feasibility analysis is carried out.</li> </ul>	<ul style="list-style-type: none"> <li>• Tool not mentioned.</li> <li>• Simulation only</li> </ul>	<ul style="list-style-type: none"> <li>• The economic analysis in terms of NPC and COE is not carried out.</li> <li>• No sensitivity analysis and adequate control strategy is applied.</li> </ul>	5.0
[41]-2019- Tao Ma <i>et al.</i>	<ul style="list-style-type: none"> <li>• Out of different configurations of PV-wind-battery, a wind-battery model is an optimal plan with 255 kWh daily load in for island electrification with ten houses in China.</li> <li>• COE is more changeable with wind energy; battery cost is the second major factor while the load is the third factor to influence COE.</li> <li>• Four sensitivity parameters (wind energy, battery storage cost, load, and solar energy) are considered.</li> </ul>	<ul style="list-style-type: none"> <li>• Tool not mentioned.</li> <li>• Simulation only</li> </ul>	<ul style="list-style-type: none"> <li>• The details of the performance tool are not elaborated.</li> <li>• The analysis is purely based on COE. An analysis with NPC is missing.</li> </ul>	5.4
[42]-2019- Neeraj Priyadarshi <i>et al.</i>	<ul style="list-style-type: none"> <li>• PV-wind-battery based adequate control scheme is applied with experimental demonstration (dSPACE).</li> <li>• ACO based MPPT for wind connected cuk converter outperforms PSO based strategy.</li> <li>• FLC based converter is used to supply the three-phase load.</li> </ul>	<ul style="list-style-type: none"> <li>• ACO, FLC</li> <li>• MATLAB</li> <li>• Simulation and prototype Experiment</li> </ul>	<ul style="list-style-type: none"> <li>• A fast battery charging may reduce life and need proper storage consideration.</li> <li>• No PV MPPT scheme is used.</li> <li>• The quality of the load</li> </ul>	4.3



TABLE 3. (Continued.) Summary of the Literature review.

	<ul style="list-style-type: none"> <li>• A fast-charging method of battery is used.</li> <li>• PV is used without the MPPT algorithm.</li> <li>• Techno-economic analysis for the optimal configuration plan is not investigated.</li> </ul>		<ul style="list-style-type: none"> <li>• voltage is very bad.</li> <li>• A low load power rating is impractical.</li> <li>• No sensitivity analysis is conducted.</li> </ul>	
[43]-2019-Sunday Olayinka Oyedepo <i>et al.</i>	<ul style="list-style-type: none"> <li>• PV-wind-diesel-battery model with 493 kWh daily load is tested for the rural domestic load of 500 households.</li> <li>• The six zones in Nigeria are selected for this purpose.</li> <li>• PV-diesel-battery is considered as the most optimal model for one site.</li> </ul>	<ul style="list-style-type: none"> <li>• HOMER</li> <li>• Simulation only</li> </ul>	<ul style="list-style-type: none"> <li>• Low wind speed shows improper consideration of wind at the initial stage of the feasibility study.</li> <li>• Emission is not considered.</li> <li>• Impractical household load (0.986 kWh/d) is estimated.</li> <li>• No sensitivity analysis is applied.</li> </ul>	2.7
[44]-2019-João Faria <i>et al.</i>	<ul style="list-style-type: none"> <li>• PV-HESS with SOC management using ANN is applied and validated using an experiment.</li> <li>• LVDC system of 60V is implemented with effective use of SC energy.</li> <li>• PSO is used to optimize HESS based PI controllers.</li> </ul>	<ul style="list-style-type: none"> <li>• PSO</li> <li>• MATLAB</li> <li>• Simulation and prototype Experiment</li> </ul>	<ul style="list-style-type: none"> <li>• Wind energy is not considered.</li> <li>• Very low power of about 400 W is used which is impractical.</li> <li>• A techno-economic analysis is not performed.</li> </ul>	3.6
[9]-2019-Xiaobing Kong <i>et al.</i>	<ul style="list-style-type: none"> <li>• PV-wind-battery based dc system with Hierarchical control using DMPC is suggested.</li> </ul>	<ul style="list-style-type: none"> <li>• MATLAB</li> <li>• Simulation and prototype Experiment</li> </ul>	<ul style="list-style-type: none"> <li>• Inverter control with an adequate control scheme is not implemented.</li> </ul>	7.1
[6]-2019-Om Krishan <i>et al.</i>	<ul style="list-style-type: none"> <li>• PV-wind-battery is presented for a rural area in India.</li> <li>• The load comprises domestic and agriculture.</li> <li>• Three configurations are compared for the optimal model.</li> <li>• PV-WT-BSS is the best suitable plan for the suggested location.</li> <li>• HRES and SOC management is applied to the most viable model.</li> <li>• The PI control scheme is used for VSI to supply a three-phase load.</li> <li>• External disturbances from sources (wind and PV) and load are analyzed.</li> </ul>	<ul style="list-style-type: none"> <li>• HOMER</li> <li>• MATLAB</li> <li>• Simulation only</li> </ul>	<ul style="list-style-type: none"> <li>• No sensitivity analysis and MPC based advanced control scheme is applied.</li> <li>• The load voltage profile shows high ripples during the PI control scheme.</li> <li>• The actual PV size (121 kW) obtained from the optimal plan is not technically implemented.</li> <li>• A dc voltage distorted during 2-6 seconds shows the improper tuning of the PI controller.</li> </ul>	7.1
[5]-2019-Erasmus Muh <i>et al.</i>	<ul style="list-style-type: none"> <li>• PV-WT-hydro-DG-BSS system is suggested for the domestic load of 100kWh/d in Camerouns.</li> <li>• PV-hydro-DG-BSS is found to be the best viable plan.</li> <li>• Four sensitivity parameters of costs (streamflow, interest, fuel, and PV cost) are considered.</li> </ul>	<ul style="list-style-type: none"> <li>• HOMER</li> <li>• Simulation only</li> </ul>	<ul style="list-style-type: none"> <li>• The studied location (Wum) having an insufficient wind speed of 2.5 m/s is not adequate to include even at the initial stage of analysis.</li> <li>• Control and</li> </ul>	5.4

TABLE 3. (Continued.) Summary of the Literature review.

			management strategy.is not implemented.	
[45]-2019-Monotosh Das et al.	<ul style="list-style-type: none"> <li>PV-biogas-hydro-battery system is suggested in India.</li> <li>A comparison of WCA and MFO with GA is based on the convergence rate for TNPC.</li> <li>WCA is found to be most efficient in terms of skewness and kurtosis.</li> <li>One sensitivity parameter (LLP) with a WCA scheme is considered.</li> <li>With the increase of LLP (from 0.03 to 0.05), TNPC and COE reduced to much lower values.</li> </ul>	<ul style="list-style-type: none"> <li>Metaheuristic optimization</li> <li>WCA, MFO, GA</li> <li>MATLAB</li> <li>Simulation only</li> </ul>	<ul style="list-style-type: none"> <li>LCOE is high even after increasing the LLP value.</li> <li>Detailed sensitivity analysis and control schemes are not presented.</li> <li>The load estimation is not elaborated in detail.</li> </ul>	4.6
[46]-2019-Xi Luo et al.	<ul style="list-style-type: none"> <li>PV-diesel-battery system is proposed for feeding load in China.</li> <li>Multi-generation energy system with demand response is presented.</li> <li>Solar subsidies are also discussed.</li> </ul>	<ul style="list-style-type: none"> <li>Bi-level optimization</li> <li>Simulation only</li> </ul>	<ul style="list-style-type: none"> <li></li> </ul>	2.1
[47]-2018-A.S. Aziz et al.	<ul style="list-style-type: none"> <li>Grid-isolated PV-diesel-battery for rural area supply in Iraq.</li> <li>A multi-year analysis is applied.</li> <li>The effect of sensitivity parameter (temperature) is used for performance analysis of PV/battery including SOC and NPC.</li> <li>Due to high temperature, battery throughput is increased while battery life and PV output are reduced due to increased chemical reactions inside the battery.</li> <li>The minimum SOC range is 30-50 % is the general recommendation.</li> </ul>	<ul style="list-style-type: none"> <li>HOMER</li> <li>Simulation only</li> </ul>	<ul style="list-style-type: none"> <li>The analysis is purely based on NPC in this paper. Further, COE is an important factor to consider during analysis which is missing.</li> <li>Only one sensitivity parameter (i.e. temperature) is considered.</li> <li>The load estimation is not elaborated in detail.</li> </ul>	2.4
[48]-2018-Neeraj Priyadarshi et al.	<ul style="list-style-type: none"> <li>PV-wind with the quasi converter is used.</li> <li>PV MPPT with the P&amp;O scheme is applied with the dc-dc SEPIC module.</li> <li>No filter requirement for the suggested inverter.</li> <li>Hardware setup (dSPACE) is used for validation.</li> </ul>	<ul style="list-style-type: none"> <li>Tool not mentioned</li> <li>Simulation and Experiment (dSPACE)</li> </ul>	<ul style="list-style-type: none"> <li>Wind MPPT modeling is not studied.</li> <li>The experimental power is very low and is impractical.</li> <li>The simulation results of the suggested model are not shown.</li> </ul>	4.3
[49]-2018-Mohammad Mehreganfar et al.	<ul style="list-style-type: none"> <li>Sensorless MPC for the AFE rectifier is applied.</li> <li>Due to the proposed scheme, two problems viz. current derivative and inductor estimation are tackled with filters and MRAS observer.</li> </ul>	<ul style="list-style-type: none"> <li>Tool not mentioned</li> <li>Simulation and Experiment</li> </ul>	<ul style="list-style-type: none"> <li>External disturbance analysis including sources and load is not examined.</li> <li>The test is conducted at a very low dc voltage.</li> </ul>	5.7
[50]-2017-Jiaxin Lu et al.	<ul style="list-style-type: none"> <li>PV-wind-diesel-battery model is suggested for the island in China.</li> <li>The weighted sum decision-making scheme is applied.</li> <li>The viable trade-off scheme of HRES is examined with SOC management.</li> <li>Three sensitivity parameters of costs (wind, PV, fuel) are considered.</li> </ul>	<ul style="list-style-type: none"> <li>HOMER</li> <li>Simulation only</li> </ul>	<ul style="list-style-type: none"> <li>Adequate control strategy.is not applied.</li> <li>Analysis of the effectiveness of the suggested scheme is not elaborated.</li> </ul>	3.7
[51]-2016-Fahd Diab et al.	<ul style="list-style-type: none"> <li>PV-wind-diesel-battery is suggested in Egypt for the domestic and industrial load.</li> </ul>	<ul style="list-style-type: none"> <li>HOMER</li> <li>Simulation only</li> </ul>	<ul style="list-style-type: none"> <li>No sensitivity analysis and adequate control</li> </ul>	2.9

TABLE 3. (Continued.) Summary of the Literature review.

[52]-2016-A. Yahiaoui <i>et al.</i>	<ul style="list-style-type: none"> <li>PV-diesel-battery model is applied in Algeria.</li> <li>Objectives: minimize [ACS, LLP, emission].</li> <li>Cost results with suggested PSO scheme are compared with HOMER generated analysis.</li> </ul>	<ul style="list-style-type: none"> <li>PSO</li> <li>MATLAB</li> <li>HOMER</li> <li>Simulation only</li> </ul>	<ul style="list-style-type: none"> <li>strategy.is applied.</li> <li>No sensitivity analysis and adequate control strategy.is applied.</li> <li>The cost analysis based on COE is not considered.</li> <li>A load estimation detail is also missing.</li> </ul>	2.1
[53]-2016-Jae-Hoon Cho <i>et al</i>	<ul style="list-style-type: none"> <li>PV-WT-DG-BSS system is proposed for electrification in South Korea.</li> <li>Objectives: minimize [TNPC, LPSP, fuel price]</li> <li>A new scheme (hybrid teaching-learning based optimization) with penalty method is presented.</li> </ul>	<ul style="list-style-type: none"> <li>GA, PSO</li> <li>TLBO</li> <li>MATLAB</li> <li>Simulation only</li> </ul>	<ul style="list-style-type: none"> <li>The load estimation detail is not presented.</li> <li>No sensitivity analysis and adequate control strategy.is applied.</li> <li>The cost analysis using COE is not presented.</li> </ul>	2.9
[54]-2015-Fahd Diab <i>et al.</i>	<ul style="list-style-type: none"> <li>PV-wind-diesel-battery model is applied in Egypt.</li> <li>Objectives: minimize [NPC, COE, GHG emission].</li> <li>Cost results with suggested PSO scheme are compared with HOMER generated analysis.</li> </ul>	<ul style="list-style-type: none"> <li>HOMER</li> <li>Simulation only</li> </ul>	<ul style="list-style-type: none"> <li>No sensitivity analysis and adequate control strategy.is applied.</li> <li>The load estimation detail is not presented.</li> </ul>	2.9
[55]-2012-Jing Li <i>et al.</i>	<ul style="list-style-type: none"> <li>PV-wind-battery is used with invariant SOC criteria for the island in China.</li> <li>Objective: minimize LCC</li> <li>With constant SOC, wind and PV units are varied with the variation of load demand.</li> </ul>	<ul style="list-style-type: none"> <li>Tool not mentioned.</li> <li>Simulation only</li> </ul>	<ul style="list-style-type: none"> <li>Comparative analysis with other schemes is not examined.</li> <li>No sensitivity analysis and adequate control strategy.is applied.</li> <li>The load estimation is not elaborated in detail.</li> </ul>	4.3

\* (BEST=10, WORST=0) Work quality is based on seven factors including number of renewable resources (PV, wind, hydro), optimization analysis, control strategy (including PI/FLLC and MPC), minimum GHG emission, number of sensitivity parameters, and load estimation/observer analysis; TSC: total system cost, UL: unmet load. CE: CO. emission.

main focus is proposed in [15] and trade-off among voltage quality and injected current, stable operation and quick response is analyzed. In [16], regulating frequency for the microgrid network is investigated with voltage adjustment for voltage-sensitive loads by using distributed MPC (D-MPC). In [17], a decentralized backstepping algorithm for voltage control as well as load sharing is applied for the standalone DC microgrid system. Coordination between the intermittent nature of wind energy and the charging load of plug-in electric vehicles (PEVs) is handled through hierarchical MPC [18]. The control strategy of grid-forming converters with transient analysis under high-signal disturbances is analyzed in [19]. In [20], the adaptive voltage control strategy is proposed to control DG and very good performance and response are observed. The adaptive scheme of static compensator (STATCOM) is investigated in [21]. PI conventional control strategy is applied in [22] for the execution of direct power control (DPC). In [23], DPC with a look-up table is applied for switching states to improve the performance of the converter. Switching harmonics is addressed with a fuzzy-based DPC scheme in [24]. Sliding mode control (SMC) is

used for the power regulation of a grid-connected system in [25].

Table 3 demonstrates a comprehensive literature work in terms of their contribution, drawbacks, HRES configurations, the applied methodologies as well as the main objectives. Results show that most literature is focused on the investigation of PI traditional schemes but rigorous analysis of the optimal design of HRES components is not considered. In this paper, the control unit of a wind turbine comprises an uncontrolled rectifier as a cheap solution. Further, it needs no IGBTs and control for generating signals for its operation and because of that, it reduces the complication and system cost.

Most published studies were not thoroughly investigated by incorporating maximum power tracking algorithms (MPPT) of WT and solar, buck-boost control to regulate dc voltage, THD investigation, and the comparative study between PI and MPC for bidirectional VSC of hybrid MG systems. Maximum literature studies have focused on either optimal HRES design components or management. This work focuses the design optimization with the best desirable and upgraded EMS scheme. First, the elaborated

techno-economic investigation with multiple HRES configurations for DG, PV, WT, BSS, and converter is used for the optimal HRES design. The obtained scheme is then applied to meet the consumer's requirements of an off-grid location selected in Pakistan with detailed feasibility analysis. Afterward, MATLAB<sup>®</sup> is employed for the execution of the proposed EMS. The most feasible HRES is then tested with the suggested EMS and the operation analysis of the presented scheme is validated for the improvement of energy quality, steady-state and transient behavior with fluctuating renewables and varying loads.

#### A. NOVELTIES OF THE PROPOSED SCHEME

After the comprehensive review of the literature, the summarized points are discussed as follows:

- The HRES models are believed to be the best solution in terms of reliability and economics as well as workable choices with low emission of toxic gases. Although multiple hybrid configurations of HRES are applicable for any specified area based on load trends, the potential of renewable energy resources, and environmental circumstances.
- The main focusing point in the literature studies is either a size optimization with a feasible plan in terms of economics or on energy management schemes. Two viewpoints are seldom presented and investigated at the same instant. Moreover, the comprehensive sensitivity analysis with eighteen (18) study cases including the ROI factor is a crucial prospect for investors in terms of economics which is not taken into consideration in the literature during design optimization of the HRES. Based on the authors' knowledge, the suggested scheme with concurrent analysis of design optimization and energy management for the PV-wind-DG-BSS-converter model with the FCS-MPC scheme of reconfigurable bidirectional VSC for a grid-isolated system is not comprehensively analyzed in the researcher's world. Further, to the best of the authors' knowledge, FCS-MPC based four modes namely. AFE rectifier mode, grid-tied inversion operation, grid-disconnected inversion operation, transitional operation from grid-connected to grid-disconnected) are not comprehensively and simultaneously considered in the literature.

Based on the literature studies, the main control for interlinking converters should be developed by keeping in view the dynamic nature of the load for the improved steady-state and transient operation with different and varying loads. Further, efficient-dynamic performance is obtained with MPC while the dedicated optimal design is also possible by improving and to regulate the voltage and frequency of DGs under grid-disconnected mode and active power control in grid-tied operation. Bidirectional VSC is the primary part of hybrid MG to deal with two-way control of active power while maintaining system stability. This work proposed an MPC based scheme of main interlinking VSC in rectification and inverter

modes with the provision of robust control operation under transient and steady-state conditions with the considerations of different varying loads.

The main contributions along with the aims and scope of the suggested study are described below:

- (1) To meet the increasing electricity demand in the world, the specified remote area in Pakistan is selected as a case study to analyze feasible HRES options with PV and wind.
- (2) An integrated and generic methodological analysis for the optimal sizing of the HRES components with management for the grid-disconnected system is demonstrated. The suggested scheme is certified with a residential case study in Pakistan.
- (3) The viable configuration plan is found with the help of comprehensive analysis in terms of cost minimization with low emission and high reliability of the model is incorporated as an objective.
- (4) A proper EMS design methodology is verified with the aid of a successfully implemented tool in Simulink<sup>®</sup>. The presented scheme is applied to keep a balanced load and constant dc voltage, with maximizing the power extracted from WT and PV while maintaining the load voltage during different perturbations.
- (5) FCS-MPC is used to achieve the best response during steady-state and transient operations.
- (6) The presented FCS-MPC scheme shows robustness during different varying loads.
- (7) Regulated voltage and suitable control of load power are obtained with a quick and precise response in grid-disconnected and grid-connected modes.
- (8) Active front end (AFE) rectifier with FCS-MPC is designed with mathematically modeled for the regulation of dc bus voltage (G2V mode).
- (9) Direct power MPC (DPMPC) is applied for grid-connected VSI mode (V2G mode) and mathematical modeling is also described.
- (10) Voltage control based MPC (MPVC) is applied for the regulation of ac voltage in grid-disconnected mode.
- (11) Transitional state from grid-connected to grid-disconnected mode is thoroughly analyzed.
- (12) The robustness and effectiveness of the considered system are validated through the applied scheme during varying loading conditions viz. balance, unbalance, and non-linear.

#### B. ADVANTAGES OF THE PROPOSED SCHEME

MPC is the most preferred option for handling the complexity of control problems [56]. The merits of the presented scheme are explained below:

- The primary significance is the simple algorithm and the conceptions are based on a heuristic rule. Further, it is intuitive as well perceivable.
- The proposed scheme can be applied more properly for multi-variable models to extend consequently.

- The presented scheme is practicable for real and on-line HRES with non-linear models.
- The presented strategy with a comprehensive outcome including optimized design and management for the selected area is not previously conducted.
- The proposed FCS-MPC controller with HRES can be easily extended from residential electrifications to commercial and agriculture load demands.
- The presented scheme chooses the most viable hres plan by addressing the objectives and constraints of the system. Hence, this scheme fulfills the need of the customers in terms of the economic advantages with fast performance while predicting the dynamic response of linear and non-linear multivariable systems.
- The applied mpc based scheme is also applicable for grid-connected applications in addition to grid-disconnected operations under transient studies. while the most widely used PI control schemes are only applicable to grid-disconnected operations.
- The settling time is minimum in the case of FCS-MPC control and is more efficient in minimizing the errors and eliminating the noises from the output signals.
- The applied scheme has no requirement of any PWM strategy and it is also capable of variable switching frequencies.
- The performance analysis during steady-state response is more efficient and better in terms of all reference frames while the complex design level is also low and its control is easily implementable in experiments.
- The suggested HRES with detailed analysis includes the incorporation of sensitivity analysis and bidirectional reconfigurable VSC for four modes of operations.

### III. SYSTEM MODELING AND COMPONENTS DESCRIPTION

Fig. 5 [57] elaborates the presented scheme for the optimized sizing of the hybrid model for grid-disconnected system and the possible energy management scheme for grid-disconnected as well as grid-connected modes of operation. Initially, the step involves comprehensive energy planning and feasibility analysis including meteorological data and the load demand of the selected location. The first step is followed by specifying the optimization objectives and constraints, viable plans of the HRES, the detailed model analysis of different HRES components is also achieved. The most viable configuration plan of HRES is suggested based on the elaborated methodology with the judgment of three prospects namely technological, economic and environmental. The succeeding step is the performance analysis of the proposed scheme for the feasibly selected model. The last step involves the proof of the suggested overall scheme and its comparative analysis with the traditional PI method. The elaboration of the suggested model and the description of the components are described below:

The proposed HRES comprises of diesel, wind, PV, BSS, and converter. The first three components including

PV, wind, and the diesel generator are taken as the main generating resources to fulfill the consumer's electricity demand. The energy storage system is considered to feed the consumers throughout the intermittent duration of solar and WT generation under different conditions which include steady-state, and transients' conditions. The power converters are considered as a substantive component of the HRES model to exchange power between buses. It is pertinent to acknowledge here that the dc-dc converters are applied to extract maximum power from solar and WT generating systems. Whereas the battery converter regulates the dc voltage.

#### A. WIND ENERGY SOURCE

The WECS consists of WT, PMSG, and MPPT mechanism. Wind turbine model which is taken from [34] is of 1 kW capacity, whereas both capital and replacement price are taken as \$ 900/kW [59], O&M is \$ 10/kW while project lifetime is 20 years.

The desirable hub height ( $V_{hub}$ ) is found from the real wind speed data at the corresponding height by applying the following logarithmic law [50]

$$V_{hub}(t) = V_{act}(t) \frac{\ln\left(\frac{H_{hub}}{L_o}\right)}{\ln\left(\frac{H_{act}}{L_o}\right)} \quad (1)$$

where,  $V_{hub}$ , and  $V_{act}$  are wind speed relevant to desirable hub height ( $H_{hub}$ ), and measurable wind speed relevant to reference height ( $H_{act}$ ) respectively.  $L_o$  is the length of surface roughness.

Wind mechanical power  $P_{mec}$  is represented as:

$$P_{mec} = \frac{1}{2} C_p(\lambda, \beta) \rho \pi R^2 v_w^3 \quad (2)$$

$$C_p = 0.22 \left( \frac{116}{\lambda_i} - 0.4\beta - 5 \right) e^{-12.5/\lambda} \quad (3)$$

$$\lambda_i = \frac{1}{\frac{1}{(\lambda+0.08\beta)} - \frac{0.035}{(\beta^3+1)}} \quad (4)$$

The formula for the blade tip speed ratio is shown as

$$\lambda = \frac{\omega_t \cdot R}{v_w} = \frac{k_g \cdot \omega_D \cdot R}{v_w} \quad (5)$$

Fig. 6 represents the maximum power coefficient ( $C_p$ ) with reference to the tip speed ( $\lambda$ ) value. Normally, the pitch angle is taken as zero during  $P_{mec}$  less than the nominal value. Therefore,  $C_p$  is the part of  $\lambda$  and its value is high i.e.  $C_{pmax}$  at a relevant  $\lambda$ . Line with zero angles represents the tip speed with a peak value of coefficient which is taken in this paper. At this instant, the wind turbine works at maximum power with the optimal rotor speed i.e.  $\omega_{Dopt}$  and at the specific wind speed i.e.  $v_w$  in (5). By substitution of (5) in (2), we get:

$$P_{MPPT}^{WG} = \frac{\rho \pi R^5 k_g^3 C_{pmax}}{2\lambda^3} \cdot \omega_D^3 = C_M \cdot \omega_D^3 \quad (6)$$

The maximum power extracting scheme of WT and the pitch angle scheme are applied for keeping power at the

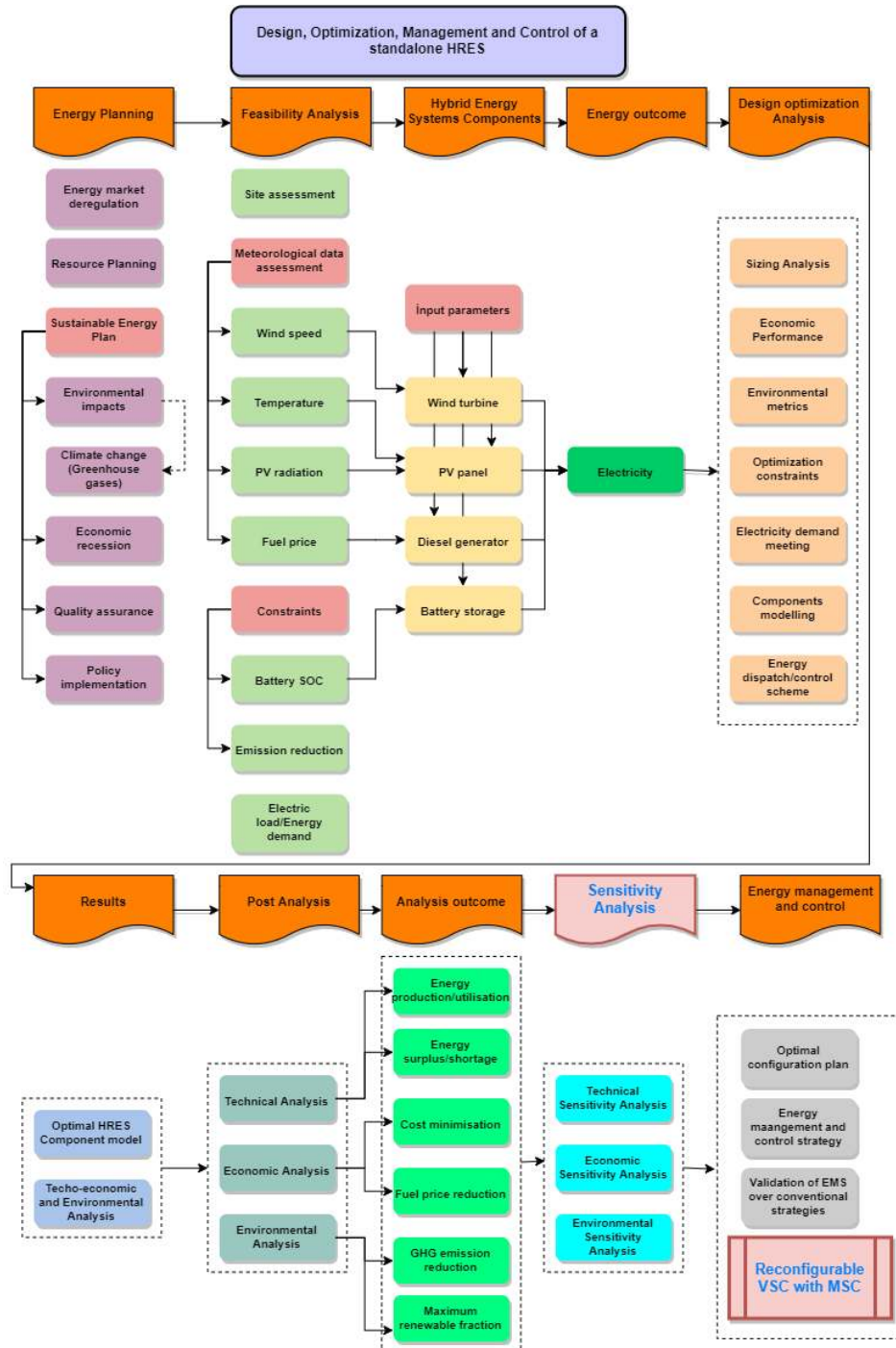


FIGURE 5. A suggested scheme for the optimal sizing, and management system [58].

desired level. The reference value of power i.e.  $P$  is found with the MPPT algorithm. The relationship to reach the optimal value of the rotor speed is represented below:

$$2H_D \cdot \omega_D \cdot \frac{d\omega_D}{dt} = P_{mec} - P_{MPPT}^{WG} \quad (7)$$

By considering the fast-electronic function, the power ( $P$ ) of the WT is considered the same as the reference power.

### B. PV SOLAR ENERGY SOURCE

The solar energy is relatively not expensive when equated with WT energy, the reason is that no wear and tear exists in the case of PV generation [9]. For MPPT, the IC scheme is employed for extracting maximum power from solar PV generator with improvement in steady-state and dynamic response and well operation during fast-alteration of atmospheric situations.

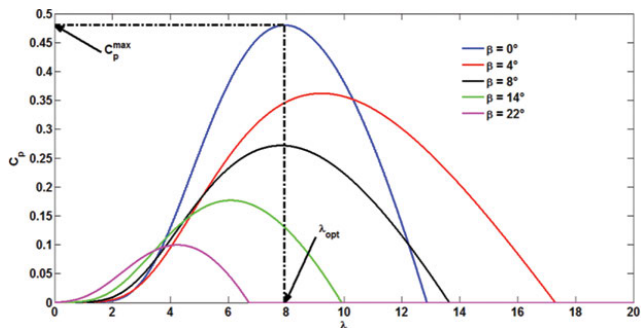


FIGURE 6. Characteristics of PV panel [60].

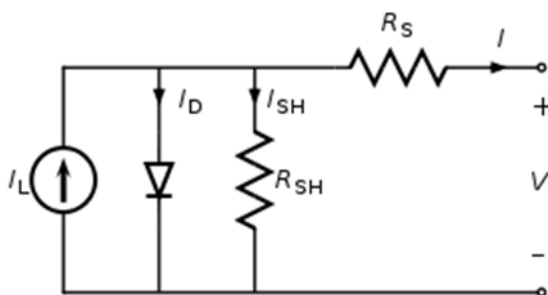


FIGURE 7. Model of the solar cell.

The clearness index ( $K_t$ ) is given by [61]

$$K_t = \frac{H_{ave}}{H_{o,ave}} \tag{8}$$

$$H_{o,ave} = \frac{\sum_{n=1}^N \frac{24}{n} G_{on} \left( \cos \varphi \cos \delta \sin \omega_s + \frac{n\omega_s}{180^\circ} \sin \varphi \sin \delta \right)}{N} \tag{9}$$

The total PV output current is computed as follows [6]

$$I = N_p I_{PV} - N_p I_O \left\{ \exp \left( \frac{V + IR_S}{nV_t} \right) - 1 \right\} - \frac{V \times N_p / N_S \times IR_S}{R_{Sh}} \tag{10}$$

The PV output power is computed as [26]

$$P_{pv}(t) = P_{SC} \cdot \frac{G_{irr}(t)}{1 kWh/m^2} \cdot \left[ 1 + \frac{\alpha}{100} \{T_{cell}(t) - 25\} \right] \cdot F_{dirt} \tag{11}$$

where  $P_{SC}$ , and  $G_{irr}(t)$  are the output power at standard conditions, and PV irradiance on tilted panel surface at hour  $t$  respectively,  $F_{dirt}$  is constant which is about 0.9,  $\alpha$  is temperature coefficient in  $\%/^\circ C$ .

$T_{cell}(t)$  is cell temperature in  $^\circ C$  which is expressed as:

$$T_{cell}(t) = T_a(t) + \left( \frac{T_{nom} - 20}{0.8} \right) \cdot \frac{G_{irr}(t)}{1 kWh/m^2} \tag{12}$$

where  $T_a(t)$  and  $T_{nom}$  are respectively the ambient and nominal temperatures of PV cell in  $^\circ C$ .

The PV Simulink diagram is shown in Fig.

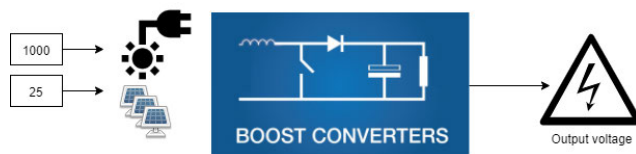


FIGURE 8. PV Simulink diagram.

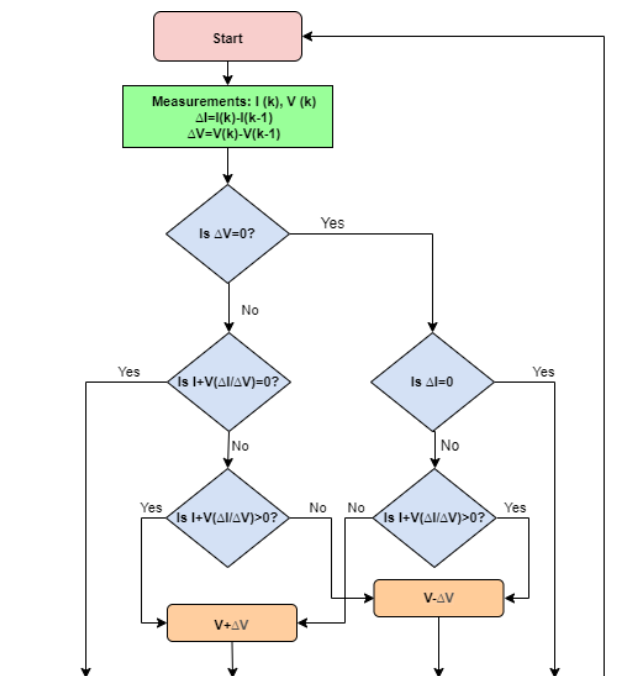


FIGURE 9. Flow chart of PV MPPT method.

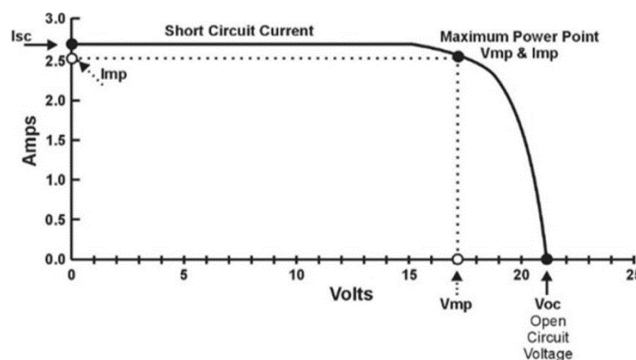


FIGURE 10. Characteristics of PV cell representing current-voltage and power-voltage curves [63].

The photovoltaic current ( $I_{PV}$ ) is linked with insolation ( $\lambda_S$ ) as follows [62]

$$I_{PV} = \{I_{SC} + k_{temp} * (T - T_{nom})\} * \frac{\lambda_S}{\lambda_{nom}} \tag{13}$$

Fig. 9 shows the flow chart for the IC method. Fig 10 shows PV cell characteristics in terms of P-V and I-V. the point where  $I_{mp}$  and  $V_{mp}$  meets is called the maximum power point (MPP) which is variable based on the atmospheric conditions.  $I_{mp}$  and  $V_{mp}$  are the current and voltage at maximum

power. R1 and Ro are the two different load lines where Ro refers to the load where the maximum power point overlaps with the operating point. Fig. 11 shows the graph between voltage (Voc) and current (Isc). Voc is linearly dependent on cell temperature and is logarithmical with irradiation, and Isc is linearly dependent on irradiation. Fig. 12 shows the PV system with the schematic diagram for DC-DC converter, where Rin and Ro are the converter input resistance and output or load resistance respectively. Approximate ranges of Rin for boost converter is shown in Fig. 13.

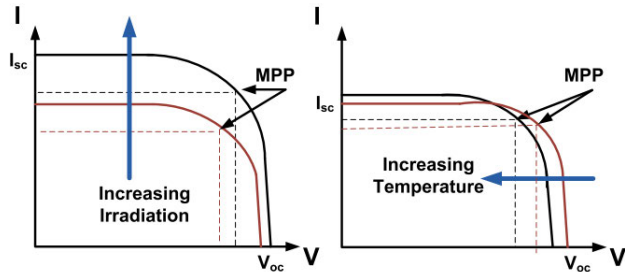


FIGURE 11. Characteristics of PV cell representing variations in ambient irradiation and temperature [63].

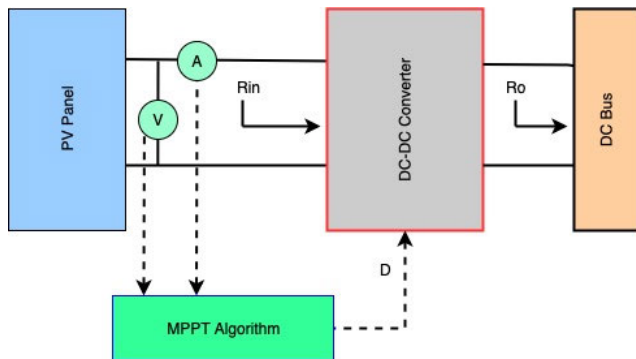


FIGURE 12. Schematic representation of the PV system.

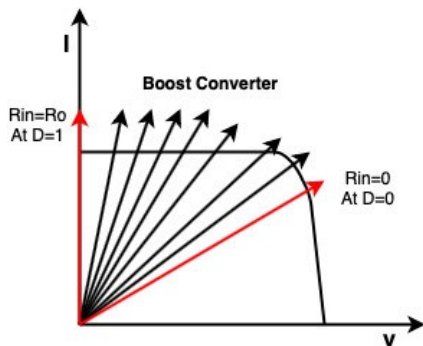


FIGURE 13. Input resistance range for DC-DC boost converter [63].

### C. BATTERY BANK

The excess energy which is available from generating energy resources is stored and then fed to the load under low generation hours. The battery capacity can be expressed as [12]

$$E_{Total} = \frac{E_{Day}}{\eta_{inv}} \quad (14)$$

The formula for battery energy is represented as

$$E_{Bat} = \frac{E_{Total} \cdot n_a}{V_{Bat} \cdot \eta_{Bat} \cdot DOD} \quad (15)$$

The total number of batteries in series ( $N_S$ ) and parallel ( $N_P$ ) are calculated by using the following relationship.

$$N_{Series} = \frac{V_{Bus}}{V_{Bat}} \quad (16)$$

$$N_{Parallel} = \frac{E_{Bat}}{E_{Bat, rated}} \quad (17)$$

The battery energy [26] in terms of production and absorption is expressed as.

$$C_{Bat}(t) = C_{Bat}(t-1) \cdot (1-\sigma) + \left[ P_{PV}(t) - \frac{P_{load}(t)}{\eta_{inv}} \right] \cdot \eta_{Bat} \quad (18)$$

with battery charging during:

$$P_{PV}(t) - \frac{P_l(t)}{\eta_{inv}} > 0 \text{ with } C_{Bat}(t-1) < C_{BatMax} \quad (19)$$

while the battery is discharging during:

$$P_{PV}(t) - \frac{P_l(t)}{\eta_{inv}} < 0 \text{ with } C_{Bat}(t-1) > C_{BatMin} \quad (20)$$

where  $C_{Bat}(t)$  is the available power of the battery bank at duration  $t$  in hours while  $C_{Bat}(t-1)$  shows the same power at the previous time ( $t-1$ ). The symbol  $\sigma$  represents the self-discharge rate. The term  $P_l(t)$  shows the load requirement at the duration  $t$  in hours. The battery/inverter efficiencies are expressed as  $\eta_{Bat}$  and  $\eta_{inv}$  respectively. The limits for  $C_{Bat}(t)$  are taken as the permissible energy point between the minimum and maximum range as:

$$C_{BatMin} \leq C_{Bat}(t) \leq C_{BatMax} \quad (21)$$

For prolonged services of the battery, the maximum charging rate is defined as:

$$SOC_{Max} = C_{Bat} N_{Bat} \quad (22)$$

where  $C_{Bat}$  and  $N_{Bat}$  are nominal battery capacity and a total number of batteries respectively. Similarly, the minimum Number of batteries is calculated as [50]

$$N_{Bat} = \frac{P_a \cdot n_A}{C_{Bat} \cdot \eta_{Bat} \cdot DOD} \quad (23)$$

The battery terminal voltage is described as [64].

$$V_{Bat} = V_{out} - i_{bat} R_{bat} - K \frac{Q}{Q - \int i_{bat} dt} + A e^{(-B \int i_{bat} dt)} \quad (24)$$

$$SOC = 100 \left( 1 - \frac{\int i_{bat} dt}{Q} \right) \quad (25)$$

The battery SOC is calculated as [50]

$$SOC(k) = \begin{cases} SOC(k-1) + \{P_a(k) - P_l(k)\} \eta_{Bat} \Delta t / C_{Bat}, & \text{for charging} \\ SOC(k-1) - \{P_l(k) - P_a(k)\} \Delta t / \eta_{Bat} C_{Bat}, & \text{for discharging} \end{cases} \quad (26)$$



**TABLE 4. Characteristics of the incremental conductance (IC) method [63].**

Circuit used	True MPPT	Sensors	Cost	Control strategy	Complexity	Accuracy/efficiency	Speed
Digital	Yes	Current, Voltage	Expensive	Sampling	Medium	Medium	Varies

**TABLE 5. Comparison of MPPT methods.**

Ref.	Study System	Standalone/Grid-connected	MPPT method	DC-DC Converter	Generation Perturbance Analysis	Interlinking inverter control
[38]	PV-WT-BSS-Converter	Standalone	IC	Buck	Irradiance	SVPWM
[37]	PV- BSS-Converter	Standalone	-	-	Irradiance	-
[44]	PV- BSS-Converter	Standalone	P&O	-	Irradiance	-
Current study	PV-WT-BSS-Converter	Standalone	IC	Boost	Irradiance & Temperature	FCS-MPC

Subject to

$$\begin{cases} SOC_{min} < SOC(k) < SOC_{max} \\ P_{ch}(k) \leq P_{ch_{max}} \\ P_{dch}(k) \leq P_{dch_{max}} \end{cases} \quad (27)$$

The relationship to design the inductor is expressed as [65].

$$L_{Bat} = \frac{V_{DC}(1-D)}{2 \cdot f_{min} \cdot \Delta I_B} \quad (28)$$

#### D. POWER CONVERTER

A bidirectional voltage source converter is applied to exchange bidirectional power between both buses. The power transmitted through the converter is [26]

$$P_{in} = \frac{P_{chg}}{\eta_{inv}} \quad (29)$$

where  $\eta_{inv}$  and  $P_{chg}$  are converter efficiency and load demand (W) in hours respectively.

The relationship for VSC capacity (C) is shown as [6]

$$C = (3 \times L_{ind}) + L_{res} \quad (30)$$

where  $L_{ind}$  and  $L_{res}$  are respectively inductive load and resistive load.

#### E. DIESEL GENERATION

A DG is used to supply a high amount of energy shortfall under the intermittent and fluctuating behavior of the generating sources. The fuel price is \$ 0.78 per liter. The fuel utilization of DG ( $F_{dg}$ ) in L/hr can be represented in Eq. (36) [66] as:

$$F_{dg} = (\alpha \times P_{nom}) + (\beta \times P_{out}) \quad (31)$$

where  $\alpha$  and  $\beta$  are coefficients of consumption in L/kWh,  $P_{nom}$ , and  $P_{out}$  are DG nominal and output capacities in kW. The DG efficiency ( $\eta_{dg}$ ) is defined as

$$\eta_{dg} = \frac{P_{out}}{F_{dg} \cdot H_{fuel}} \quad (32)$$

where  $H_{fuel}$  is the value of fuel consumption heating in kWh/L (ranges from 10-11.6). The values of  $\alpha$  and  $\beta$  are 0.246 and 0.08145 respectively [26].

#### IV. TECHNO-ECONOMIC INVESTIGATION USING HOMER

The comparison of different optimal sizing tools is described in [67], while these tools are used in the research studies for the sizing of HRES models. Out multiple available tools [68], [69]–[73], HOMER (Hybrid Optimization of Multiple Electric Renewables) tools are the best often applied and extremely commended in different literature works.

HOMER is a robust design optimization software for design optimization [32] which takes into account the adaptable circumstances to investigate different configurations and optimal HRES models [32].

Its algorithms of design optimization permit the designer and planners to judge the feasible scenarios under different technical criteria related to the changing technological trends and resource accessibility. Hence, HOMER is selected in this study for the techno-economic investigation to determine the most feasible option to meet the load requirements for the selected area.

HOMER assesses viable configuration schemes among various possible solutions with frequent and easy process. The suggested flow chart of the optimization design is demonstrated in Fig. 14 [34]. It optimizes the component sizing [6]. Its design optimization is purely based on the input parametric values which include load requirements, gener-

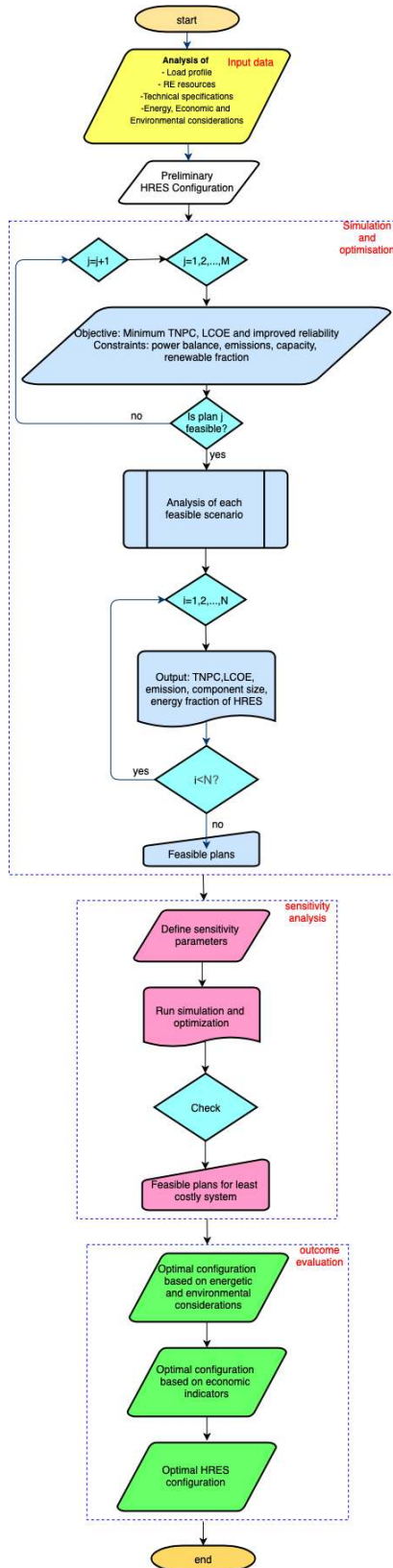


FIGURE 14. Applied scheme for optimal sizing of HRES [34].

ation profiles, economic and technical circumstances, modeling constraints, suggested energy management, scheme, GHG evaluation parameters [6], [32] with TNPC as the main

objective of design optimization scheme [32]. HOMER calculates a one-year optimal design to evaluate different aspects of HRES which includes technical, environmental, and economic considerations [74]. Subsequently, extrapolation of costs operates for the remaining years throughout the project life, to ensure reliable generation and consumption balance on an hourly basis [32]. After finishing the testing stage for all possible configurations, the viable plans are selected and ranked in terms of design objective.

**A. OBJECTIVE FUNCTION AND CONSTRAINTS**

The past literature studies have taken into account different evaluation standards reported in [34] which are applied to determine the viable configuration plan of HRES. In this study, the annualized cost of the system (ASC) is used as the main objective function with LLP and emission as the main constraints are described as follows.

Annualized system cost (ASC) or annualized total cost (ATC) in \$/yr is the sum of system capital cost per annum, annualized maintenance cost, and annualized replacement cost for each model component which is expressed as follows

$$ASC = A_{capt, cost} + A_{maint, cost} + A_{repl, cost} + A_{fuel, cost} \quad (33)$$

with

$$A_{capt, cost} = C_{capt} \cdot CRF(i, n) \quad (34)$$

where  $C_{capt}$  is the capital value for each HRES component (in US\$),  $i$  is annualized interest and  $n$  is project life.  $CRF$  is described as

$$CRF = \frac{i(1+i)^n}{(1+i)^n - 1} \quad (35)$$

where  $i$  is expressed as

$$i = \frac{i_{nom} - f_{inf}}{1 + f_{inf}} \quad (36)$$

Operation and maintenance cost are represented as

$$A_{maint, cost} = A_{maint, cost}(n1) \cdot (1 + f_{inf})^n \quad (37)$$

$A_{maint, cost}(n1)$  is the first-year cost of the corresponding component. Replacement cost is related as

$$A_{repl, cost} = C_{repl} \cdot SFF(i, n_{repl}) \quad (38)$$

where  $C_{repl}$  is the replacement cost of each component (in US\$),  $n_{repl}$  is the component of life in years.  $SFF$  is given below.

$$SFF = \frac{i}{(1+i)^n - 1} \quad (39)$$

LCOE in \$/kWh is the ratio of ASC and generated electricity which is derived as

$$LCOE = \frac{ASC}{TE_{gen}} \quad (40)$$

LCC in \$ is the sum of recurring and non-recurring costs during the system lifespan, which include operating, installation, capital, upgrading, maintenance costs, and salvage value which is written as

$$LCC = \sum_{i=1}^m C_{C,i} + C_{R,i} + C_{OM,i} \quad (41)$$

LPSP is mentioned as.

$$LPSP = \frac{\sum_{t=1}^M LPS(t)}{\sum_{t=1}^M LD(t)} \quad (42)$$

LLP is defined as

$$LLP = \frac{\sum_{t=1}^{8760} E_{deficit}(t)}{\sum_{t=1}^{8760} E_{demand}(t)} \quad (43)$$

where  $LLP \leq \varepsilon_{LLP}$ ,  $E_{deficit}$ , and  $E_{demand}$  are energy shortage and unmet load respectively.

LOA is the reliability index which is defined as one minus a total hour when a load has not served to the system operation hours as expressed below.

$$LOA = 1 - \frac{T_{load,NS}}{T_{operation}} \quad (44)$$

ELF is the ratio between forced outage duration and the total system operation time (hours). ELF is less than 0.1 for an off-grid system which is expressed as follows.

$$ELF = \frac{1}{T} \sum_{t=1}^J \frac{E(Q(t))}{LD(t)} \quad (45)$$

The mathematical relation for renewables fraction [?] is written as

$$RF = 1 - \frac{E_{NR}}{E_S} \quad (46)$$

The power balance constraint is [75].

$$\sum_{j=1}^N P_{PV} + \sum_{j=1}^N P_{WT} + P_{diesel} + P_{bat} - P_{load} = 0 \quad (47)$$

The limits of generation and battery operation [75] are.

$$P_{charge}^{max} \leq P_{bat} \leq P_{discharge}^{max} \quad (48)$$

The DG creates pollution in the form of toxic gases and carbon dioxide is the primary toxic gas and is taken into account in this work which is expressed as follows [26].

$$CO_{2W} = \sum_{t=1}^{8760} L_{fuel} \cdot F_{em} \quad (49)$$

where  $CO_{2W}$  should be less than or equal to  $\varepsilon_{CO_2}$  (i.e.  $CO_{2W} \leq \varepsilon_{CO_2}$ ) while  $F_{em}$  is the emission factor (in kg/L) based on DG type with its engine attributes and ranges from 2.4-2.8.

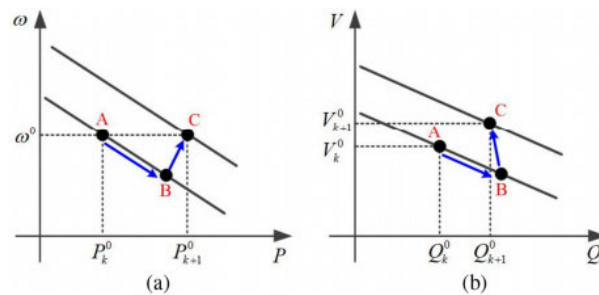


FIGURE 15. Principle of droop: (a) P- $\omega$  curve, and (b) Q-V curve [10].

## V. TECHNICAL ANALYSIS USING MATLAB

### A. SYSTEM DESCRIPTION

A microgrid comprises of energy resources including distributed generators (DG), battery storage system (BSS), and renewable energy sources (RESs). The DG output power in an ac grid is calculated as:

$$P_g = P_g^{ref} + k_p (\omega^{ref} - \omega) \quad (50)$$

$$Q_g = Q_g^{ref} + k_q (V^{ref} - V) \quad (51)$$

where  $P_g^{ref}$  and  $Q_g^{ref}$  represent active and reactive powers respectively.  $k_p$  and  $k_q$  are the droop coefficients of two curves viz.  $P - \omega$  and  $Q - V$  (see Fig. 15) respectively.  $\omega$  and  $V$  demonstrate the values of frequency and voltage magnitude respectively. For the dc grid, the output power of DGs is expressed as.

$$P_g = P_g^{ref} + k_p (V^{ref} - V) \quad (52)$$

Fig. 16 shows the general concept of the MPC scheme. The prediction step of the system is incorporated in the optimization model to address the issue which is based on the predicted time horizon as shown in Fig. 17.

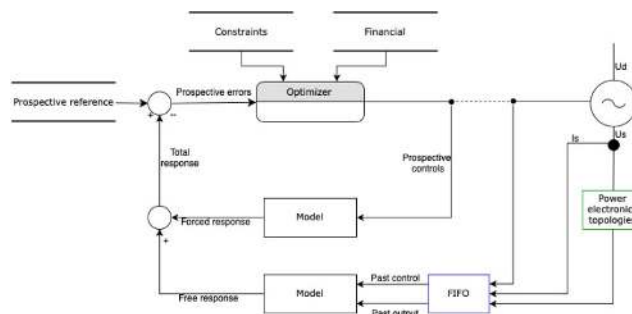


FIGURE 16. The general framework of MPC for reconfigurable VSC.

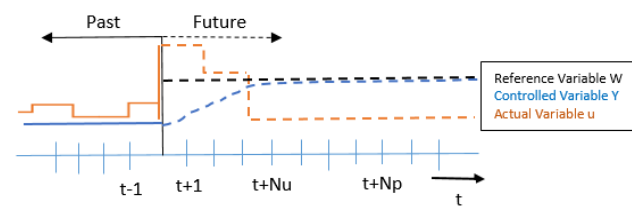


FIGURE 17. Predicted horizon during MPC operation.

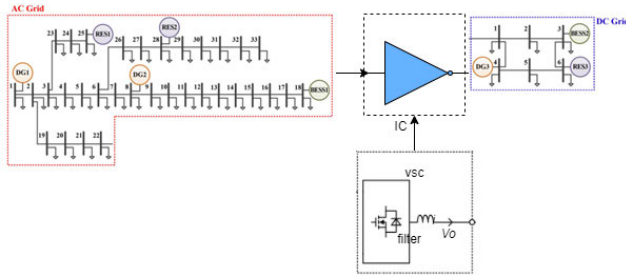


FIGURE 18. Demonstration of HMG test system.

FCS-MPC is implemented for a bidirectional VSC converter to regulate the load voltage. FCS-MPC scheme with 2-level 3-phase VSC is suggested in this work. The applied control strategy chooses the most feasible state from seven switching states for minimizing the cost function. Simulation results demonstrate compensation of disturbance from loads, and sources while the load voltage is in continuous mode for tracking the reference signal of the voltage. A buck-boost control is used for the regulation of the dc voltage. The renewables converters of PV and WT are implemented to extract maximum power. The following section discusses the control as well as management strategies.

Fig. 19 depicts the applied FCS-MPC concept. The parameters required to address and resolve the particular issue is highlighted with symbol  $v$ . The external perturbation is symbolized with  $d$ . The control signal is highlighted with symbol  $c$ . The forecasting parameter is expressed with a symbol  $w$ . With the measurement values of the current system ( $v$ ) and forecasting parameter ( $d$ ), the simulation is executed with an optimizer.

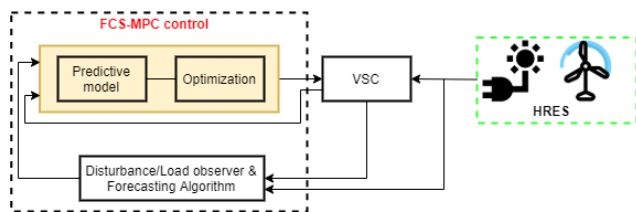


FIGURE 19. Suggested FCS-MPC scheme of a bidirectional VSC.

MPC strategy is used for main VSC control. Contrary to the conventional controls, FCS-MPC does not need to apply the control with inner and outer loops or PWM techniques. The working rule of the suggested methodology is described in [57].

### B. PREDICTIVE CONTROL OF VOLTAGE SOURCE CONVERTERS IN MICROGRIDS DURING RECONFIGURATION

#### 1) AFE RECTIFICATION MODE

For the development of the AFE rectifier model as shown in Fig. 20, the continuous state-space model of VSC is

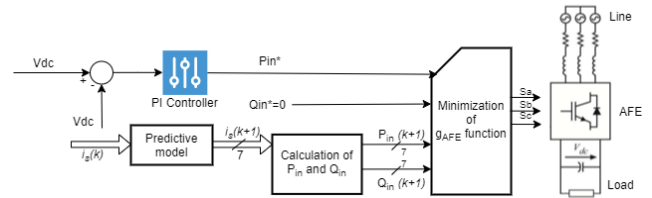


FIGURE 20. Predictive power control of AFE VSC.

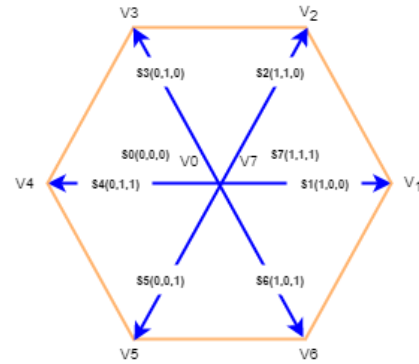


FIGURE 21. Possible switching states of a 2-level, 3-phase VSC.

explained as follows:

$$L_s \frac{di_s}{dt} = v_s - v_r - R_s i_s \quad (53)$$

where  $L_s$ ,  $R_s$  are respectively the inductance and resistance of the RLC filter. The parameters like  $v_s$ ,  $v_r$  and  $i_s$  are representing respectively the voltages of source, rectifier and input current. Fig. 21 shows the generated voltage vectors of VSC. Discrete-time state-space modeling for the prediction of current is represented as:

$$i_s(k+1) = \left(1 - \frac{R_s T_s}{L_s}\right) i_s(k) + \frac{T_s}{L_s} [v_s(k) - v_r(k)] \quad (54)$$

$$\begin{bmatrix} i_{s\alpha}(k+1) \\ i_{s\beta}(k+1) \end{bmatrix} = \left(1 - \frac{R_s T_s}{L_s}\right) \begin{bmatrix} i_{s\alpha}(k) \\ i_{s\beta}(k) \end{bmatrix} + \frac{T_s}{L_s} \begin{bmatrix} v_{s\alpha}(k) - v_{r\alpha}(k) \\ v_{s\beta}(k) - v_{r\beta}(k) \end{bmatrix} \quad (55)$$

where  $T_s$  shows the sampling time and the following relationships represent the predicted value for instantaneous powers (active and reactive):

$$P_i(k+1) = \text{Re} \{v_s(k+1)i_s(k+1)\} = v_{s\alpha}i_{s\alpha} + v_{s\beta}i_{s\beta} \quad (56)$$

$$Q_i(k+1) = \text{Im} \{v_s(k+1)i_s(k+1)\} = v_{s\alpha}i_{s\beta} - v_{s\beta}i_{s\alpha} \quad (57)$$

The following cost function is applied for the predictive power control.

$$g_r = |Q_i^* - Q_i(k+1)| + |P_i^* - P_i(k+1)| \quad (58)$$

where  $Q_i^*$ ,  $P_i^*$  are the reference values of reactive and active powers respectively. Fig. 22 shows the flow chart of the FCS-MPC algorithm which is applied for the control of AFE VSC.

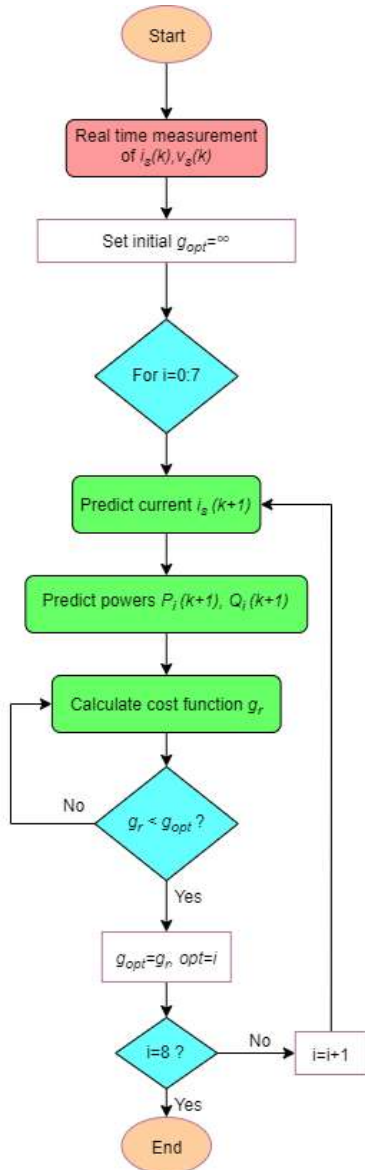


FIGURE 22. The applied flow chart for predictive power scheme of AFE VSC.

2) VOLTAGE MAGNITUDE/FREQUENCY CONTROL OF VSI DURING GRID-DISCONNECTED MODE

The filter model is shown in Fig. 23 and predictive voltage control is described in Fig.24 with the following relationship.

$$\frac{d}{dt} \begin{bmatrix} i_f \\ v_c \\ i_o \end{bmatrix} = \begin{bmatrix} 0 & -\frac{1}{L} & 0 \\ \frac{1}{C} & 0 & -\frac{1}{C} \\ 0 & 0 & 0 \end{bmatrix} \begin{bmatrix} i_f \\ v_c \\ i_o \end{bmatrix} + \begin{bmatrix} \frac{1}{L} \\ 0 \\ 0 \end{bmatrix} v_i + \begin{bmatrix} 0 \\ 0 \\ f(i_o, v_c) \end{bmatrix} \quad (59)$$

where  $V_c, V_i, I_f, R_f, L$  are respectively the voltage vectors on the load side of VSC, VSC output voltage, current, resistance, and inductance of RLC filter. Continuous state-space

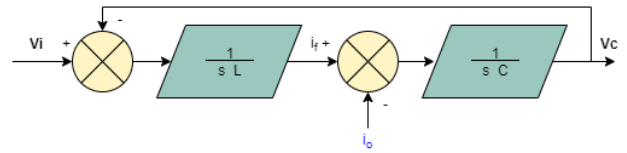


FIGURE 23. Filter model for VSC based HMGS.

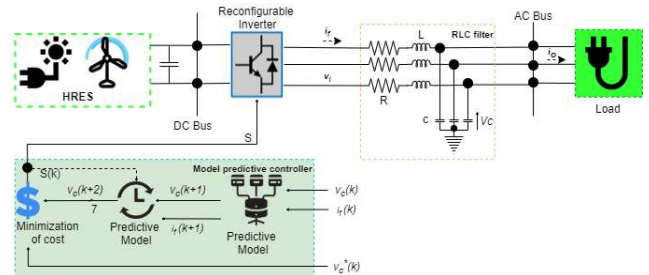


FIGURE 24. FCS-MPC strategy of VSC as an inverter mode.

modeling of the above-mentioned relationship is expressed as follows.

$$\frac{dx}{dt} = Ax + Bv_i + u_d(k) \quad (60)$$

To determine the voltage value at the next sampling time, the discrete state-space model is expressed as follows

$$x(k + 1) = A_q x(k) + B_q v_i(k) + u_d(k) \quad (61)$$

By solving the above-mentioned relationship for the discrete state space, we get the following equation.

$$\begin{bmatrix} V_c \\ I_f \end{bmatrix}^{k+1} = A_d \begin{bmatrix} V_c \\ I_f \end{bmatrix}^k + B_d \begin{bmatrix} V_i \\ I_o \end{bmatrix}$$

$$\text{Where } A_q = e^{AT_s}, B_q = \int_0^{T_s} e^{A\tau} B d\tau \quad (62)$$

and  $V_i$  represent the voltage vector with seven switching states for VSC switches viz.  $S_a, S_b,$  and  $S_c$  with the following relation.

$$V_i = \begin{cases} \frac{2}{3} V_{dc} e^{j(i-1)\frac{\pi}{3}} & \text{for } i = 1, 2, \dots, 6 \\ 0 & \text{for } i = 0, 7 \end{cases} \quad (63)$$

The load disturbance observer is applied by defining the objective function as,

$$g_{inv} = (v_{\alpha}^* - v_{c\alpha})^2 + (v_{\beta}^* - v_{c\beta})^2 \quad (64)$$

Fig. 25 demonstrates the flow chart of an algorithm for VSC as an inverter operation in the grid-disconnected state.

The real power (P) is controlled with the VSC output voltage and the imaginary power (Q) is controlled with the frequency of the VSC. The output voltage ( $V_{nom}$ ) and frequency ( $\omega_{nom}$ ) of VSC are used to control the powers (P and Q) as mentioned in the following expressions.

$$\omega_i = \omega_{nom} - m_i P_i \quad (65)$$

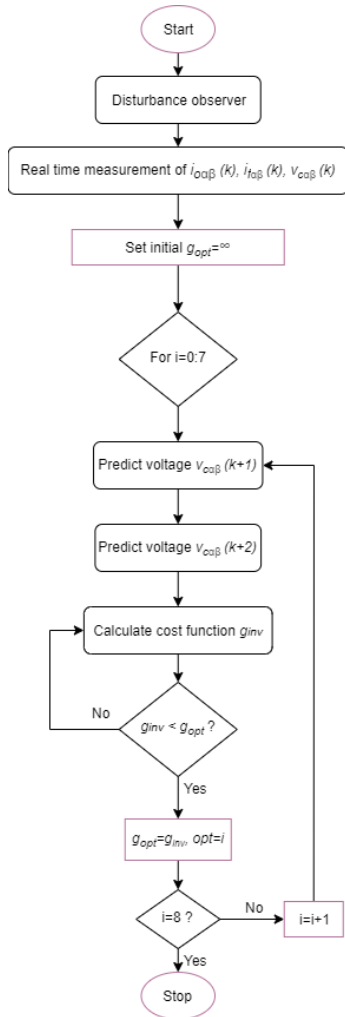


FIGURE 25. The implemented flow chart of FCS-MPC scheme for VSC as an inverter mode.

$$V_i = V_{nom} - n_i Q_i \quad (66)$$

the coefficients namely  $m$  and  $n$  are chosen so that the system stability is ensured with the following relationship.

$$m_i = \frac{\Delta\omega}{Q_{max}} \quad (67)$$

$$n_i = \frac{\Delta V}{P_{max}} \quad (68)$$

where  $P_{max}$  and  $Q_{max}$  are the maximum values of powers furnished by VSC. The other parameters like  $\Delta\omega$  and  $\Delta V$  demonstrate the deviations with an upper limit for frequency and voltage amplitude of the VSC output signal. The parameters,  $m$ , and  $n$  are set to 0.0014 and 0.0008 respectively.

### 3) DIRECT POWER CONTROL (DPC) WITH GRID-TIED MODE

For the development of the DP-MPC model in the grid-connected state as demonstrated in Fig. 26, the following relationships show the output voltage and field current vectors in

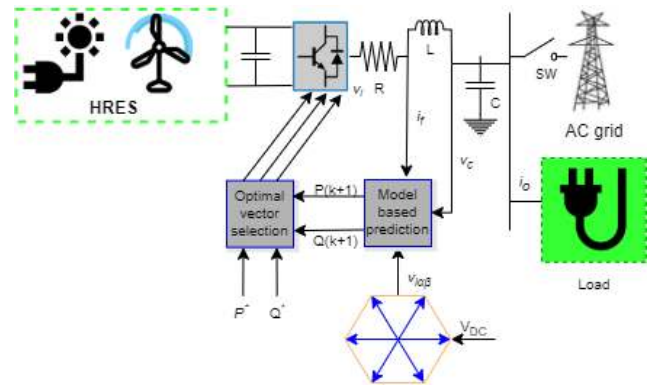


FIGURE 26. Predictive direct power control (DP-MPC) for grid-tied VSC.

the  $\alpha\beta$  reference frame [76].

$$v_{c\alpha\beta} = \begin{bmatrix} v_{c\alpha} \\ v_{c\beta} \end{bmatrix} = \frac{2}{3} \begin{bmatrix} 1 & -\frac{1}{2} & -\frac{1}{2} \\ 0 & \frac{\sqrt{3}}{2} & -\frac{\sqrt{3}}{2} \end{bmatrix} \begin{bmatrix} v_{ca} \\ v_{cb} \\ v_{cc} \end{bmatrix} \quad (69)$$

$$i_{f\alpha\beta} = \begin{bmatrix} i_{f\alpha} \\ i_{f\beta} \end{bmatrix} = \frac{2}{3} \begin{bmatrix} 1 & -\frac{1}{2} & -\frac{1}{2} \\ 0 & \frac{\sqrt{3}}{2} & -\frac{\sqrt{3}}{2} \end{bmatrix} \begin{bmatrix} i_{fa} \\ i_{fb} \\ i_{fc} \end{bmatrix} \quad (70)$$

For balanced loading conditions, the relation for line current is expressed as follows.

$$v_{c\alpha\beta} = L \frac{di_f}{dt} + R i_{f\alpha\beta} + v_{i\alpha\beta} \quad (71)$$

$$C \frac{dv_c}{dt} = \frac{3}{2} (i_{f\alpha} S_\alpha + i_{f\beta} S_\beta) - i_o \quad (72)$$

where  $v_{c\alpha\beta}$ ,  $v_{i\alpha\beta}$ ,  $i_{f\alpha\beta}$ , and  $i_o$  are respectively the voltage vectors of output, and input of VSC, the current values of filter, and load. The exchangeable power ( $P$  and  $Q$ ) with the grid is determined with the following relationship.

$$\begin{bmatrix} P \\ Q \end{bmatrix} = \frac{3}{2} \begin{bmatrix} v_{c\alpha} & v_{c\beta} \\ v_{c\beta} & -v_{c\alpha} \end{bmatrix} \begin{bmatrix} i_{f\alpha} \\ i_{f\beta} \end{bmatrix} \quad (73)$$

Substituting (78) and (79) in (80) and then taking the derivative, the following mathematical relationship is found.

$$\frac{d}{dt} \begin{bmatrix} P \\ Q \end{bmatrix} = \frac{3}{2} \left( i_{f\alpha} \frac{d}{dt} \begin{bmatrix} v_{c\alpha} \\ v_{c\beta} \end{bmatrix} + \frac{di_{f\alpha}}{dt} \begin{bmatrix} v_{c\alpha} \\ v_{c\beta} \end{bmatrix} + i_{f\beta} \frac{d}{dt} \begin{bmatrix} v_{c\beta} \\ -v_{c\alpha} \end{bmatrix} + \frac{di_{f\beta}}{dt} \begin{bmatrix} v_{c\beta} \\ -v_{c\alpha} \end{bmatrix} \right) \quad (74)$$

For load voltage underbalanced and sinusoidal waveform, the following expression is obtained.

$$\vec{v}_c = v_{ca} + jv_{cb} = |\vec{v}_c| e^{j\omega t} \quad (75)$$

$$\vec{v}_c = v_{ca} + jv_{cb} = |\vec{v}_c| e^{j\omega t} \quad (76)$$

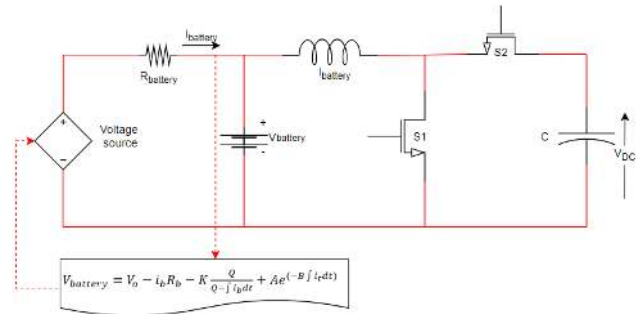


FIGURE 27. Diagram of the BSS Model.

To calculate the instantaneous powers ( $P$  and  $Q$ ), (21) can be modified by substituting (76) and (83) into (81) as

$$\frac{d}{dt} \begin{bmatrix} P_i \\ Q_i \end{bmatrix} = -\frac{R}{L} \begin{bmatrix} P_i \\ Q_i \end{bmatrix} + \omega \begin{bmatrix} -Q_i \\ P_i \end{bmatrix} + \frac{3}{2L} \begin{bmatrix} |\vec{v}_c|^2 - \text{Re}(\vec{v}_c \vec{v}_{ii}^*) \\ -\text{Im}(\vec{v}_c \vec{v}_{ii}^*) \end{bmatrix} \quad (77)$$

where a distinctive space vector is expressed by  $\vec{v}_{ii}$  in  $\alpha\beta$  frame of reference with the following relation.

$$\begin{bmatrix} v_{ii\alpha} \\ v_{ii\beta} \end{bmatrix} = \frac{2}{3} V_{dc} \begin{bmatrix} S_{ia} - \frac{1}{2}(S_{ib} + S_{ic}) \\ \frac{\sqrt{3}}{2}(S_{ib} - S_{ic}) \end{bmatrix} \quad (78)$$

where  $S_{ia}$ ,  $S_{ib}$ ,  $S_{ic}$  are the switching states of the VSC. For constant dc bus voltage, the power prediction for the next instant i.e.  $k+1$  during the end of the sampling period ( $T_s$ ) is expressed as follows.

$$\begin{bmatrix} P_i^{k+1} \\ Q_i^{k+1} \end{bmatrix} = T_s \left( -\frac{R}{L} \begin{bmatrix} P_i^k \\ Q_i^k \end{bmatrix} + \omega \begin{bmatrix} -Q_i^k \\ P_i^k \end{bmatrix} + \frac{3}{2L} \begin{bmatrix} |\vec{v}_c|^2 - \text{Re}(\vec{v}_c \vec{v}_{ii}^*) \\ -\text{Im}(\vec{v}_c \vec{v}_{ii}^*) \end{bmatrix} \right) + \begin{bmatrix} P_i^k \\ Q_i^k \end{bmatrix} \quad (79)$$

The feasible switching state with corresponding minimum voltage ripples is chosen for VSC switching with the expression of the following cost function.

$$g_{vsc} = \sqrt{(P^* - P_i^{k+1})^2 + (Q^* - Q_i^{k+1})^2} \quad (80)$$

**C. BATTERY CONTROL UNIT**

To regulate the dc bus voltage, Fig. 27 demonstrates the BSS model and Fig. 28 represents the buck-boost controller.

The net power is maintained and is described as follows.

$$P_{net} = P_{PV} + P_{Wind} + P_{Diesel} + P_{Load} \quad (81)$$

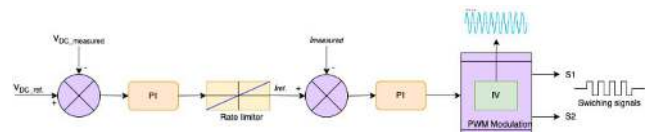


FIGURE 28. A battery controller.

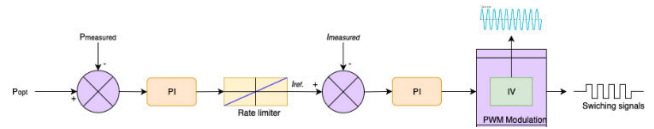


FIGURE 29. A Wind MPPT control with a dc-dc boost converter.



FIGURE 30. The selected site area for electrical load in Pakistan [77].

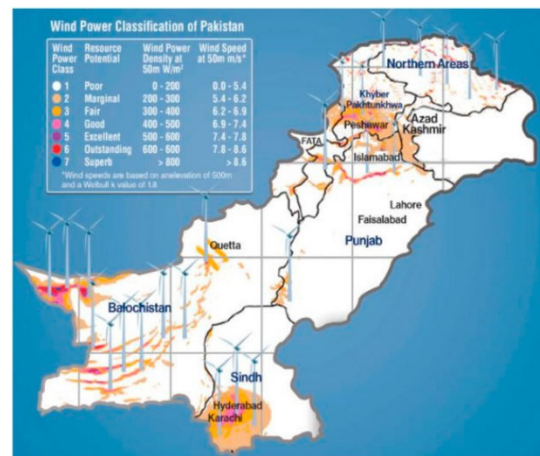


FIGURE 31. Wind generation details of Pakistan [78].

**D. WIND MPPT CONTROLLER**

A WT with a constant (zero) pitch angle and fluctuating wind input is applied, and the parameters detail of PMSG and wind is given in [34]. Fig. 29 shows the MPPT boost controller for a wind energy conversion system.

**VI. CASE STUDY**

Pakistan is located in the territory of South Asia and further detailed investigation of the territory of Pakistan is comprehensively discussed in [57] along with site description, energy resource assessment, and electric load estimation. The domestic area of Kharan district is shown in Fig. 30 and is located at the latitude and longitude of 28° 44.0' N

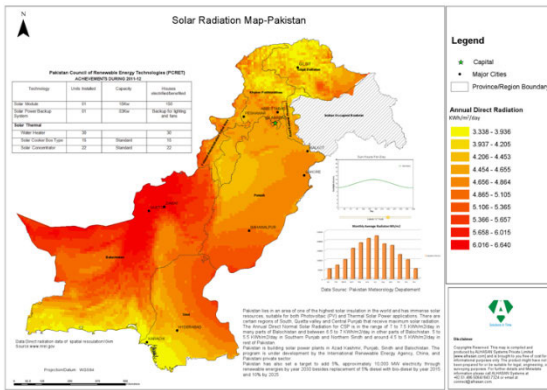


FIGURE 32. Solar generation details of Pakistan [79].

and 65° 3.3' E respectively as shown in Fig 31 with wind generation details. And the annual radiation is shown in Fig. 32. The wind speed, solar irradiance, and temperature are shown in Fig. 33, and Fig. 34 respectively. The estimated peak load is 6.03 kW and the annual energy demand

is 35.94 kWh/day. Fig. 35 shows the load profile for two households with detailed load estimation in Table 6.

## VII. RESULTS AND DISCUSSIONS

### A. DESIGN OPTIMIZATION AND OPERATION INVESTIGATION USING HOMER

The economic prospects and technological analysis are investigated for each component of HRES which includes PV, wind, diesel, battery, and VSC with load profile, real-time solar irradiance, temperature and wind speed. The suppositions and constraints are taken into considerations for the development of the HRES model and simulation studies as demonstrated in Fig. 36 and described as follows.

- Project lifetime is set to be 20 years to find the best computations of the HRES model.
- The nominal discount value is taken as 10 % which is based on the routine trends in Pakistan while inflation is set as 4 %.
- To guarantee the maximum system reliability, zero capacity shortage is considered during the simulation.

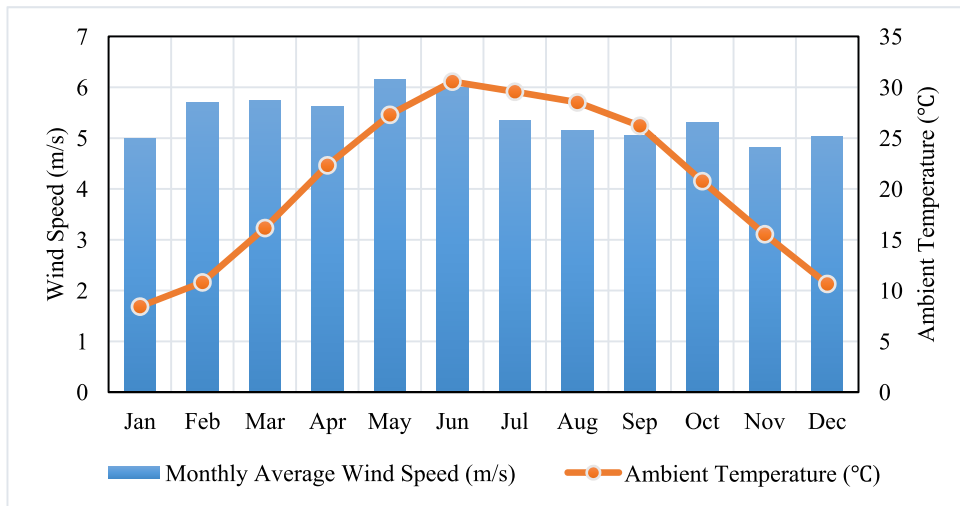


FIGURE 33. Wind profile with temperature.

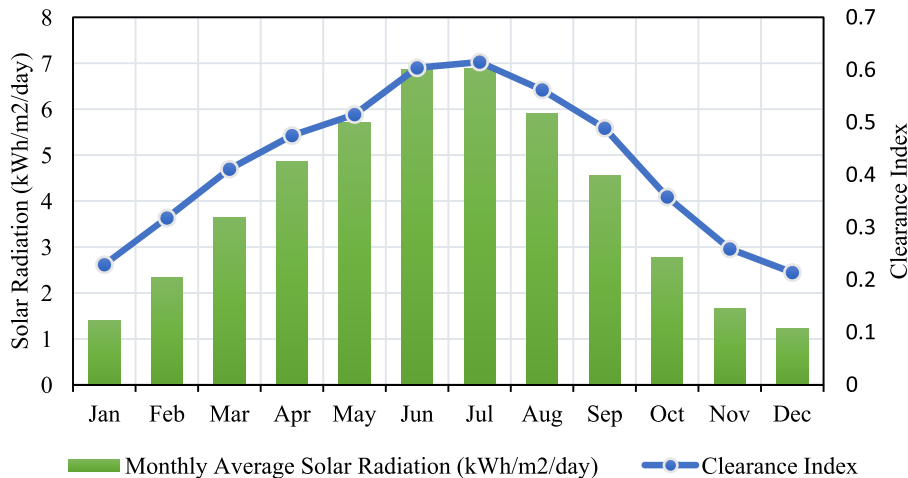


FIGURE 34. Profile of monthly average solar radiation and clearance index.



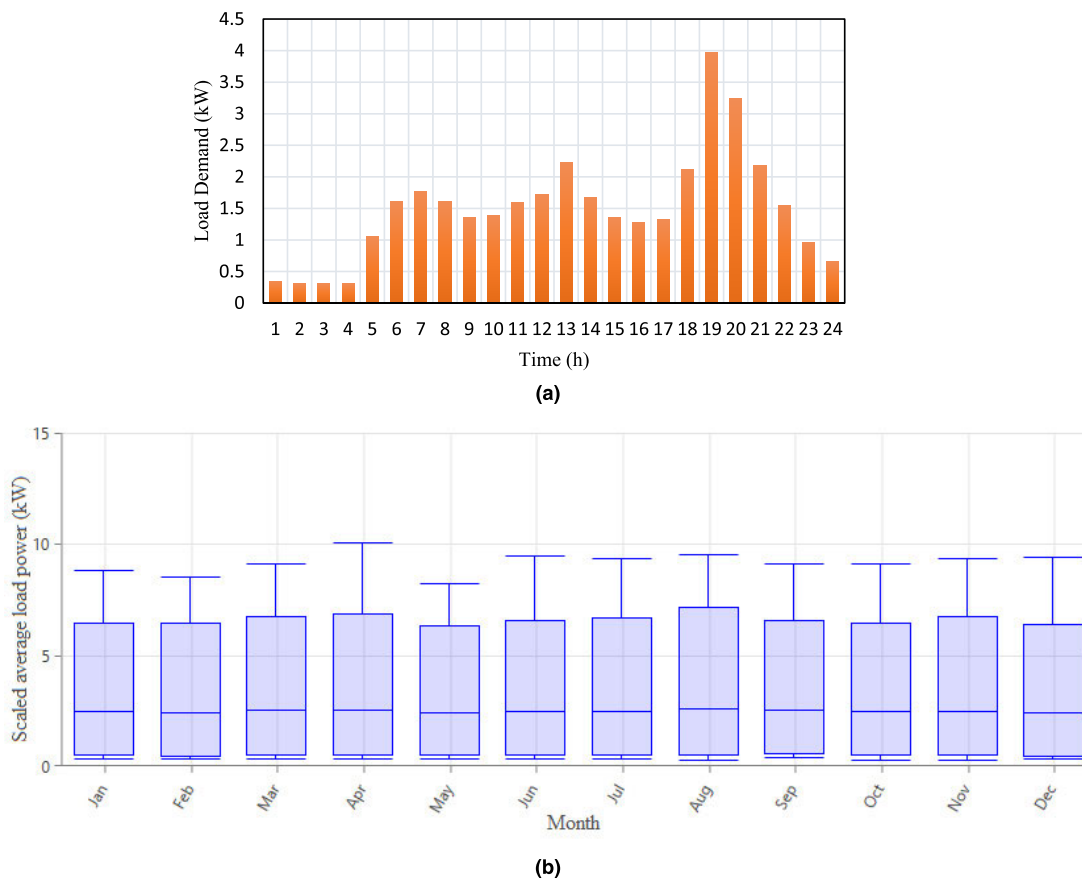


FIGURE 35. Load profile of two houses.

TABLE 6. Estimation analysis of household load.

Appliance name	AC power (Watt)	Quantity	Switch ON duration (Hours/day)	Total load (Wh/day)
Lights	25	7	8	1400
Toaster	1300	1	0.1	130
Coffee maker	800	1	0.35	280
Roof fan	50	3	10	1500
Vacuum cleaner	700	1	0.35	245
Microwave	1300	1	0.3	390
Air Cooler	75	1	5	375
Laptop	50	1	5	250
Television	150	1	3	450
Blender	300	1	0.1	30
Mobile Charger	5	2	7	70
Air conditioner	1500	1	5	7500
Washing machine	500	1	0.5	250
Water Pump	500	1	1.5	750
Dishwasher	1500	1	0.5	750
Refrigerator	150	1	24	3600
Total (one house)				17,970
<b>Total (Two houses)</b>				<b>35,940</b>

- A 10 % reserve is assumed to cover the fluctuating load. The wind and solar energy reserves are chosen to be 15% for compensating random variations in wind speed and solar irradiance.

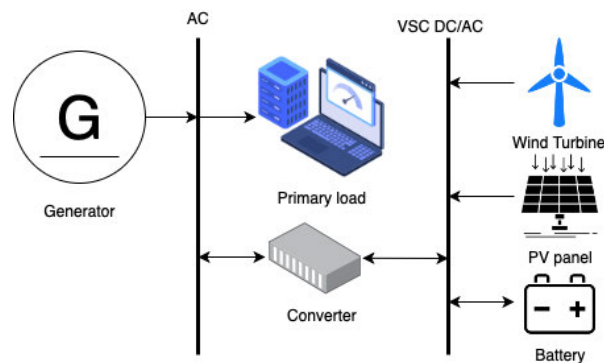


FIGURE 36. HOMER model for the suggested HRES configuration plan.

- A GHG emission penalty of \$ 20/tons is considered as one of the constraints.
- Power flow among different components of HRES is controlled by using the proposed dispatch scheme. Fig. 37 [36] demonstrates the flow chart to produce adequate electricity from a diesel generator which can meet the load requirement. To charge the battery and to serve the deferrable load, low priority objectives are set which depend on renewable power generation capacity. LF strategy is applied to achieve the maximum profit from RERs as well as to reduce fuel consumption. LF preserves the battery by

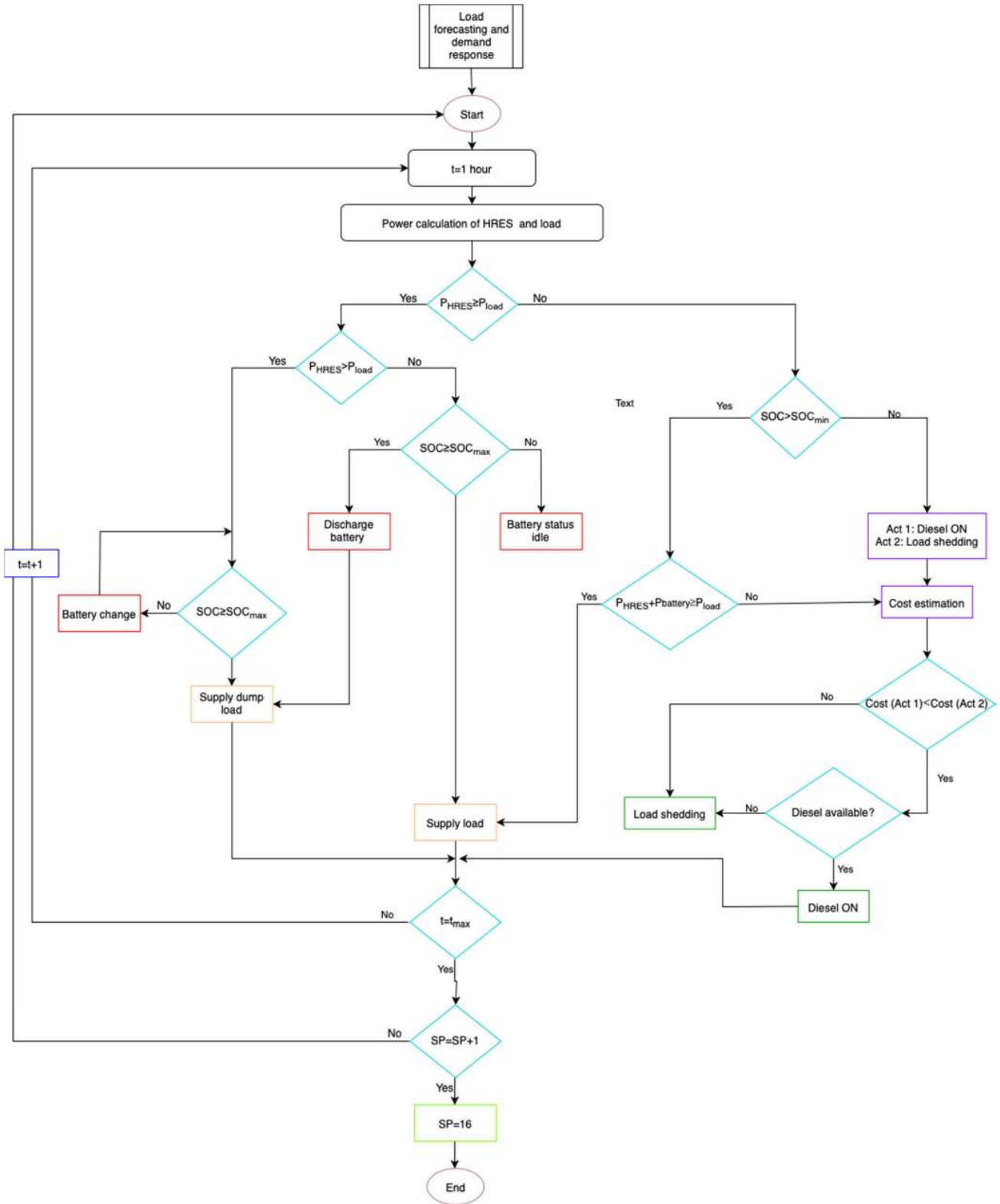


FIGURE 37. Applied dispatch methodology for PV-WT-DG-BSS-converter HRES [36].

avoiding over-charging and over-discharging [36]. Feasible outcomes of all possible configuration plans of the presented HRES models are shown in Table 9 in terms of techno-economic investigation and are ranked

based on TNPC. The concluding remarks about these above-mentioned results are described as follows.

- Among all available HRES configurations, PV-WT-BSS-converter is the most viable option with higher

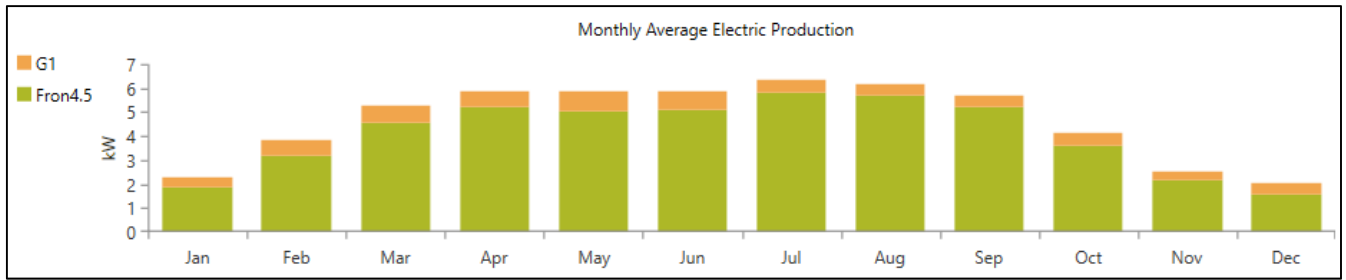


FIGURE 38. Energy generation scheduling.

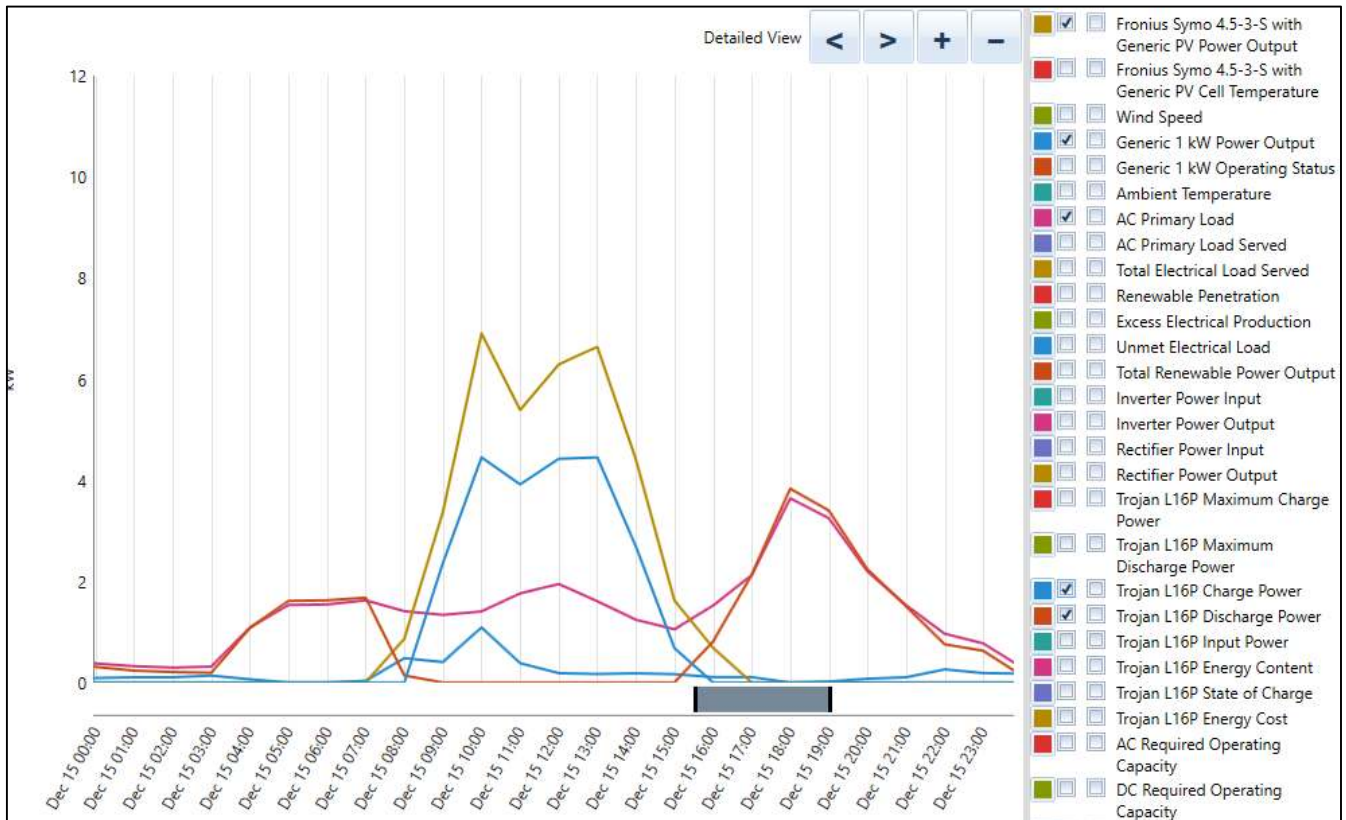


FIGURE 39. Power Dispatch for one day of 15 December on an hourly basis.

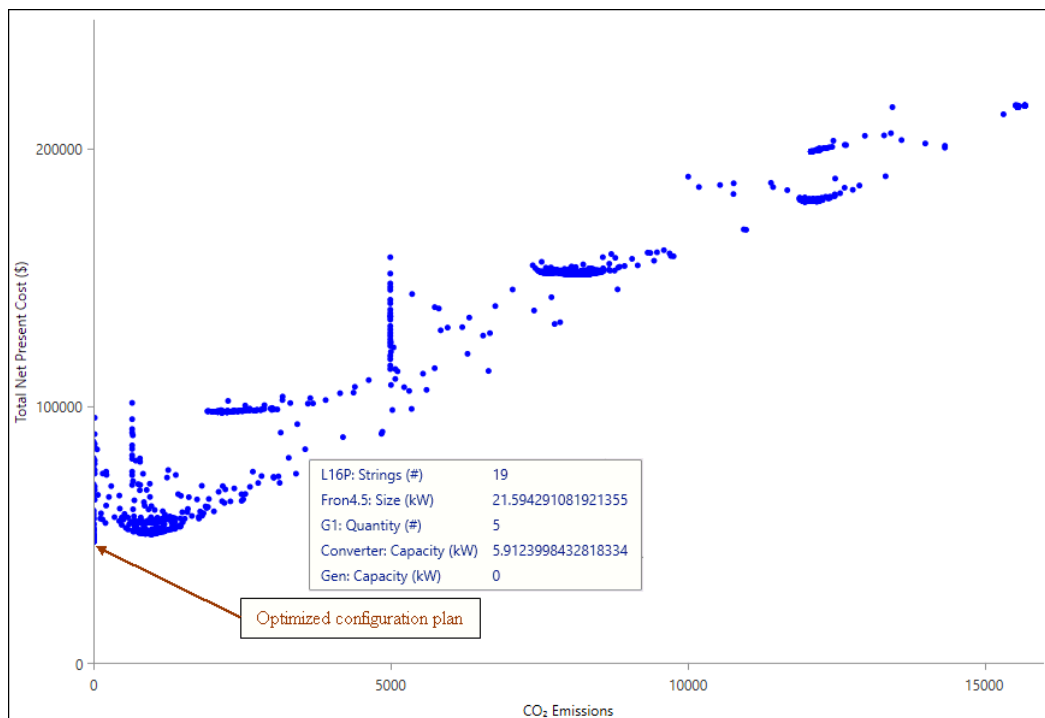
performance attributes for supplying the load at the designated location with the extra energy of 26,034 kWh per year (i.e. 63.9 %).

- The viable model as shown in Table 7 consists of 21.1 kW PV, five (5) WT units of 1 kW each, thirty-eight (38) battery units with each capacity of 2.37 kWh, and 5.96 kW power converter.
- The final optimized configuration is obtained with minimum TNPC (\$ 47,398), LCOE (\$ 0.309/kWh), 100 % renewable penetration (RF) without having any fuel consumption and GHG emission. These findings will assist as a benchmark to select the viable HRES option for an off-grid remote location in Pakistan.
- The base case which includes only diesel is the normal trend in Pakistan which demonstrates the least

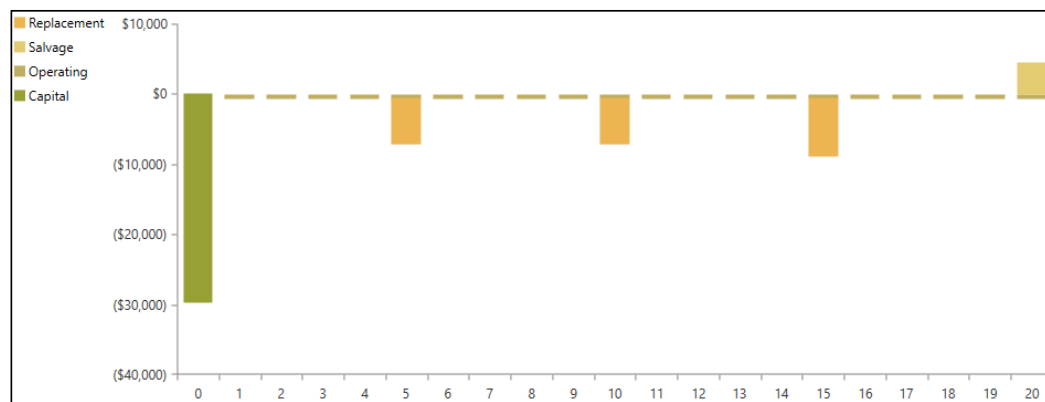
prioritized case scenario in this work with the highest TNPC (\$ 258,845), LCOE (\$ 1.69/kWh). O&M cost (\$ 45,685), annual fuel usage (67,440 L/year) and GHG penalty (19,364 kg/year).

Fig. 38 shows the electricity produced and shared between PV and WT. MPPT is applied for extracting maximum power for meeting the load requirement. It is noticed that the generation from PV source is high in July due to maximum radiations while June has next-top value and these observations are also justified in Fig. 34.

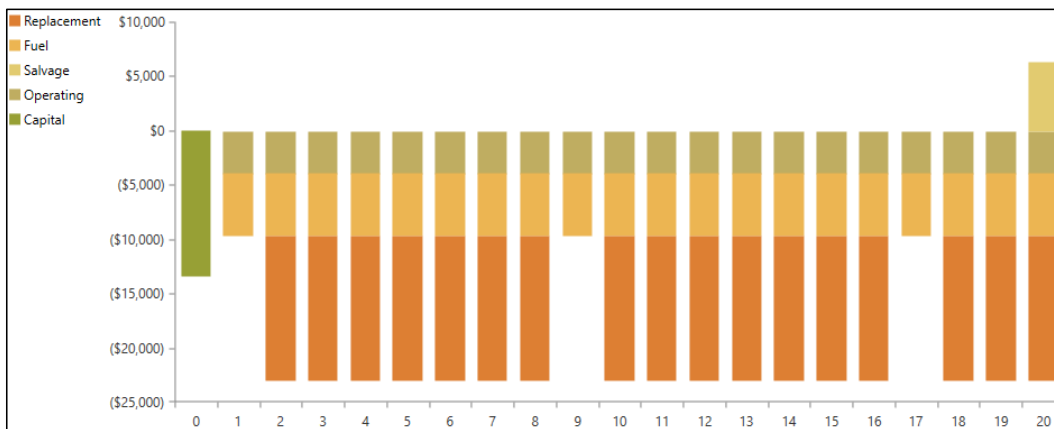
The on-line energy scheduling scheme including generation and load profiles is demonstrated in Fig. 39 for December 15. The critical analysis of Fig. 39 reveals many important prospects for the suggested configuration plan. It is observed that both solar and wind energy generations



(a) The optimized solution set with multiple solutions



(b) Optimal case



(c) Base case

FIGURE 40. Optimized solution set and Nominal cash flow results.

**TABLE 7.** Details of the optimized system.

<i>Comp.</i>	<i>Initial</i>	<i>O&amp;M</i>	<i>Replacement</i>	<i>Salvage</i>	<i>Total</i>
BSS	6,650	3,553.13	11,685.88	0.00	21,889.01
Power Converter	1,787.50	0.00	770.65	388.12	2,170.03
PV	16,887.79	2,467.29	0.00	1,100.06	18,255.03
WT	4,500	584.40	0.00	0.00	5,084.40
System	29,825.29	6,604.82	12,456.53	1,488.18	47,398.46

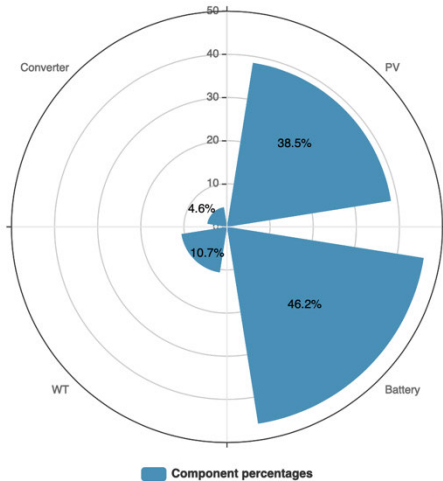


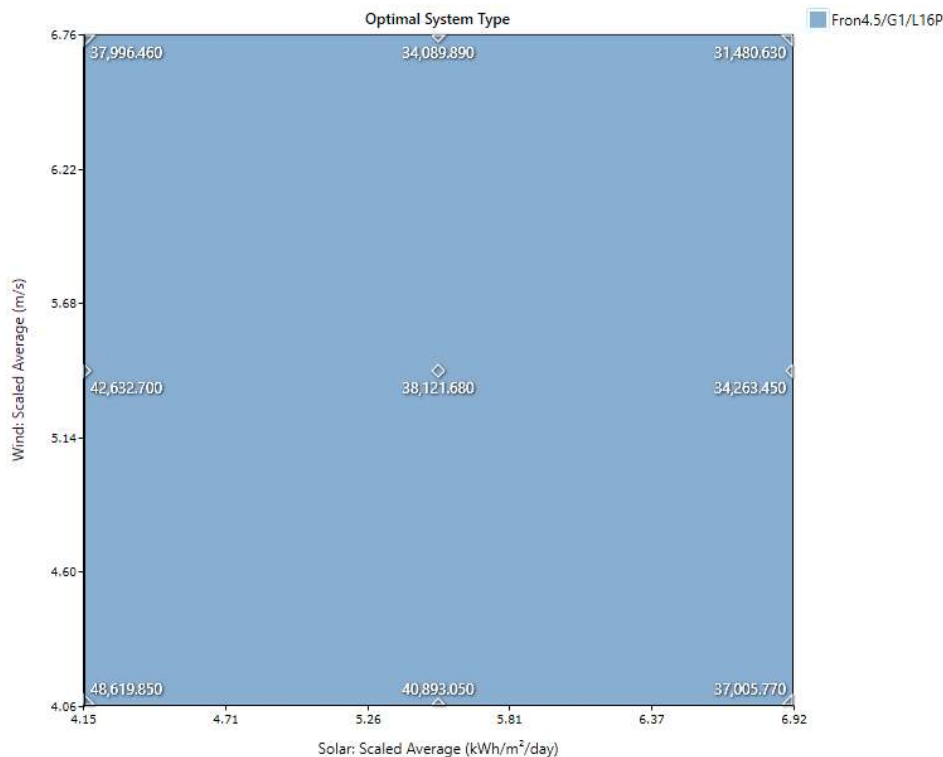
**FIGURE 41.** Component cost as a percentage of the total values for the optimal configuration plan.

are available from 0800 onward and are not available after 1700. During these nine hours, solar power is more than the wind power and all the load is supplied by renewable

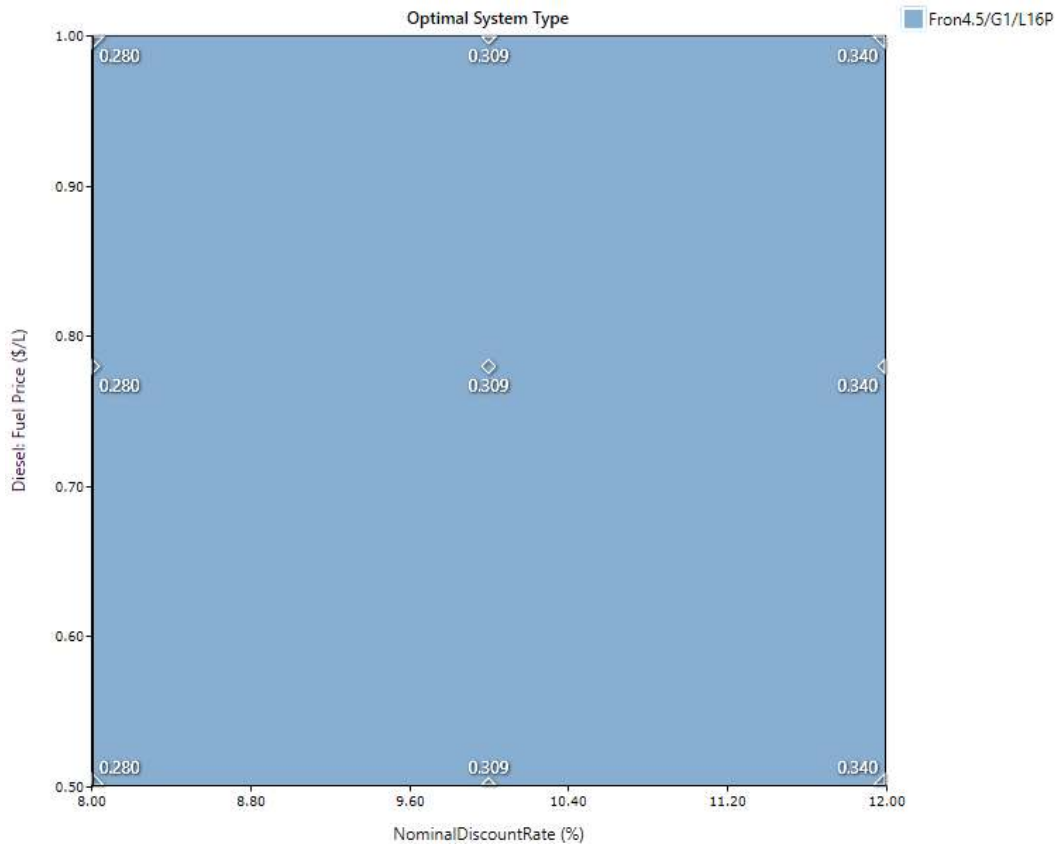
generation. Moreover, excess energy is also used to charge the battery units. During this time, the battery remains in idle state and hence the life of the battery is improved. Due to the non-availability of PV and wind energy before 0800 and after 1700, all the load is supplied by the battery storage units. In this way, the optimized operation of the HRES components is ensured with proper dispatch and management strategy.

Table 7 concludes the costs of the component of the proposed configuration plan. The PV initial cost is about four times the initial cost of WT. And BSS has 1.5 times cost as compared to wind. The O&M cost of the BSS is slightly higher than that of PV, and it is six times greater as compared to wind. Based on the total cost, PV and BSS have almost the same values while wind has three times lower cost than that of PV and four times lower cost than BSS.

Fig. 40 shows the optimal solution set and the cash flow summary of two cases viz. base case (DG only) and the optimized HRES (PV-WT-BSS) for a 20 years plan. The optimal system maintains minimum cash flow during the entire lifetime of the project, whereas the cash flow for the base



**FIGURE 42.** Sensitivity analysis by varying solar radiation and wind speed at constant values of fuel price (\$1.0/Ltr), nominal discount rate (8%), and scaled average load (26.96 kWh/day).



**FIGURE 43.** Sensitivity analysis with variable nominal discount and fuel cost at constant values of wind speed (5.41, PV radiation (5.54), and scaled load (35.94).

**TABLE 8.** Electricity production/consumption (kWh/yr) of the optimal configuration plan.

PV	35,654	87.5%	Electrical load	13,109	100
WT	5,115	12.5%	Excess energy	26,034	63.9
DG	0	0%	Unmet load	9.45	0.0721
Total	40,770	100%	Energy Shortage	13.1	0.0997

case keeps on attaining the higher values until it touches the highest scales in the end. Fig 41 shows the costs in percentage for each component of an optimal system.

### 1) SENSITIVITY ANALYSIS

Table 11 shows the sensitivity parameters which are used for the comprehensive analysis and impact of important factors on different costs and emissions. Fig. 42 shows the TNPC by varying solar irradiance and wind speed while other parameters are kept constant. It is observed that TNPC has a direct relationship with wind speed and solar irradiance for the selected area. An increase in either of the two parameters will reduce the TNPC. Fig. 43 shows the impact on LCOE with the variations of nominal discount rate and fuel price while keeping another parameter constant. LCOE is reduced with a low discount rate while diesel fuel

has no impact due to the case when DG is not present. Fig. 44 shows the impact on TNPC with the variations of load and fuel price. There is the pivotal value of loading i.e. 35.94 kWh/d where the optimal configuration plan is changed from 100 % renewables (Case-7) to diesel-based HRES system (Case-8). Therefore, it is important to mention here that the load will decide whether a 100 % renewables system is possible for the selected location or not. In this study, 100 % renewables are only possible up to 35.94 kWh daily load. While DG needs to be incorporated above this specified load. It means that the present study is conducted for two households while the system can be extended for more households while keeping the DG part of the MG system.

Table 12 shows the impact of different parameters on the system performance in terms of techno-economic and environmental context. The discount rate has a minor impact on

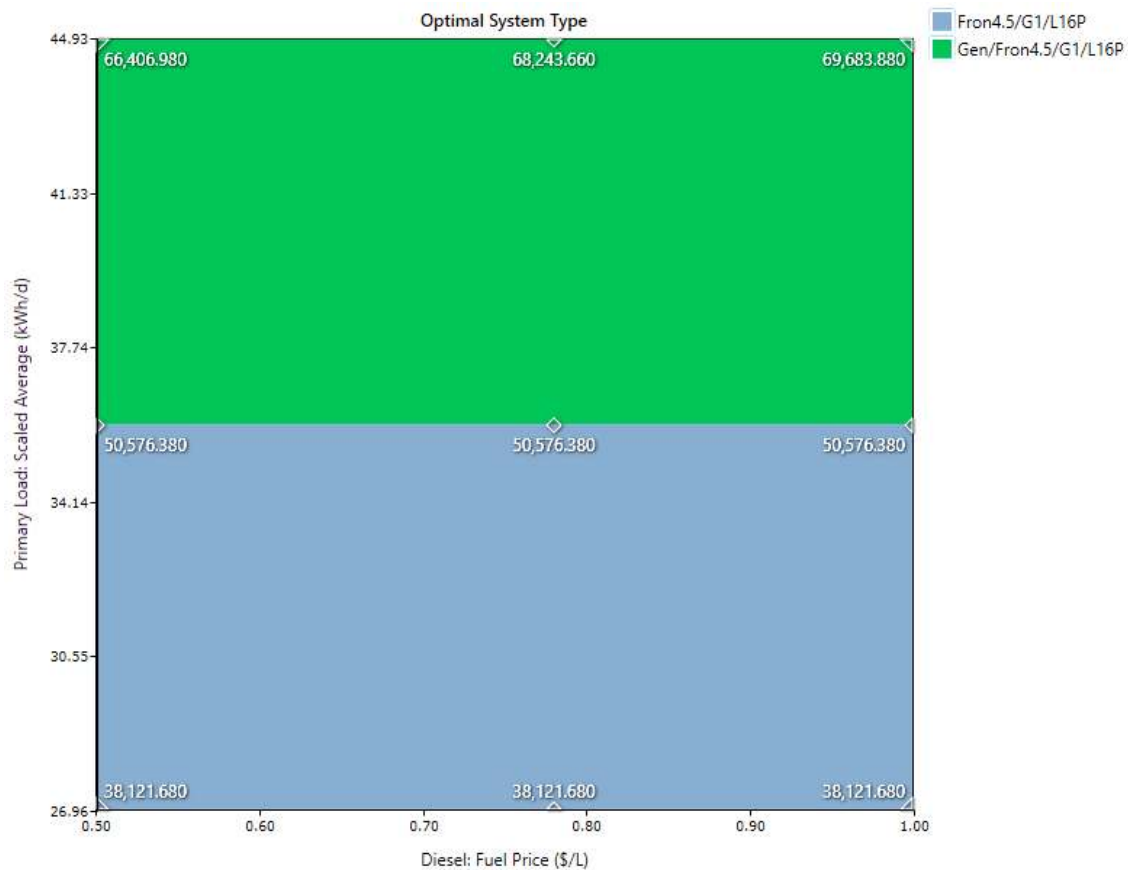


**FIGURE 44.** Sensitivity analysis by varying diesel fuel price and scaled average load at constant values of wind speed (5.41 m/s), solar radiation (5.54 kWh/m<sup>2</sup>/day), and nominal discount rate (8 %).

**TABLE 9.** All possible configuration models with ranking in terms of NPC.

Ranking	Case	HRES Plan	TNPC (\$)	LCOE (\$/kWh)	ROI (%)	RF (%)	Fuel (L/yr)	DG Opr. (hr/yr)	GHG (kg/yr)	Cost COE&NPC (%)	Reduction, (%)
1	7	PV-WT- Battery-Converter	47,398.46	0.309	112.6	100	0	0	0	81.7	
2	8	PV-WT-DG-Battery-Converter	50,450	0.329	87.9	93.8	371	463	971	80.5	
3	4	PV-DG-Battery-Converter	54,808	0.357	80.5	93.6	389	493	1,019	78.9	
4	5	WT-DG-Battery-Converter	97,663	0.637	39.5	85.9	825	999	2,159	62.3	
5	6	PV-WT-DG-Converter	151,134	0.986	30.6	45.9	3,136	3,767	8,209	41.7	
6	2	PV-DG-Converter	179,433	1.170	42.7	19.6	4,572	5,362	11,968	30.8	
7	3	WT-DG-Converter	198,738	1.30	21.1	21.1	4,614	5,609	12,078	23.1	
8	1	DG-Battery-Converter	216,040	1.41	164.5	0.0	5,945	7,077	15,561	16.6	
9	9	DG (base case)	258,845	1.69	0.0	0.0	7,398	8,760	19,364	0.0	

PV sizes while WT size is reduced from six to four units as the discount rate increases while battery size increases two units. TNPC is reduced while LCOE is increased with an increase in discount. Initial capital cost remains almost the same while

O&M cost is reduced to about 75 %. Variations of solar irradiance have more impact on PV sizes while battery units remain the same. TNPC and LCOE are reduced significantly with the increase in solar irradiance. During the variation

TABLE 10. All possible configuration models with results in terms of optimal design.

Case	Component sizing					Cost results				
	PV (kW)	WT (Qty)	DG (kW)	Converter (kW)	BSS (Qty)	Initial (\$)	O&M (\$/yr)	Replacement (\$)	Fuel (\$)	Salvage (\$)
1	-	-	6.70	1.62	10	15,636.91	37,824.06	112,183.32	54,193.97	3,797.95
2	20.2	-	6.70	3.56	-	30,602.08	30,348.40	79,286.38	41,683.49	2,487.53
3	-	30	6.70	5.50	-	42,050.00	32,683.77	85,711.77	42,063.68	3,771.17
4	19.7	-	6.70	5.97	28	35,874.87	7,478.76	9,382.69	3,549.41	1,478.09
5	-	29	6.70	5.94	56	51,083.44	13,824.12	25,633.26	7,517.76	395.97
6	16.4	21	6.70	5.51	-	47,061.76	23,988.11	54,740.95	28,589.92	3,246.45
7	21.1	5	-	5.96	38	29,825.29	6,604.82	12,456.53	0.00	1,488.18
8	13.5	5	6.70	5.94	22	34,326.07	6,620.78	7,534.14	3,381.98	1,413.13
9	-	-	6.70	-	-	13,400	45,685.76	134,414.00	67,440.42	2,094.88

TABLE 11. Parameters for sensitivity analysis of the optimal configuration plan.

SN	Parameter name	Max/Min Range (%)	Parameter values
1	Wind scaled average speed (m/s)	±25	4.0588, 5.4117, 6.7646
2	Solar scaled average radiation (kWh/m <sup>2</sup> /day)	±25	4.1531, 5.5375, 6.9219
3	Scaled average load (kWh/day)	±25	26.955, 35.94, 44.925
4	Diesel fuel price (\$/Ltr)	+36, -28	0.5, 0.78, 1.0
5	Nominal discount rate (%)	±20	8, 10, 12
6	Minimum SOC (%) with incorporation of temperature effects	-50, -100, -150	20, 30, 40, 50
7	Minimum SOC (%) without incorporation of temperature effects (20.57 °C)	±50, -100, -150, -200, -250	10, 20, 30, 40, 50, 60, 70
8	DOD (%)	±12.5, 25, 37.5, 50, 62.5	90, 80, 70, 60, 50, 40, 30
9	Battery string size (units)	-150, -300, -450, -600	2, 5, 8, 11, 14
10	Capital cost of PV (% of initial cost)	100, 50, 25	800, 400, 200
11	Capital cost of WT (% of initial cost)	100, 50, 25	900, 450, 225
12	Capital cost of battery (% of initial cost)	100, 50, 25	175, 87.5, 43.75
13	Inflation rate (%)	±50	2, 4, 6
14	Load variations (kWh/day)	86, 72, 58, 44, 30, 17, -11, -25	5, 10, 15, 20, 25, 30, 35.94, 40, 45
15	CO <sub>2</sub> emission (kg/year)	95, 90, 80, 69, 59, 49, 39, 28, 18, 8, -53, -156, -258, -360, -462, -565, -667	50, 100, 200, 300, 400, 500, 600, 700, 800, 900, 1500, 2500, 3500, 4500, 5500, 6500, 7500
16	LLP (%)	±100, -300, -500, -800, -1100	0, 0.1, 0.2, 0.4, 0.6, 0.9, 1.2
17	Incorporation of temperature effects	51, -46, -95	10, 20.57, 30, 40

of load, PV and WT sizes and TNPC reduced significantly with a decrease in load while LCOE increases. High wind speed reduced the PV and battery sizes as well as TNPC and LCOE while WT size remains almost the same. Variations of diesel price have no significant impact on PV and WT sizes while battery size is reduced significantly with the increase of TNPC and LCOE. The impact of SOC with the incorporation of temperature effects is interesting. With the increase in temperature, while keeping the value of SOC same, there is

no major change in PV, while a minor decrease in WT sizes and a minor increase in battery sizes are observed. TNPC and LCOE are increased with an increase in temperature. During SOC variation from 10 % to 70 %, while keeping the temperature constant, PV size remains almost the same till 50 % SOC while it is reduced drastically with the increase of 20 % SOC. TNPC and LCOE are increased and directly proportional to the SOC while DOD has the opposite relation as compared to SOC. Battery string sizes have a major impact



**TABLE 12. Sensitivity analysis with a variation of different sensitivity parameters for optimal configuration plan with 100% RF and no emission.**

Parameter value	PV (kW)	WT (Qty)	DG (kW)	BSS (Qty)	Converter (kW)	NPC (\$/kWh)	COE (\$)	Initial capital (\$)	O&M (\$/yr.)
Discount rate (%)									
8	21.7	6	-	36	5.92	50,576	0.280	30,858	7,788
10 (initila value)	21.1	5	-	38	5.96	47,398	0.309	29,825	6,604
12	22	4	-	38	5.98	44,778	0.340	29,644	5,666
Scaled solar average radiation (kWh/m <sup>2</sup> /day)									
4.15	22.0	15	-	38	5.87	58,304	0.380	39,510	7,877
4.15 (Case-8)	15.7	6	8.3	22	5.96	57,049	0.372	40,229	7,375
5.54	21.1	5	-	38	5.96	47,398	0.309	29,825	6,604
6.92	17.1	4	-	38	5.83	42,899	0.280	25,709	6,023
Scaled average load (kWh/day)									
27.0	16.8	3	-	28	5.25	35,632	0.310	22,626	4,933
35.9	21.1	5	-	38	5.96	47,398	0.309	29,825	6,604
44.9 (Case-8)	17.0	6	8.3	30	5.99	64,666	0.337	42,652	8,727
Scaled average wind speed (m/s)									
4.06	21.9	9	-	42	5.74	54,412	0.355	34,727	7,543
5.41 (initila value)	21.1	5	-	38	5.96	47,398	0.309	29,825	6,604
6.76	15.4	8	-	34	5.94	43,236	0.282	27,285	5,918
Diesel fuel price (\$/Ltr)									
0.50	21.1	5	-	38	5.96	47,398	0.309	29,825	6,604
0.50 (Case-8)	13.0	5	8.3	22	5.94	51,779	0.338	37,138	6,802
0.78 (initila value)	21.1	5	-	38	5.96	47,398	0.309	29,825	6,604
0.78 (Case-8)	13.9	5	8.3	22	5.98	53,012	0.346	37,903	6,694
1.00	21.1	5	-	38	5.96	47,398	0.309	29,825	6,604
1.00 (Case-8)	13.9	5	8.3	24	5.96	53,931	0.352	38,246	6,618
Minimum SOC (%) with the incorporation of temperature effects									
20.57 °C									
20 (initial vlaue)	21.1	5	-	38	5.96	47,398	0.309	29,825	6,604
30	20.9	4	-	42	5.86	48,509	0.317	29,466	6,842
40	22.0	5	-	40	5.94	49,313	0.322	30,881	6,895
50	21.9	7	-	40	5.90	51,252	0.334	32,595	7,118
10 °C									
20	20.8	5	-	38	5.96	47,137	0.308	29,583	6,569
30	21.5	4	-	40	5.93	47,850	0.312	29,569	6,718
40	21.5	4	-	42	5.87	49,029	0.320	29,946	6,912
50	21.5	7	-	40	5.87	50,927	0.332	32,296	7,076
30 °C									
20	21.3	4	-	40	5.90	47,716	0.311	29,446	6,702
30	21.2	5	-	40	5.98	48,649	0.318	30,265	6,804
40	21.8	6	-	40	5.81	50,086	0.327	31,560	6,985
50	21.8	5	-	44	5.98	51,423	0.336	31,401	7,241
40 °C									
20	20.9	4	-	42	5.89	48,521	0.317	29,475	6,842
30	21.7	5	-	40	5.89	49,045	0.320	30,636	6,862
40	21.3	7	-	40	6.00	50,801	0.332	32,174	7,052
50	21.5	6	-	44	5.97	52,241	0.341	32,117	7,331
Minimum SOC (%) without incorporation of temperature effects (20.57 °C)									
10	21.4	4	-	38	5.89	46,584	0.304	29,115	6,519
20 (initial vlaue)	21.1	5	-	38	5.96	47,398	0.309	29,825	6,604
30	20.9	4	-	42	5.86	48,509	0.317	29,466	6,842
40	22.0	5	-	40	5.94	49,313	0.322	30,881	6,895
50	21.9	7	-	40	5.90	51,252	0.334	32,595	7,118
60	15.4	4	-	26	5.53	53,421	0.348	35,543	7,148
70	15.9	3	-	34	5.46	56,702	0.370	36,391	7,667

**TABLE 12. (Continued.) Sensitivity analysis with a variation of different sensitivity parameters for optimal configuration plan with 100% RF and no emission.**

DOD (%)									
90	21.4	4	-	38	5.89	46,584	0.304	29,115	6,519
80 (initial vlaue)	21.1	5	-	38	5.96	47,398	0.309	29,825	6,604
70	20.9	4	-	42	5.86	48,509	0.317	29,466	6,842
60	22.0	5	-	40	5.94	49,313	0.322	30,881	6,895
50	21.9	7	-	40	5.90	51,252	0.334	32,595	7,118
40	15.4	4	-	26	5.53	53,421	0.348	35,543	7,148
30	15.9	3	-	34	5.46	56,702	0.370	36,391	7,667
Battery string size (units)									
2 (initial value)	21.1	5	-	38	5.96	47,398	0.309	29,825	6,604
5	20.9	4	-	40	6.00	47,348	0.309	29,102	6,647
8	20.9	4	-	40	5.96	47,376	0.309	29,129	6,653
11	19.6	4	-	44	5.91	48,500	0.317	28,740	6,870
14	20.2	4	-	42	5.90	47,848	0.312	28,853	6,751
The capital cost of PV (% of the initial cost)									
100% (initila value)	21.1	5	-	38	5.96	47,398	0.309	29,825	6,604
50%	21.7	6	-	36	5.96	39,100	0.255	22,173	6,605
25%	21.8	6	-	36	5.85	34,746	0.227	17,819	6,617
The capital cost of WT (% of the initial cost)									
100% (initila value)	21.1	5	-	38	5.96	47,398	0.309	29,825	6,604
50%	19.8	11	-	34	5.93	45,083	0.294	28,501	6,776
25%	15.7	24	-	32	5.94	42,342	0.276	25,309	7,627
The capital cost of the battery (% of the initial cost)									
100% (initila value)	21.1	5	-	38	5.96	47,398	0.309	29,825	6,604
50%	22.0	4	-	38	5.99	43,840	0.286	26,324	6,591
25%	22.0	4	-	38	6.00	42,179	0.275	24,663	6,591
Inflation rate (%)									
2%	22.0	4	-	38	5.98	44,610	0.343	29,644	5,602
4% (initila value)	21.1	5	-	38	5.96	47,398	0.309	29,825	6,604
6%	21.7	6	-	36	5.92	50,693	0.279	30,858	7,838

**TABLE 13. Impact of load variations on different parameters.**

Load variations (kWh/day)	ASC (US\$)		COE (\$/kWh)		LLP (%)		CO <sub>2</sub> emission (kg/year)		Renewable penetration, RF (%)		ROI (%)	
	7	8	7	8	7	8	7	8	7	8	7	8
Study Cases	7	8	7	8	7	8	7	8	7	8	7	8
5	7,346	18,325	0.345	0.859	0.096	0	0	91	100	95.9	58.3	0.8
10	15,342	24,269	0.360	0.569	0.003	0	0	146	100	96.7	5.6	0.5
15	19,763	29,720	0.309	0.464	0.100	0	0	287	100	95.6	1636	0.0
20	28,488	35,242	0.334	0.413	0.096	0	0	509	100	94.2	831.9	204.1
25	32,832	40,774	0.308	0.382	0.098	0	0	641	100	94.1	606.2	159.8
30	39,406	46,436	0.308	0.363	0.096	0	0	709	100	94.6	302.4	130.9
35.94 (initial value)	47398	53,173	0.309	0.347	0.100	0	0	978	100	93.7	180.5	110.9
40	-	57,953	-	0.340	-	0	-0	1070	-	93.8	-	99.7
45	-	64,904	-	0.338	-	-	-	-	-	93.4	-	-

on PV, wind and battery sizes while TNPC is increased slightly with the increase of LCOE. PV capital cost has no impact on PV size while TNPC is reduced and LCOE is increased with a 75 % reduction in PV capital cost. The same but more significant impact on TNPC and LCOE is observed during wind capital cost. By reducing wind capital costs up to 75 %, the PV and battery sizes are reduced significantly while WT units are increased in a significant number. The capital cost of battery banks has no major impact on PV and WT sizes while a drastic reduction in TNPC and LCOE

is observed. Therefore, storage cost has a major impact on the overall system cost. More efficient and low-cost storage systems will help to develop the models of HRES in a cost-effective manner. The inflation rate has a direct impact on TNPC while indirectly proportional to the LCOE.

Table 13 shows the effect of load perturbation on different parameters for the two cases when DG is available for one case. without DG i.e., case-7, the highest value of ROI is found when a load is decreased to about half of the main value i.e. 15 kWh/d with no emission while LLP is the same as the

**TABLE 14. Impact of load variations on components sizing.**

Load (kWh/day)	PV size (kW)		WT size (units)		DG sizing (kW)		BSS size (units)		Power converter sizing (kW)	
	7	8	7	8	7	8	7	8	7	8
Study Cases										
5	4.28	2.76	1	1	-	8.40	4	4	0.880	0.946
10	9.17	4.73	1	2	-	8.40	10	8	1.75	1.88
15	8.79	6.33	2	2	-	8.40	16	12	2.51	2.71
20	18.3	7.20	1	3	-	8.40	18	14	3.46	3.51
25	15.4	10.3	3	3	-	8.40	26	16	4.15	4.41
30	18.6	11.8	3	4	-	8.40	32	20	5.09	5.29
35.94 (initial value)	21.1	13.7	5	5	-	8.40	38	22	5.96	6.00
40	-	15.4	-	5	-	8.40	-	26	-	5.98
45	-	18.3	-	6	-	8.40	-	28	-	6.00

**TABLE 15. Impact of load variations on different costs.**

Load variations (kWh/day)	Capt. (US\$)		O&M (US\$)		Repl. (US\$)		Fuel (US\$)		Optimal Case
	7	8	7	8	7	8	7	8	
Study Cases									
5	5,291	20,893	992	1,046	1344	1352	0	316	PV-WT-bat (case-7)
10	10,508	24,352	2,123	1,911	3,302	2,703	0	509	PV-bat (case-10)
15	12,383	26,576	2,757	2,834	5,245	4,041	0	1000	PV-WT-bat (case-7)
20	19,745	28,764	3,941	3,810	5,983	4,760	0	1773	PV-WT-bat (case-7)
25	20,792	31,871	4,578	4,698	8,532	5,490	0	2,231	PV-WT-bat (case-7)
30	24,692	34,964	5,515	5,538	10,499	6,834	0	2,470	PV-WT-bat (case-7)
35.94 (initial value)	29,825	37,871	6,605	6,728	12,457	7,542	0	3,405	PV-WT-bat (case-7)
40**	-	39,999	-	7,539	-	8,770	-	3,727	PV-WT-DG-bat (case-8)
45**	-	43,578	-	8,728	-	14,895	-	4,489	PV-WT-DG-bat (case-8)

\*\*no optimal PV-WT-bat configuration is found.

**TABLE 16. Impact of emission on different costs.**

CO <sub>2</sub> emission (kg/year)	Capt.	Repl.	O&M	Fuel	ASC	COE (\$/kWh)	Renewable penetration, RF (%)
	(US\$)						
Study Cases-8							
50	42,725	12,462	6,664	164	42,725	0.367	99.7
100	42,312	11,847	6,582	342	55,685	0.363	99.4
200	41,738	10,612	6,497	693	54,503	0.355	98.7
300	40,492	9,999	6,387	1,027	53,445	0.349	98.1
400	38,956	10,002	6,421	1,371	52,740	0.344	97.5
500	38,084	9,387	6,421	1,737	52,099	0.340	96.8
600	37,507	8,767	6,417	2,072	51,692	0.337	96.2
700	36,793	8,152	6,441	2,434	51,218	0.334	95.6
800	35,463	8,156	6,494	2,773	50,703	0.331	94.9
900	34,578	8,150	6,578	3,119	50,735	0.331	94.2
1500	34,326	7,534	6,621	3,382	50,450	0.329	93.8
2500	34,326	7,534	6,621	3,382	50,450	0.329	93.8
3500	34,326	7,534	6,621	3,382	50,450	0.329	93.8
4500	34,326	7,534	6,621	3,382	50,450	0.329	93.8
5500	34,326	7,534	6,621	3,382	50,450	0.329	93.8
6500	34,326	7,534	6,621	3,382	50,450	0.329	93.8
7500	34,326	7,534	6,621	3,382	50,450	0.329	93.8

baseload of 35.94 kWh/d. Table 14 shows the effect of load perturbation on components sizes. Table 15 shows the effect of load perturbation on different costs and have a directly proportional relationship. When a load is decreased to about three times i.e. 10 kWh/d, the new case with PV-battery is

found to be more economical without wind and diesel units. When the load is increased beyond the base value, diesel generator becomes part of the HRES. Table 16 shows the effect of emissions on different costs. Table 17 shows the effect of LLP on different costs. TNPC and LCOE are drastically reduced

TABLE 17. Impact of LLP on different costs.

LLP	Capt.		Repl.		O&M		Fuel		ASC		COE		Renewable penetration	
(%)	(US\$)										(\$/kWh)		RF (%)	
Study Cases	7	8	7	8	7	8	7	8	7	8	7	8	7	8
0 (initial value)	29,825	34,326	12,457	7,534	6,605	6,621	0	3,382	47,398	50,450	0.309	0.329	100	93.8
0.1	18,115		6,789		3,730				27,691		0.197			
0.2	14,307		5,362		2,969				21,968		0.171			
0.4	12,244		4,120		2,400				18,186		0.157			
0.6	10,643		2,804		1,938				14,837		0.145			
0.9	8,465		2,140		1,501				11,694		0.130			
1.2	7,696		975		1,124				9,248		0.124			

TABLE 18. Electrical parameters for simulation.

Parameter	Symbol	Value
PV specifications	-	SunPower SPR-305
PV power (upper-limit)	-	16.50 kW
Wind Power (max)	-	4.000 kW
RLC Filter resistance	$R_f$	0.100 $\Omega$
RLC Filter inductance	$L_f$	10.00 mH
RLC Filter capacitance	$C_f$	250.0 $\mu$ F
Load resistance	$R_L$	25.00 $\Omega$ (variable)
Frequency	$f$	50.00 Hz
DC voltage	$V_{dc}$	510.0 V
Grid voltage	$V_{g, RMS}$	110.0 V
DC link capacitor	$C$	2,000 $\mu$ F
Sampling time	$T_s$	33.00 $\mu$ s
PI controller (wind)	$K_p, K_i$	0.0510, 1.0000
PI controller (battery inner loop)	$K_p, K_i$	4.9830, 10.7520
PI controller (battery outer loop)	$K_p, K_i$	0.4490, 1.0650

with the increase of LLP value from initially zero to 1.2 % while the cost reduction is more than half of the base value.

**B. OPERATIONAL INVESTIGATION OF OPTIMIZED MODEL**

An EMS with FCS-MPC based control strategies is applied by considering the load fluctuations and generation perturbations as shown in Fig 45. The PI controllers’ parameters including wind boost and battery buck-boost and the electrical parameters of the suggested model are shown in Table 18. The case studies for the validation of the proposed strategies are discussed one by one as follows.

**1) MPC CASE WITH UPPER SOC**

The impact of external disturbances including generation and load is observed while applying MPC strategy during upper SOC limits. Smooth voltage and current waveforms are obtained as shown in Fig 46. Fig 47 shows that as the SOC crosses the upper limit i.e. 80 %, the load switch-2 operates and the secondary load is incorporated to the model to ensure the extra power absorbed by the load. Fig 48 shows the power-sharing among different components while supplying

the load requirement. The extra power is supplied to the BSS in charging mode while abrupt fluctuations are also handled through the battery storage system.

**2) MPC CASE WITH LOWER SOC**

The impact of external disturbances including generation and load is observed while applying MPC strategy during lower SOC limits. Smooth voltage and current waveforms are obtained as demonstrated in Fig 49. Fig 50 shows that as the SOC crosses the lower limit i.e. 20 %, the load switch-1 operates and the secondary load is linked to the generation to ensure the extra power absorbed by the load. Fig 51 shows the power-sharing among different components while supplying the load demand. The extra power is supplied to the BSS in charging mode while abrupt fluctuations are also handled through the battery storage system.

**3) PI WITH UPPER SOC**

The impact of external disturbances including generation and load is observed while applying PI strategy during upper SOC limits. Irregular with high transients in voltage and current waveforms are observed as demonstrated in Fig 52. Fig 53 shows that as the SOC crosses the upper limit i.e. 80 %, the load switch-2 operates and the secondary load is linked to the model to ensure the extra power absorbed by the load. Fig 54 shows the power-sharing among different components while supplying the load requirement. The extra power is supplied to the BSS in charging mode while abrupt fluctuations are also handled through the battery storage system. Low power and voltage quality are obtained in the case of PI control.

**4) AFE RECTIFIER**

The first operational model is shown in Fig 55 for the implementation of the AFE rectifier to feed the dc load from the ac supply which can be ac generation from distributed energy resources or from the ac grid.

A constant dc load with fixed resistance is applied for the performance of the AFE in rectification mode. The FCS-MPC based control of AFE rectifier tracks the reference value of dc bus voltage at 510 V. The constant three-phase ac voltage is depicted while the three-phase ac source current shows some

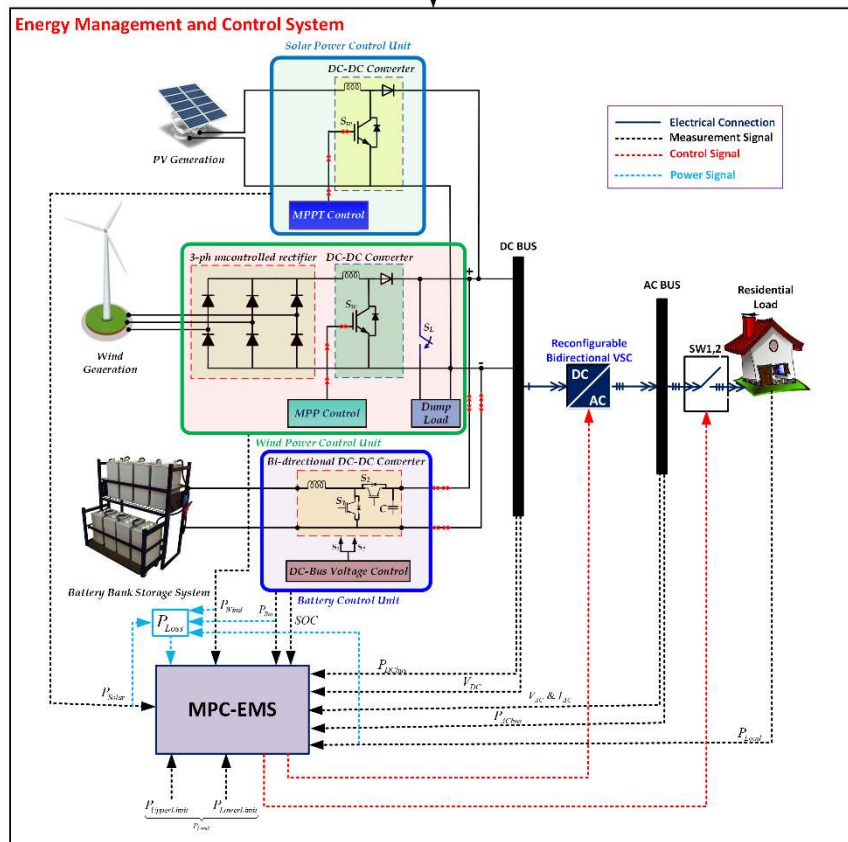
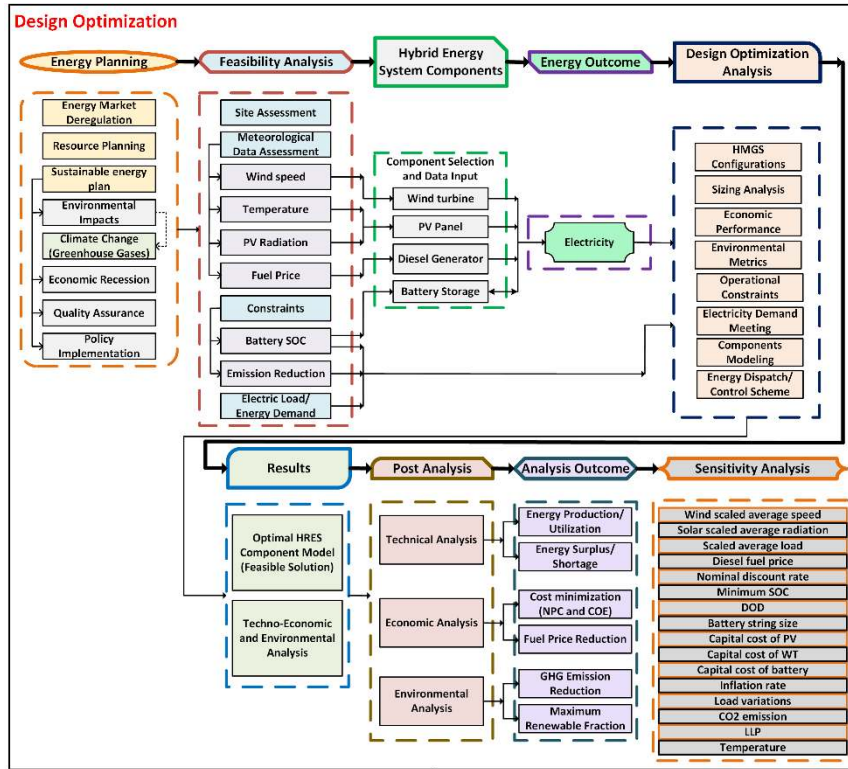


FIGURE 45. The applied to control and management strategy for an optimized model.

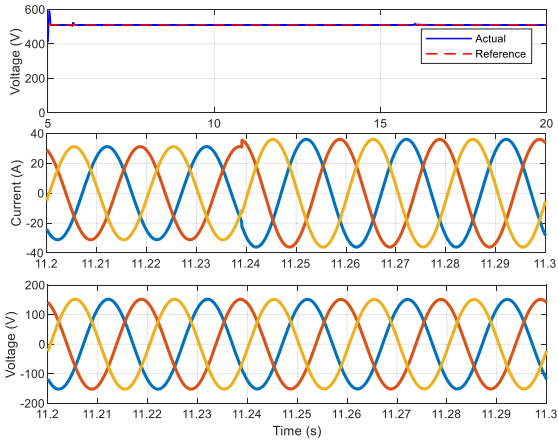


FIGURE 46. The voltages of dc and ac buses and load current during the MPC scheme.

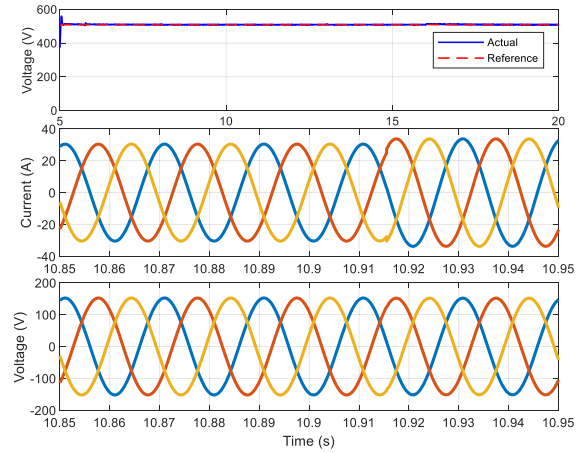


FIGURE 49. The buses voltages and load current with the MPC scheme.

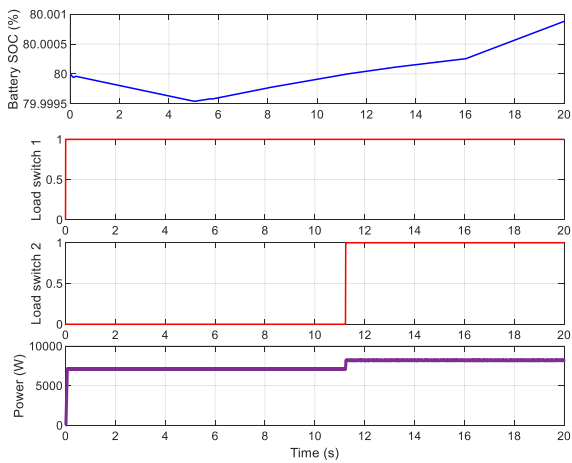


FIGURE 47. Battery SOC, switching signals and load power (MPC).

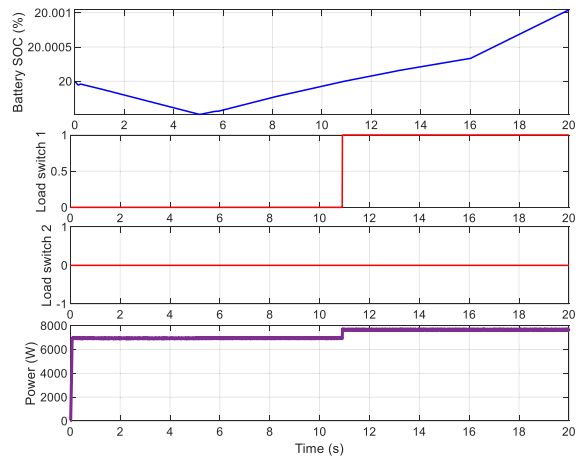


FIGURE 50. Battery SOC, switching signals and load power (MPC).

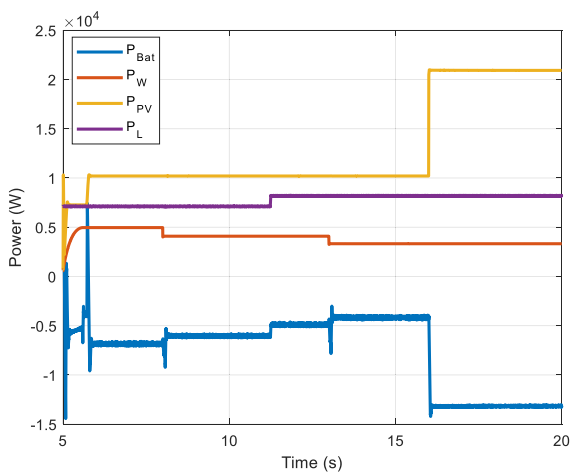


FIGURE 48. Power-sharing among HRES components (MPC).

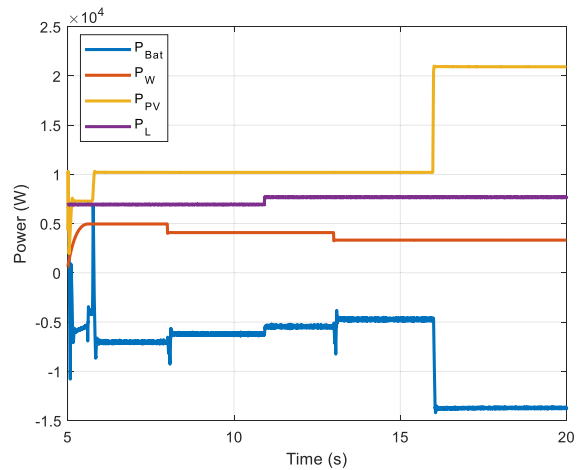


FIGURE 51. Power-sharing among HRES components (MPC).

high magnitude transients during the initial 30 ms due to the rise time for the real dc voltage to track the reference dc voltage through the FCS-MPC control. The reactive power is

zero while the real power of 5.3 kW is fed through the rectifier to the dc load.

A dc bus voltage changed from 510 V to 400 V at 0.5 s to check the performance of the suggested AFE rectifier.

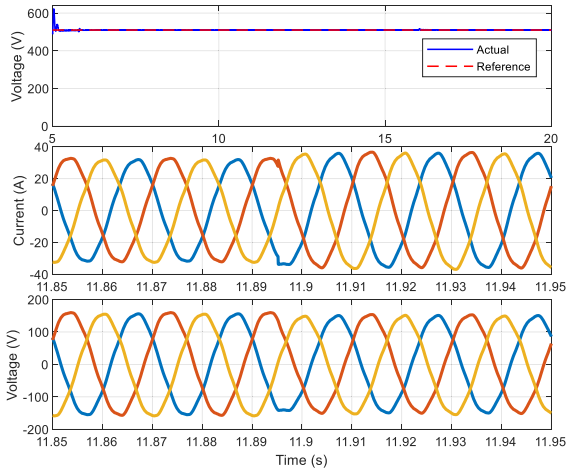


FIGURE 52. The buses voltages and load current with the PI scheme.

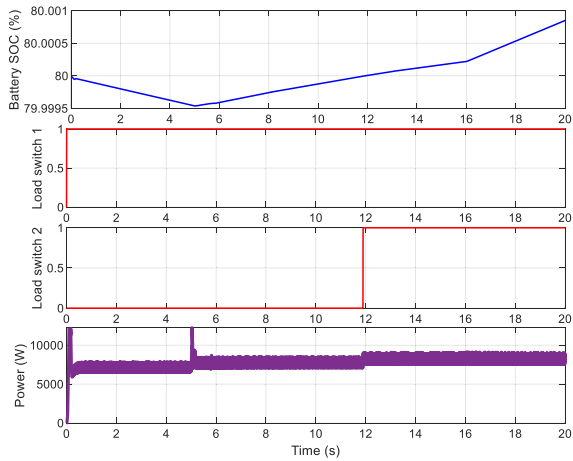


FIGURE 53. Battery SOC, switching signals and load power (PI).

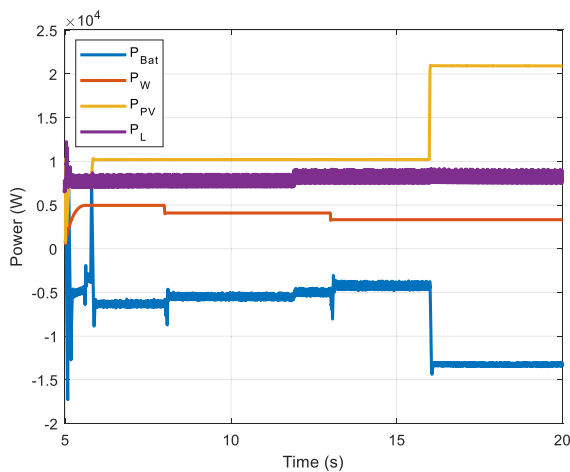


FIGURE 54. Power-sharing among HRES components (PI).

Fig 56 shows that the controller is exactly tracking the reference voltage. A 27.5 % reduction in dc voltage reduces the three-phase ac current to 37.5 %, while the active power

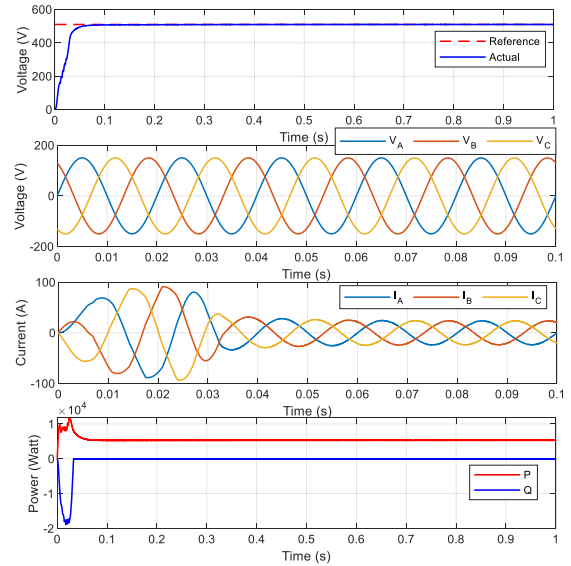


FIGURE 55. Performance analysis of AFE rectifier.

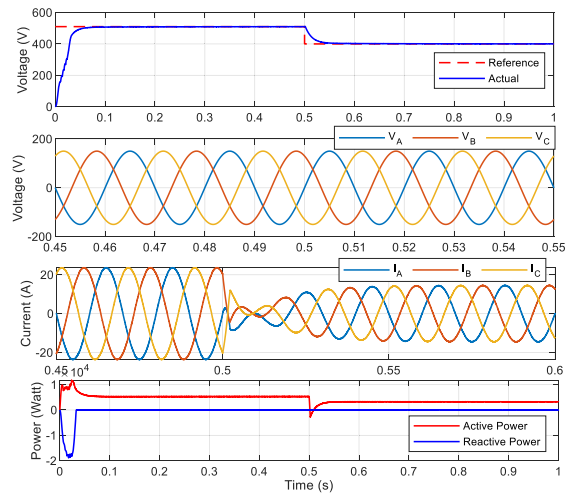


FIGURE 56. Performance analysis of AFE rectifier.

is reduced to 38.7 % (3.25 kW). the reactive power (Q) remained zero.

dc load resistance is changed from 50 to 75 ohms at 0.5 s to the controller performance for regulating the dc bus voltage. During the abrupt change in dc load, a 3.5 % change in the dc voltage (i.e. 328 V) is observed as shown in Fig 57 while the controller is tracking the dc reference voltage after the abrupt load variation. The 33.3 % reduction in three-phase ac current while real power is reduced from 5.3 kW to 3.5 kW.

The dc voltage is kept constant while the active power of dc load is changed from 2 kW to 3.5 kW as shown in Fig 58.

#### 5) GRID-CONNECTED VSI FOR DPC

The second case study includes the grid-connected operation of the VSC in grid-feeding mode. The DC constant voltage

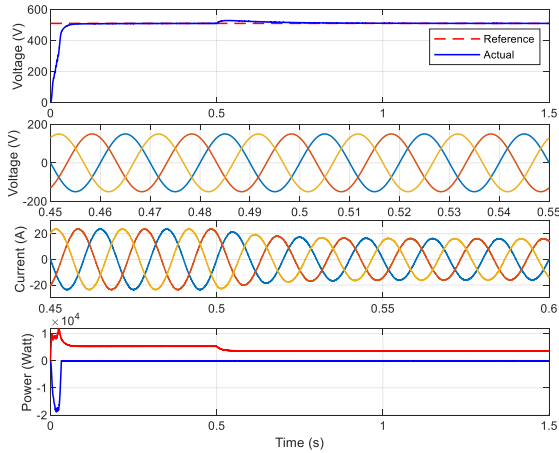


FIGURE 57. Performance analysis of AFE rectifier.

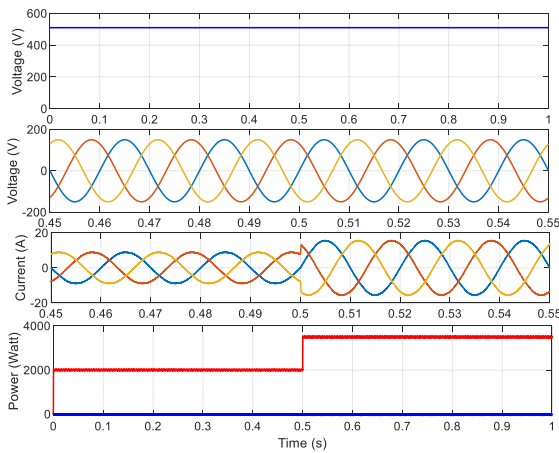


FIGURE 58. Performance analysis of AFE rectifier.

source of 510 V is connected to the DC side while the AC output is connected to the grid as shown in Fig 59.

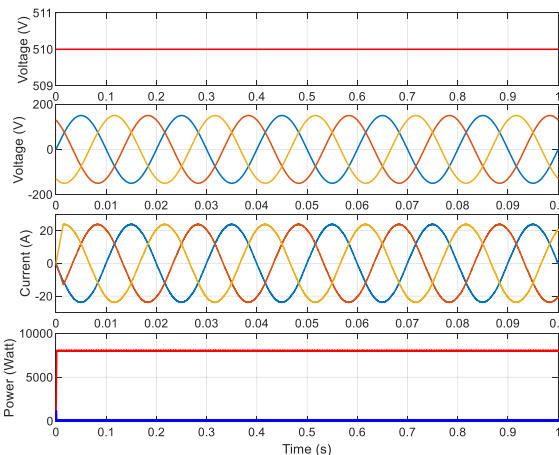


FIGURE 59. Performance analysis of grid-connected VSI.

The DC voltage is fixed at 510 V while the AC active power is fixed at 8 kW as shown in Fig 15. The reactive power (Q) in

this case is taken as zero. It can be observed that the constant voltage and current set by the infinity bus (i.e. utility grid) is not disturbed while the direct power transfer from DC source to the AC grid is carried out.

A DC bus voltage is fixed at 510 V while the active power flow is varied from 8 kW to 12 kW at 0.5 s by keeping the reactive power fixed at zero as shown in Fig 60. Constant three-phase AC voltage is observed while variation in three-phase AC load due to the variation in active power validate the proposed strategy of reconfigurable microgrid after direct power flow control from DC source to AC grid.

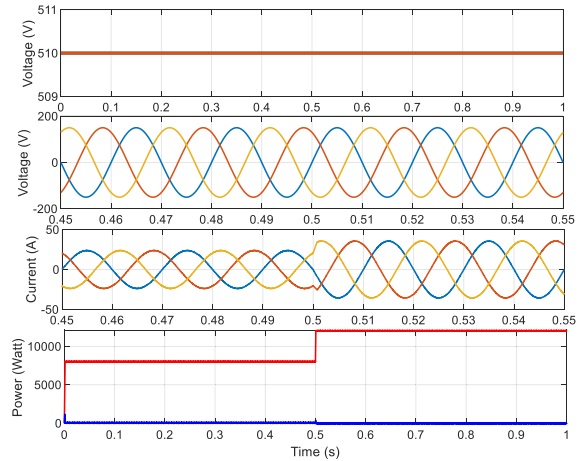


FIGURE 60. Performance analysis of grid-connected VSI.

The DC bus voltage remained constant at 510 V while both active and reactive powers are changed from 8 kW to 12 kW and 0 kW to 5 kW respectively as shown in Fig 61. Constant three-phase AC voltage while the variation in magnitude of three-phase AC current is more due to the reason that the reactive power transfer of 5 kW is also included in this case.

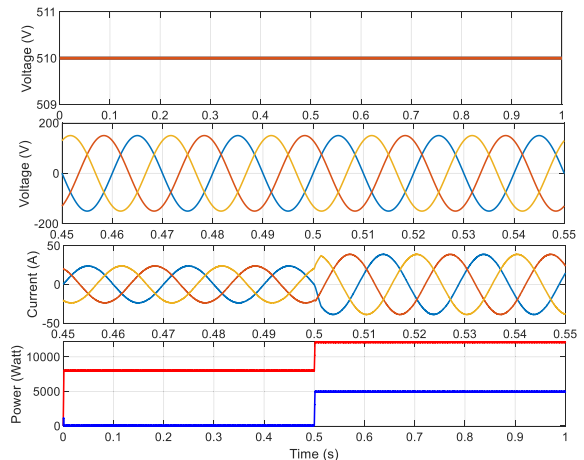


FIGURE 61. Performance analysis of grid-connected VSI.

The unbalanced three-phase load with each phase resistance of 40, 200 and 7500 ohms respectively is taken. The DC voltage is again fixed at 510 V while the active power is set to



8 kW (see Fig 62) with zero reactive power. The three-phase AC voltage and the unbalanced load can be seen from three-phase unbalanced AC current. The active power of 8 kW is successfully supplied to the grid in a reconfigurable fashion.

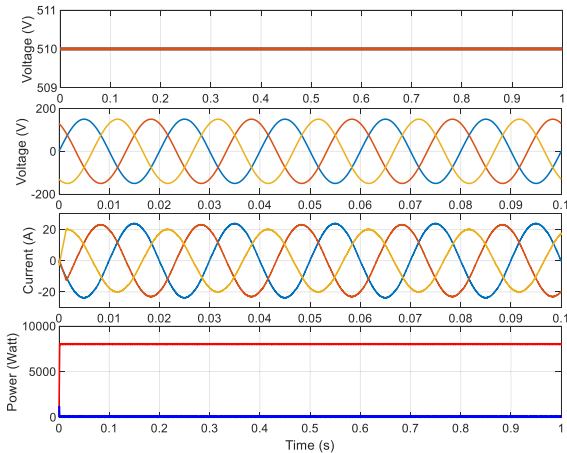


FIGURE 62. Performance analysis of grid-connected VSI.

6) ISLANDED VSI FOR VOLTAGE REGULATION

The third case study includes the standalone microgrid configuration to control the voltage magnitude and its frequency in grid-forming mode and voltage control-based FCS-MPC (FCS-MPVC) strategy is used in this case.

The three-phase balanced and constant load is taken with zero reactive power at a fixed DC voltage of 510 V. The regulated voltage is demonstrated in Fig 63 and the load current. The three-phase AC active power of 3 kW is fed to the load.

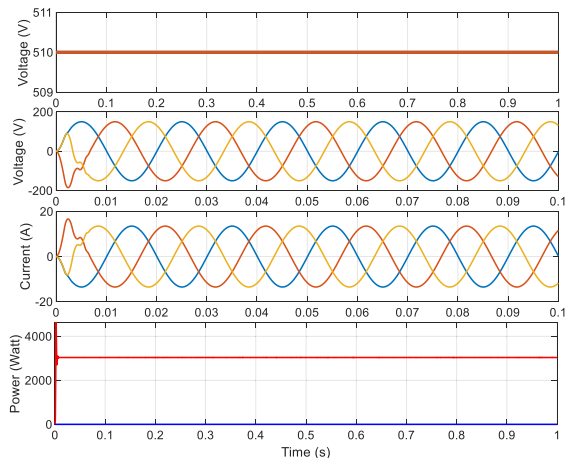


FIGURE 63. Performance analysis of islanded VSI.

The three-phase load is varied from 20 ohms to 10 ohms at 0.5 s while the DC source voltage is fixed at 510 V. The real power is changed from 1.69 kW to 3.37 kW at 0.5 s while the imaginary power is zero. Fig 64 shows the three-phase load voltage which is regulated by the FCS-MPC control strategy.

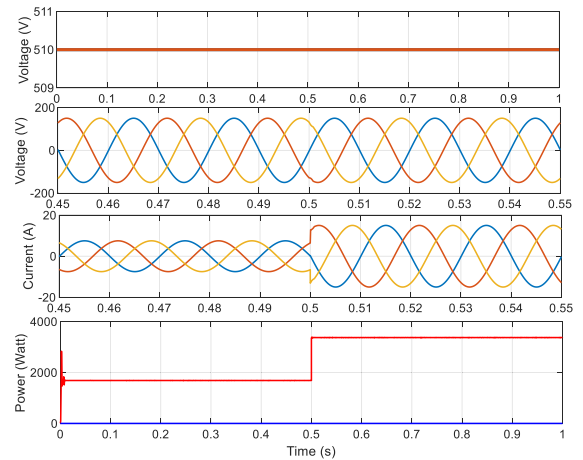


FIGURE 64. Performance analysis of islanded VSI.

Three-phase current is changed from 7.5 A to 15 A during the load variation at 0.5 s.

The linear load of 20 ohms is changed to a non-linear load of 25 ohms at 0.5 s as shown in Fig 65 while maintaining the constant voltage with the variations of active and reactive power.

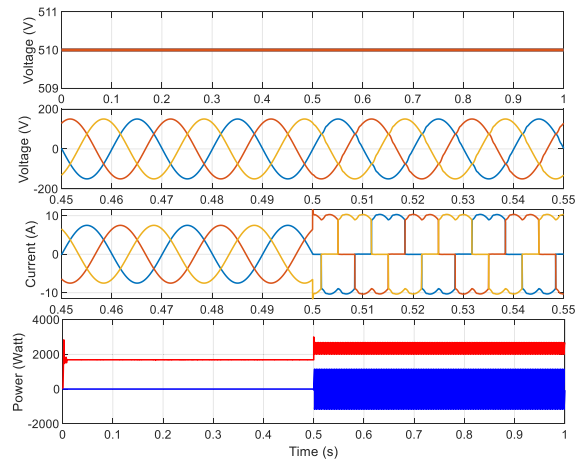


FIGURE 65. Performance analysis of islanded VSI.

7) INVERTER RECONFIGURATION FROM GRID-DISCONNECTED MODE TO GRID-TIED MODE

A seamless transformation from grid-isolated to grid-connected mode is implemented. Fig 66 shows the regulated DC voltage during the operation of the AFE rectifier in rectification mode. The voltage is tracking the reference value without any transient in voltage magnitude. The transformation from rectification to grid-tied mode is accomplished at 0.5 s while the three-phase voltage remained purely sinusoidal. The seamless transformation from grid-tied to grid-isolated mode is implemented at 1s where the zoomed view of voltage shows the magnitude variations of voltage phases for a short time while maintaining the voltage magnitude and its

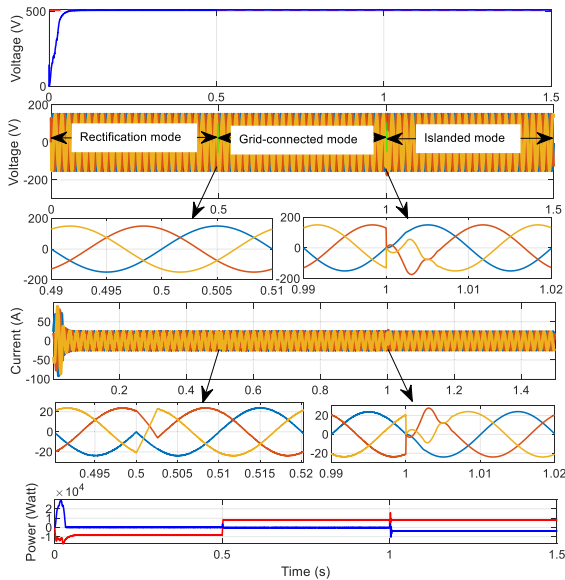


FIGURE 66. Performance analysis from grid-connected to islanded mode.

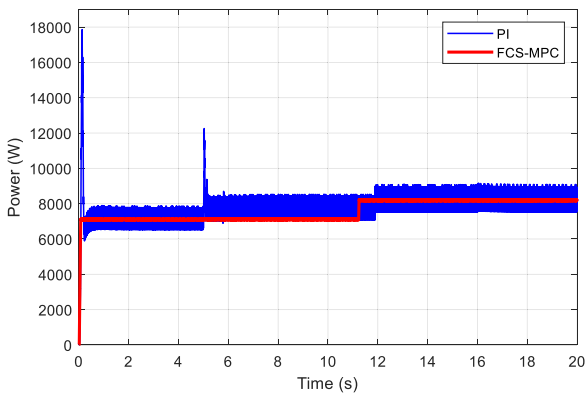


FIGURE 67. Comparison of power oscillations.

frequency at fixed reference peak value. The corresponding three-phase current is shown with the real and imaginary power flow during these transitions. The reactive power is zero during rectification mode while the active power of 8 kW is flowing. During grid-connected mode at 0.5 s, the power flow is opposite while the same active power of 8 kW is flowing to supply the grid. The reactive power is almost zero. During the third seamless transformation from grid-tied to grid-isolated mode at 1 s, the almost same active power of 8 kW is flowing due to the fixed load resistance, while reactive power of 4 kW is flowing to feed the AC load.

8) POWER OSCILLATIONS AND THD COMPARISON OF FCS-MPC WITH CONVENTIONAL CONTROLS

Fig. 67 shows load powers and Tables 19-21 shows the comparison of harmonic distortion value for both FCS-MPC and conventional control methods for voltage and current waveforms which validated the superior performance of the proposed FCS-MPC strategy. Fig 70 and Fig 71 show

TABLE 19. THD with PI and FCS-MPC (inverter mode).

Load	PI	FCS-MPC
No load	1.220	0.570
Resistive (balanced)	1.220	0.570
Non-linear	4.310	1.000

TABLE 20. THD with FCS-MPC strategy.

VSC Mode	THD	
	Current	Voltage
AFE Rectifier	0.560	-
Grid-connected	0.430	-
Islanded (linear load)	0.560	0.500
Islanded (non-linear load)	-	1.000

TABLE 21. THD with different control strategies (inverter mode).

Ref.	Control Strategy	THD (voltage)	
		Non-linear load	Linear load
[80]	PR	4.60	1.40
[81]	SMC	2.66	-
[82]	PI	42.0	16.0
[83]	Deadbeat	4.80	2.10
Current Study	FCS-MPC	1.0	0.50

the THD values (0.28 %) of HMGS with MPC. THD of 3.71 % is recorded in the case of PI control as shown in Fig 68 and Fig 69. Table 23 summarizes the THD and voltage mismatch.

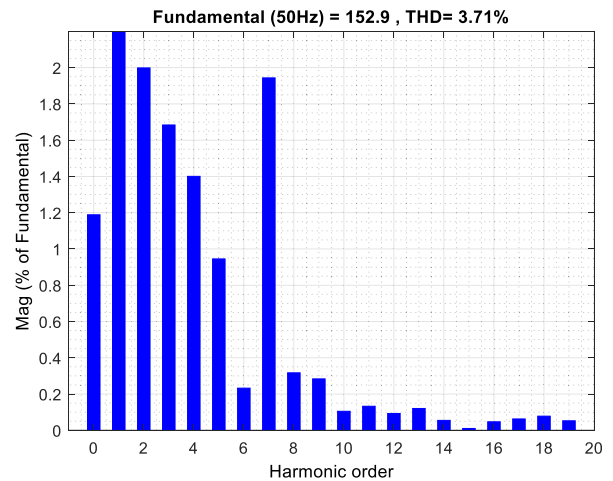


FIGURE 68. THD values for load voltage (PI control).

VIII. PROMINENT ASPECTS OF PROPOSED STRATEGY AND RELATIVE ANALYSIS WITH LITERATURE

Table 22 compares the cost results of different optimal design models with the presented hybrid model. With the consideration of components sizes and capital cost, the TNPC is definitely not the same as all literature models as well

**TABLE 22. Comparison of techno-economic results of the proposed optimized system with research studies.**

REF	LOCATION	Hybrid Configuration	TNPC (\$)	LCOE (\$/kWh)
[84]	Philippines	PV-wind-diesel-FC-BSS-Converter	72,500,000	0.696
[85]	Saudi Arabia	PV-BSS-Converter	45,188	0.281
[86]	Suhag, Egypt	PV-diesel-FW-BSS-Converter	28,500,000	0.200
[87]	Geladin, Ethiopia	PV-wind-diesel-BSS-Converter	24,949,272	0.110
[88]	Taxila, Pakistan	PV-Hydro-DG-BSS-Converter	40407000	0.175
[5]	Southern Camerouns	PV-MHT-diesel-BSS-Converter	191,700	0.443
[89]	Canary, Spain	PV-wind-diesel-BSS-Converter	473,013	0.404
[39]	Kuala Lumpur, Malaysia	PV-diesel-BSS-converter	965,261	0.194
[90]	Akure, Nigeria	Grid-PV-BESS-Converter	302,543	1.247
[51]	New Borg El Arab, Egypt	PV-wind-diesel-BSS-converter	1,684,118	0.190
[26]	Tamanrasset, Algeria	PV-diesel-BSS-converter	8585.14	0.380
[27]	Bandar Abbas, Iran	Grid-PV-wind	86394	1.550
[57]	Sherani, Pakistan	PV-wind-diesel-BESS-Converter	28,620	0.311
[28]	Sakran Erbil, Iraq	PV-Hydro-diesel-BSS-Converter	113201	0.054
[30]	Alaris, Saudi Arabia	PV-wind-BSS-converter	35449	0.226
[91]	Neom, Saudi Arabia	PV-wind-diesel-BESS-Converter	8,130,000	0.164
[33]	Victoria, Canada	NGG (residential)	29,300,000	0.285
[33]	Victoria, Canada	NGG (commercial)	34,400,000	0.286
[33]	Victoria, Canada	NGG (industrial)	32,500,000	0.298
[33]	Victoria, Canada	PV-wind-NGG-BSS-Converter (residential)	30,900,000	0.301
[33]	Victoria, Canada	PV-wind-NGG-BSS-Converter (commercial)	32,200,000	0.268
[33]	Victoria, Canada	PV-wind-NGG-BSS-Converter (industrial)	28,700,000	0.263
[33]	Victoria, Canada	PV-wind-BGG-BSS-Converter (residential)	42,900,000	0.418
[33]	Victoria, Canada	PV-wind-BGG-BSS-Converter (commercial)	48,000,000	0.399
[33]	Victoria, Canada	PV-wind-BGG-BSS-Converter (industrial)	41,900,000	0.385
[92]	Tehran, Iran	PV-wind-BESS-Converter	676,345	0.274
[45]	Silchar, India	PV-BG-PHES-BSS-Converter	763,406	0.4073
[6]	Haryana, India	PV-wind-BESS-Converter	228,353	0.288
[93]	Madhya Pradesh, India	PV-wind-diesel-BSS-Converter	517277	0.458
[43]	Six sites, Nigeria	PV-wind-diesel-BSS-Converter	2370131	0.700
[36]	Diyala, Iraq	PV-diesel-BSS-Converter (LF)	138,704	0.264
[36]	Diyala, Iraq	PV-diesel-BSS-Converter (CC)	115,722	0.220
[36]	Diyala, Iraq	PV-diesel-BSS-Converter (CD)	110,191	0.210
[94]	Tuludimtu, Ethiopia	PV-wind	-	0.350
[34]	Quetta, Pakistan	Wind-diesel-BSS-Converter	14,846	0.309
[41]	Island, China	Wind-BESS-Converter	-	0.187
[95]	Istanbul, Turkey	PV-wind-FC-Converter	607,298	1.306
[96]	The random site, Bangladesh	PV-wind-diesel-BSS-Converter	200,000	0.500
[97]	Kaduna, Nigeria	PV-wind-diesel-BESS-Converter	379,914	0.487
[51]	Borg El Arab, Egypt	PV-wind-diesel-BESS-Converter	1,684,118	0.190
[98]	Tazouta, Morocco	PV-diesel-BSS-Converter	10,195.56	0.570
<b>Present study</b>	<b>Kharan, Pakistan</b>	<b>PV-wind-diesel-BSS-Converter</b>	<b>47,398</b>	<b>0.309</b>

**TABLE 23. Comparative analysis of applied MPC scheme with PI.**

Ref	Studied model	Voltage level	Voltage magnitude error (%)	% THD (V)	% THD (I)
[38]	PV-WT-BSS	326.70	-5.048	1.830	2.670
[34]	WT-BSS	308.70	0.739	0.260	--
[57]	PV-WT-BSS	314.90	-1.254	0.300	0.300
<b>Present study</b>	<b>PV-WT-BSS</b>	<b>151.90</b>	<b>-1.266</b>	<b>0.280</b>	<b>0.280</b>

as the proposed model. Nevertheless, LCOE is an alternative parameter and judging tool as a crucial parameter to compare the cost of HRES based generated power.

Iraq, Saudi Arabia, India, Egypt, Malaysia, China, Canada, Ethiopia, and Pakistan have the lowest LCOE in terms of comparison with the relevant parameter of other countries.

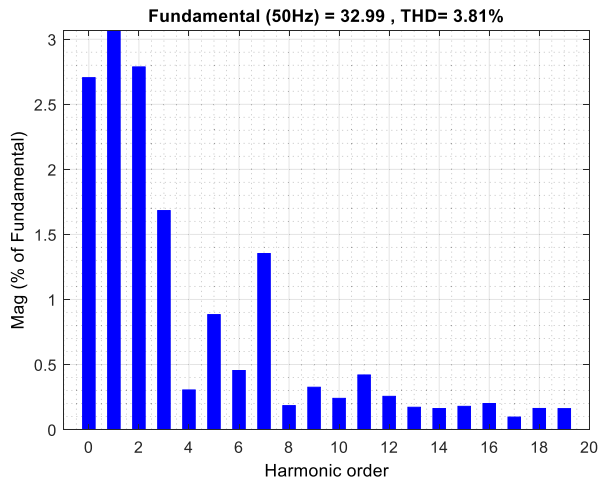


FIGURE 69. THD of three-phase load current (PI).

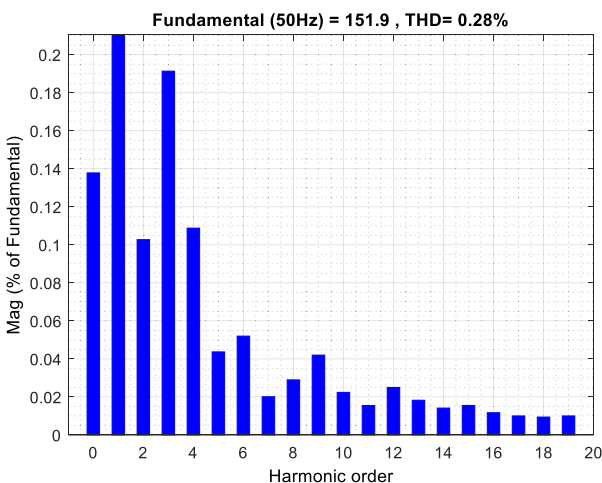


FIGURE 70. THD values for load voltage (FCS-MPC).

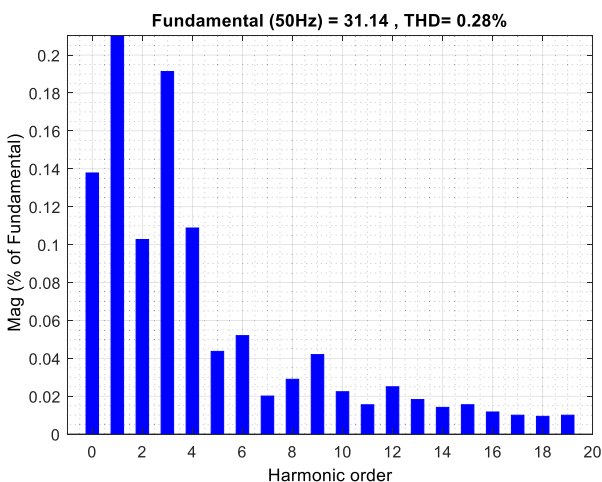


FIGURE 71. THD values for load current (FCS-MPC).

While LCOE in the Philippines, Camerouns, Spain, Turkey, Bangladesh, Morocco, and Nigeria are the highest. With the obtained solutions, the comparative analysis also shows reasonable trade-off with the literature studies and demonstrates a clear understanding of the feasibility of economic aspects of HRES in Pakistan.

The comparative THD values are shown in Table 24. The THD value for the FCS-MPC scheme is found to be 0.28 % which is less than the relevant THD values mentioned in [57] under the same conditions. The probable reason is the different component sizing, dc/ac voltage level, and load profiles. Another model consisting of the wind-battery scheme which is analyzed in [34] has the same THD value under the MPC scheme without incorporating PV source. The comparison of load power ripples is examined between PI and MPC control schemes. Lower values of THD and power ripples during the MPC scheme show superior performance. It is relevant to describe the reason for very low values of THD during the MPC scheme for different case studies that can be examined from the output signals of voltage and current of Fig 46 and Fig 52.

The major outcomes of the proposed study are concluded below:

- The optimized model is obtained with PV-wind-BSS-converter and the TNPC is found to be \$ 47,398 while the value of LCOE is \$ 0.309/kWh. In this way, generation incorporation with 100 % renewable energy resources is ascertained, without any supply shortage.
- The value of LCOE is found to be high which is \$ 1.690/kWh for the base case including DG only (case-9). Hence, it is examined that the diesel generator shows a critical role in terms of GHG emission.
- The TNPC of the proposed HRES is \$ 47,398 that is about six times less than the value of base case which is \$ 258,845. Hence, the stand-alone system with DG only is not commended, which is the usual case in Pakistan.
- No GHG emission is found and fuel consumption is not required for the presented HRES model whereas 19,364 kg/yr emission and fuel consumption of 7,398 L/yr is found for the base case.
- Remarkable outcomes are obtained during the implementation of the presented EMS scheme under the intermittent generation of PV, and wind with fluctuating load.
- With the MPC scheme, improved power quality and voltage regulation are obtained for a standalone system.
- The proposed MPC scheme is robust during transient analysis and fluctuating dc voltage level.
- Only 0.28 % of THD of the output ac voltage which is well below the value of 5 % as specified by IEEE standard 929, 2000 and IEEE-519 standards [6].
- The PI controllers' parameters for wind/solar boost and battery BSS converter are selected with a trial and error approach.
- The operation analysis of reconfigurable bidirectional VSC during generation intermittency and fluctuating load demand is implemented through simulations and different case studies.
- The proposed study will assist the government of Pakistan as well as developing countries to incorporate multiple standalone and grid-connected scheme with state-of-the-art schemes. Energy sector planners can implement appropriate action plans to integrate further

**TABLE 24. Analysis of THD and power quality (inverter mode).**

Ref	Study System	DC/AC voltage	Component sizes	LOAD	Methodology	THD (%)	Load Power Ripples
[34]	WT-BSS	710/311	PV: 0 WT: 2.4 BSS: 53.9	11.25	PI	3.71	±1000 W (5-8 s) ±1200W (8-11 s) ±1000W (11-15 s)
					FCS-MPC	0.28	±20W (5-8 s) ±30W (8-11 s) ±20W (11-15 s)
[57]	PV-WT-BSS	750/311	PV: 13.4 WT: 4.0 BSS: 47.4	21.57	PI	5.44	±480W (5-10 s) ±1000W (10-20 s)
					FCS-MPC	0.30	±30 W (5-20 s)
Present Study	PV-WT-BSS	510/150	PV: 21.1 WT: 5.0 BSS: 90.1	35.94	PI	3.71	±1500 W (5-20 s)
					FCS-MPC	0.28	±30 W (5-20 s)

renewable energy resources to ensure the system more reliable, economical, and environmentally safe. These analysis outcomes will assist new viewpoints for the designers, energy planners and researchers to design and apply the models in an effective and efficient way by penetrating more intermittent energy resources like PV and wind while handling the increasing demands of irregular and fluctuating load requirements.

## IX. CONCLUSION

As determined by techno-economic analysis carried out through HOMER and MATLAB, a grid-disconnected model with PV-wind-BSS configurations is selected as the best suitable optimized plan, to fulfill the residential electricity requirements of Kharan region in the Baluchistan Province of Pakistan. The first step involves optimal components sizing through HOMER. Simulation studies for the region are carried out with practical and real load profile and weather data, with constraints including sixteen (16) sensitivity parameters. Out of nine possible models as examined in this work, PV-WT-BSS was found to be the best optimal choice with better economic considerations. The minimum value of TNPC is observed to be \$ 47,398 while LCOE is recorded as \$ 0.309/kWh. This represents an 81.7 % decrease in overall cost while a 100 % reduction in GHG emissions while fulfilling 100 % of the load requirements with 63.9 % of excess available energy. The suggested model consists of 21.1 kW PV, 5 kW WT, 5.96 kW power converter, and 38 BSS units with 2.37 kWh each capacity.

For technical analysis, optimized sizes are obtained from the initial step, are therefore chosen and proposed management scheme in simulink with FCS-MPC for bidirectional VSC. The technical analysis which is based on different parameters including power balance among HRES components, constant level of DC and AC voltages, Safe operation of battery SOC, improved quality of an ac voltage. The analysis is carried out by observing the intermittent nature of PV irradiance, WT speed, and fluctuating load requirement. The result outcomes are formalized through simulation case studies. The total harmonic distortion (THD) was found to be 0.28 % which is well below the permissible values as specified by IEEE-929 as well as IEEE-519 standards, and

considerably lower than 3.71 % THD with the conventional PI control scheme.

The suggested strategy could assist the governments, energy planners, and data analysts to inquire about proper action plans, to effectively and efficiently design of the hybrid model. Increased demand with external perturbations can be effectively treated with more generation penetration of renewable sources to achieve the system with better reliability, economically viable, and environmentally safe. The future work will incorporate biomass energy with a comparative analysis between sliding mode and model predictive control.

## ACKNOWLEDGMENT

The authors would like to acknowledge the King Fahd University of Petroleum and Minerals for providing the support to conduct the present study.

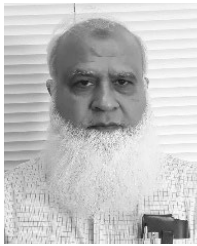
## REFERENCES

- [1] F. Vivas, A. De Las Heras, F. Segura, and J. Andújar, "A review of energy management strategies for renewable hybrid energy systems with hydrogen backup," *Renew. Sustain. Energy Rev.*, vol. 82, pp. 126–155, Feb. 2018.
- [2] IRENA Renewable Energy Capacity Statistics. Accessed: Nov. 16, 2019. [Online]. Available: [https://www.irena.org/-/media/Files/IRENA/Agency/Publication/2019/Jul/IRENA\\_Renewable\\_energy\\_statistics\\_2019.pdf](https://www.irena.org/-/media/Files/IRENA/Agency/Publication/2019/Jul/IRENA_Renewable_energy_statistics_2019.pdf)
- [3] A. L. Bukar and C. W. Tan, "A review on stand-alone photovoltaic-wind energy system with fuel cell: System optimization and energy management strategy," *J. Cleaner Prod.*, vol. 221, pp. 73–88, Jun. 2019.
- [4] J. Kumari, P. Subathra, J. E. Moses, and D. Shruthi, "Economic analysis of hybrid energy system for rural electrification using HOMER," in *Proc. Int. Conf. Innov. Electr., Electron., Instrum. Media Technol. (ICEEIMT)*, Feb. 2017, pp. 151–156.
- [5] E. Muh and F. Tabet, "Comparative analysis of hybrid renewable energy systems for off-grid applications in Southern Cameroons," *Renew. Energy*, vol. 135, pp. 41–54, May 2019.
- [6] O. Krishan and S. Suhag, "Techno-economic analysis of a hybrid renewable energy system for an energy poor rural community," *J. Energy Storage*, vol. 23, pp. 305–319, Jun. 2019.
- [7] E. Eriksson and E. Gray, "Optimization and integration of hybrid renewable energy hydrogen fuel cell energy systems—A critical review," *Appl. Energy*, vol. 202, pp. 348–364, Sep. 2017.
- [8] A. Saleh, A. Deihimi, and R. Iravani, "Model predictive control of distributed generations with feed-forward output currents," *IEEE Trans. Smart Grid*, vol. 10, no. 2, pp. 1488–1500, Mar. 2019.
- [9] X. Kong, X. Liu, L. Ma, and K. Y. Lee, "Hierarchical distributed model predictive control of standalone wind/solar/battery power system," *IEEE Trans. Syst., Man, Cybern., Syst.*, vol. 49, no. 8, pp. 1570–1581, Aug. 2019.
- [10] J.-O. Lee, Y.-S. Kim, and S.-I. Moon, "Novel supervisory control method for islanded droop-based AC/DC microgrids," *IEEE Trans. Power Syst.*, vol. 34, no. 3, pp. 2140–2151, May 2019.

- [11] F. Blaabjerg, Y. Yang, K. Ma, and X. Wang, "Power electronics—The key technology for renewable energy system integration," in *Proc. Int. Conf. Renew. Energy Res. Appl. (ICRERA)*, Nov. 2015, pp. 1618–1626.
- [12] C. Ndukwe and T. Iqbal, "Sizing and dynamic modelling and simulation of a standalone PV based DC microgrid with battery storage system for a remote community in Nigeria," *J. Energy Syst.*, vol. 32, pp. 67–85, Jun. 2019.
- [13] Y. Han, G. Zhang, Q. Li, Z. You, W. Chen, and H. Liu, "Hierarchical energy management for PV/hydrogen/battery island DC microgrid," *Int. J. Hydrogen Energy*, vol. 44, no. 11, pp. 5507–5516, Feb. 2019.
- [14] R. Heydari, M. Gheisarnejad, M. H. Khooban, T. Dragicevic, and F. Blaabjerg, "Robust and fast voltage-source-converter (VSC) control for naval shipboard microgrids," *IEEE Trans. Power Electron.*, vol. 34, no. 9, pp. 8299–8303, Sep. 2019.
- [15] J. Liu, Y. Miura, and T. Ise, "Cost-function-based microgrid decentralized control of unbalance and harmonics for simultaneous bus voltage compensation and current sharing," *IEEE Trans. Power Electron.*, vol. 34, no. 8, pp. 7397–7410, Aug. 2019.
- [16] K. Liu, T. Liu, Z. Tang, and D. J. Hill, "Distributed MPC-based frequency control in networked microgrids with voltage constraints," *IEEE Trans. Smart Grid*, vol. 10, no. 6, pp. 6343–6354, Nov. 2019.
- [17] H. Amiri, G. A. Markadeh, and N. M. Dehkordi, "Voltage control and load sharing in a DC islanded microgrid based on disturbance observer," in *Proc. 27th Iranian Conf. Electr. Eng. (ICEE)*, Apr. 2019, pp. 825–830.
- [18] P. Kou, Y. Feng, D. Liang, and L. Gao, "A model predictive control approach for matching uncertain wind generation with PEV charging demand in a microgrid," *Int. J. Electr. Power Energy Syst.*, vol. 105, pp. 488–499, Feb. 2019.
- [19] D. Pan, X. Wang, F. Liu, and R. Shi, "Transient stability of voltage-source converters with grid-forming control: A design-oriented study," *IEEE J. Emerg. Sel. Topics Power Electron.*, to be published.
- [20] H. Li, F. Li, Y. Xu, D. T. Rizey, and J. D. Kueck, "Adaptive voltage control with distributed energy resources: Algorithm, theoretical analysis, simulation, and field test verification," *IEEE Trans. Power Syst.*, vol. 25, no. 3, pp. 1638–1647, Aug. 2010.
- [21] Y. Xu and F. Li, "Adaptive PI control of STATCOM for voltage regulation," *IEEE Trans. Power Del.*, vol. 29, no. 3, pp. 1002–1011, Jun. 2014.
- [22] D. Zhi, L. Xu, and B. W. Williams, "Improved direct power control of grid-connected DC/AC converters," *IEEE Trans. Power Electron.*, vol. 24, no. 5, pp. 1280–1292, May 2009.
- [23] S. Vazquez, J. Sanchez, J. Carrasco, J. Leon, and E. Galvan, "A Model-Based Direct Power Control for Three-Phase Power Converters," *IEEE Trans. Ind. Electron.*, vol. 55, no. 4, pp. 1647–1657, Apr. 2008.
- [24] A. Bouafia, F. Krim, and J.-P. Gaubert, "Fuzzy-logic-based switching state selection for direct power control of three-phase PWM rectifier," *IEEE Trans. Ind. Electron.*, vol. 56, no. 6, pp. 1984–1992, Jun. 2009.
- [25] J. Hu, L. Shang, Y. He, and Z. Q. Zhu, "Direct active and reactive power regulation of grid-connected DC/AC converters using sliding mode control approach," *IEEE Trans. Power Electron.*, vol. 26, no. 1, pp. 210–222, Jan. 2011.
- [26] F. Fodhil, A. Hamidat, and O. Nadjemi, "Potential, optimization and sensitivity analysis of photovoltaic-diesel-battery hybrid energy system for rural electrification in Algeria," *Energy*, vol. 169, pp. 613–624, Feb. 2019.
- [27] M. Jahangiri, A. Haghani, A. Alidadi Shamsabadi, A. Mostafaipoor, and L. M. Pomares, "Feasibility study on the provision of electricity and hydrogen for domestic purposes in the south of Iran using grid-connected renewable energy plants," *Energy Strategy Rev.*, vol. 23, pp. 23–32, Jan. 2019.
- [28] A. S. Aziz, M. F. N. Tajuddin, M. R. Adzman, A. Azmi, and M. A. Ramli, "Optimization and sensitivity analysis of standalone hybrid energy systems for rural electrification: A case study of Iraq," *Renew. Energy*, vol. 138, pp. 775–792, Aug. 2019.
- [29] C. Y. Acevedo-Arenas, A. Correcher, C. Sánchez-Díaz, E. Ariza, D. Alfonso-Solar, C. Vargas-Salgado, and J. F. Petit-Suárez, "MPC for optimal dispatch of an AC-linked hybrid PV/wind/biomass/H<sub>2</sub> system incorporating demand response," *Energy Convers. Manage.*, vol. 186, pp. 241–257, Apr. 2019.
- [30] S. M. Shaahid, L. M. Alhems, and M. K. Rahman, "Techno-economic assessment of establishment of wind farms in different Provinces of Saudi Arabia to mitigate future energy challenges," *Therm. Sci.*, vol. 2018, no. 5, pp. 2909–2918, 2018.
- [31] K. Murugaperumal and P. Ajay D. Vimal Raj, "Energy storage based MG connected system for optimal management of energy: An ANFMDA technique," *Int. J. Hydrogen Energy*, vol. 44, no. 16, pp. 7996–8010, Mar. 2019.
- [32] E. Diemuodeke, A. Addo, C. Oko, Y. Mulugetta, and M. Ojapah, "Optimal mapping of hybrid renewable energy systems for locations using multi-criteria decision-making algorithm," *Renew. Energy*, vol. 134, pp. 461–477, Apr. 2019.
- [33] M. Bagheri, S. H. Delbari, M. Pakzadmanesh, and C. A. Kennedy, "City-integrated renewable energy design for low-carbon and climate-resilient communities," *Appl. Energy*, vol. 239, pp. 1212–1225, Apr. 2019.
- [34] H. U. R. Habib, S. Wang, M. R. Elkadeem, and M. F. Elmorshedy, "Design optimization and model predictive control of a standalone hybrid renewable energy system: A case study on a small residential load in Pakistan," *IEEE Access*, vol. 7, pp. 117369–117390, 2019.
- [35] M. Guezgouz, J. Jurasz, and B. Bekkouche, "Techno-economic and environmental analysis of a hybrid PV-WT-PSH/BB standalone system supplying various loads," *Energies*, vol. 12, no. 3, p. 514, Feb. 2019.
- [36] A. Aziz, M. Tajuddin, M. Adzman, M. Ramli, and S. Mekhilef, "Energy management and optimization of a PV/diesel/battery hybrid energy system using a combined dispatch strategy," *Sustainability*, vol. 11, no. 3, p. 683, Jan. 2019.
- [37] W. Jing, C. H. Lai, D. K. Ling, W. S. Wong, and M. D. Wong, "Battery lifetime enhancement via smart hybrid energy storage plug-in module in standalone photovoltaic power system," *J. Energy Storage*, vol. 21, pp. 586–598, Feb. 2019.
- [38] P. S. Sikder and N. Pal, "Modeling of an intelligent battery controller for standalone solar-wind hybrid distributed generation system," *J. King Saud Univ. Eng. Sci.*, to be published.
- [39] E.-T. Chok, Y. S. Lim, and K. H. Chua, "Novel fuzzy-based control strategy for standalone power systems for minimum cost of electricity in rural areas," *Sustain. Energy Technol. Assessments*, vol. 31, pp. 199–211, Feb. 2019.
- [40] J. Carroquino, J.-L. Bernal-Agustín, and R. Dufo-López, "Standalone renewable energy and hydrogen in an agricultural context: A demonstrative case," *Sustainability*, vol. 11, no. 4, p. 951, Feb. 2019.
- [41] T. Ma and M. S. Javed, "Integrated sizing of hybrid PV-wind-battery system for remote island considering the saturation of each renewable energy resource," *Energy Convers. Manage.*, vol. 182, pp. 178–190, Feb. 2019.
- [42] N. Priyadarshi, V. Ramachandaramurthy, S. Padmanaban, and F. Azam, "An ant colony optimized MPPT for standalone hybrid PV-wind power system with single Cuk converter," *Energies*, vol. 12, no. 1, p. 167, Jan. 2019.
- [43] S. O. Oyedepo, T. Uwoghien, P. O. Babalola, S. C. Nwanya, O. Kilanko, R. O. Leram, A. K. Aworinde, T. Adekeye, J. A. Oyebanji, and O. A. Abidakun, "Assessment of decentralized electricity production from hybrid renewable energy sources for sustainable energy development in Nigeria," *Open Eng.*, vol. 9, no. 1, pp. 72–89, Mar. 2019.
- [44] J. Faria, J. Pombo, M. Calado, and S. Mariano, "Power management control strategy based on artificial neural networks for standalone PV applications with a hybrid energy storage system," *Energies*, vol. 12, no. 5, p. 902, Mar. 2019.
- [45] M. Das, M. A. K. Singh, and A. Biswas, "Techno-economic optimization of an off-grid hybrid renewable energy system using metaheuristic optimization approaches—Case of a radio transmitter station in India," *Energy Convers. Manage.*, vol. 185, pp. 339–352, Apr. 2019.
- [46] X. Luo, J. Liu, Y. Liu, and X. Liu, "Bi-level optimization of design, operation, and subsidies for standalone solar/diesel multi-generation energy systems," *Sustain. Cities Soc.*, vol. 48, Jul. 2019, Art. no. 101592.
- [47] A. S. Aziz, M. F. N. Tajuddin, M. R. Adzman, and M. A. M. Ramli, "Feasibility analysis of PV/diesel/battery hybrid energy system using multi-year module," *Int. J. Renew. Energy Res.*, vol. 8, no. 4, pp. 1980–1993, Dec. 2018.
- [48] N. Priyadarshi, S. Padmanaban, D. M. Ionel, L. Mihet-Popa, and F. Azam, "Hybrid PV-wind, micro-grid development using quasi-Z-source inverter modeling and control—Experimental investigation," *Energies*, vol. 11, no. 9, p. 2277, 2018.
- [49] M. Mehreganfar, M. H. Saedinia, S. A. Davari, C. Garcia, and J. Rodriguez, "Sensorless predictive control of AFE rectifier with robust adaptive inductance estimation," *IEEE Trans. Ind. Informat.*, vol. 15, no. 6, pp. 3420–3431, Jun. 2019.
- [50] J. Lu, W. Wang, Y. Zhang, and S. Cheng, "Multi-objective optimal design of stand-alone hybrid energy system using entropy weight method based on HOMER," *Energies*, vol. 10, no. 10, p. 1664, Oct. 2017.
- [51] F. Diab, H. Lan, L. Zhang, and S. Ali, "An environmentally friendly factory in Egypt based on hybrid photovoltaic/wind/diesel/battery system," *J. Cleaner Prod.*, vol. 112, pp. 3884–3894, Jan. 2016.

- [52] A. Yahiaoui, K. Benmansour, and M. Tadjine, "Control, analysis and optimization of hybrid PV-Diesel-Battery systems for isolated rural city in Algeria," *Solar Energy*, vol. 137, pp. 1–10, Nov. 2016.
- [53] J.-H. Cho, M.-G. Chun, and W.-P. Hong, "Structure optimization of standalone renewable power systems based on multi object function," *Energies*, vol. 9, no. 8, p. 649, Aug. 2016.
- [54] F. Diab, H. Lan, L. Zhang, and S. Ali, "An environmentally-friendly tourist village in egypt based on a hybrid renewable energy system—Part two: A net zero energy tourist village," *Energies*, vol. 8, no. 7, pp. 6945–6961, Jul. 2015.
- [55] J. Li, W. Wei, and J. Xiang, "A simple sizing algorithm for standalone PV/wind/battery hybrid microgrids," *Energies*, vol. 5, no. 12, pp. 5307–5323, Dec. 2012.
- [56] S. Vadi, S. Padmanaban, R. Bayindir, F. Blaabjerg, and L. Mihet-Popa, "A review on optimization and control methods used to provide transient stability in microgrids," *Energies*, vol. 12, no. 18, p. 3582, Sep. 2019.
- [57] E. A. Al-Ammar, H. U. R. Habib, K. M. Kotb, S. Wang, W. Ko, M. F. Elmorschedy, and A. Waqar, "Residential community load management based on optimal design of standalone HRES with model predictive control," *IEEE Access*, vol. 8, pp. 12542–12572, 2020.
- [58] L. Li, Z. Yao, S. You, C.-H. Wang, C. Chong, and X. Wang, "Optimal design of negative emission hybrid renewable energy systems with biochar production," *Appl. Energy*, vol. 243, pp. 233–249, Jun. 2019.
- [59] *Wind System Installation*. Accessed: Dec. 7, 2019. [Online]. Available: <http://www.windenergy.com>
- [60] K. Belmokhtar, T. W. Energy, and H. Ibrahim, "A maximum power point tracking control algorithms for a PMSG-Based WECS for isolated applications: Critical review," in *World's Largest Science*. Amsterdam, The Netherlands: IOS Press, Jul. 2016.
- [61] S. Ebrahimi, M. Jahangiri, H. A. Raiesi, and A. R. Ariae, "Optimal planning of on-grid hybrid microgrid for remote island using HOMER software, Kish in Iran," *Int. J. Energetica*, vol. 3, no. 2, pp. 13–21, 2018.
- [62] A. Tani, M. B. Camara, and B. Dakyo, "Energy management in the decentralized generation systems based on renewable energy—ultracapacitors and battery to compensate the wind/load power fluctuations," *IEEE Trans. Ind. Appl.*, vol. 51, no. 2, pp. 1817–1827, Mar. 2015.
- [63] M. A. Husain, A. Tariq, S. Hameed, M. S. B. Arif, and A. Jain, "Comparative assessment of maximum power point tracking procedures for photovoltaic systems," *Green Energy Environ.*, vol. 2, no. 1, pp. 5–17, Jan. 2017.
- [64] J. Hu, Y. Xu, K. W. Cheng, and J. M. Guerrero, "A model predictive control strategy of PV-battery microgrid under variable power generations and load conditions," *Appl. Energy*, vol. 221, pp. 195–203, Jul. 2018.
- [65] N. Bizon, "Effective mitigation of the load pulses by controlling the battery/SMES hybrid energy storage system," *Appl. Energy*, vol. 229, pp. 459–473, Nov. 2018.
- [66] F. K. Abo-Elyousr and A. Elnozahy, "Bi-objective economic feasibility of hybrid micro-grid systems with multiple fuel options for islanded areas in Egypt," *Renew. Energy*, vol. 128, pp. 37–56, Dec. 2018.
- [67] S. Sinha and S. Chandel, "Review of software tools for hybrid renewable energy systems," *Renew. Sustain. Energy Rev.*, vol. 32, pp. 192–205, Apr. 2014.
- [68] M. D. A. Bin Rozmi, G. S. Thirunavukkarasu, E. Jamei, M. Seyedmahmoudian, S. Mekhilef, A. Stojcevski, and B. Horan, "Role of immersive visualization tools in renewable energy system development," *Renew. Sustain. Energy Rev.*, vol. 115, Nov. 2019, Art. no. 109363.
- [69] A. Mills, "Simulation of hydrogen-based hybrid systems using Hybrid2," *Int. J. Hydrogen Energy*, vol. 29, no. 10, pp. 991–999, Aug. 2004.
- [70] Y. Pan, L. Liu, T. Zhu, T. Zhang, and J. Zhang, "Feasibility analysis on distributed energy system of Chongming county based on RETScreen software," *Energy*, vol. 130, pp. 298–306, Jul. 2017.
- [71] G. Zubi, R. Dufo-López, G. Pasaoglu, and N. Pardo, "Techno-economic assessment of an off-grid PV system for developing regions to provide electricity for basic domestic needs: A 2020–2040 scenario," *Appl. Energy*, vol. 176, pp. 309–319, Aug. 2016.
- [72] M. S. Saleem, "Design and optimization of hybrid solar-hydrogen generation system using TRNSYS," *Int. J. Hydrogen Energy*, to be published.
- [73] S. Ferrari, F. Zagarella, P. Caputo, and M. Bonomolo, "Assessment of tools for urban energy planning," *Energy*, vol. 176, pp. 544–551, Jun. 2019.
- [74] C. Bastholm and F. Fiedler, "Techno-economic study of the impact of blackouts on the viability of connecting an off-grid PV-diesel hybrid system in Tanzania to the national power grid," *Energy Convers. Manage.*, vol. 171, pp. 647–658, Sep. 2018.
- [75] R. Lingamuthu and R. Mariappan, "Power flow control of grid connected hybrid renewable energy system using hybrid controller with pumped storage," *Int. J. Hydrogen Energy*, vol. 44, no. 7, pp. 3790–3802, Feb. 2019.
- [76] X. Shi, J. Zhu, L. Li, and Y. Qu, "Model predictive control of PWM AC/DC converters for Bi-directional power flow control in microgrids," in *Proc. Australasian Universities Power Eng. Conf. (AUPEC)*, Sep. 2015, pp. 1–4.
- [77] (2005). *Encyclopaedia Britannica, Geographical Map of Pakistan*. Accessed: Dec. 7, 2019. [Online]. Available: <https://www.britannica.com/place/Pakistan>
- [78] W. U. K. Tareen, Z. Anjum, N. Yasin, L. Siddiqui, M. Darwish, M. Aamir, L. W. Chek, I. Farhat, S. A. Malik, S. Mekhilef, B. Horan, and M. Seyedmahmoudian, "The prospective non-conventional alternate and renewable energy sources in Pakistan—A focus on biomass energy for power generation, transportation, and industrial fuel," *Energies*, vol. 11, no. 9, p. 2431, 2018.
- [79] *Solar Generation of Pakistan*. Accessed: Jan. 13, 2020. [Online]. Available: [https://jouetmusee.com/wear\\_rm.php](https://jouetmusee.com/wear_rm.php)
- [80] A. Hasanzadeh, O. Onar, H. Mokhtari, and A. Khaligh, "A proportional-resonant controller-based wireless control strategy with a reduced number of sensors for parallel-operated UPSs," *IEEE Trans. Power Del.*, vol. 25, no. 1, pp. 468–478, Jan. 2010.
- [81] H. Komurcugil, "Rotating-sliding-line-based sliding-mode control for single-phase UPS inverters," *IEEE Trans. Ind. Electron.*, vol. 59, no. 10, pp. 3719–3726, Oct. 2012.
- [82] P. Chiang Loh, M. Newman, D. Zmood, and D. Holmes, "A comparative analysis of multiloop voltage regulation strategies for single and three-phase UPS systems," *IEEE Trans. Power Electron.*, vol. 18, no. 5, pp. 1176–1185, Sep. 2003.
- [83] P. Mattavelli, "An improved deadbeat control for UPS using disturbance observers," *IEEE Trans. Ind. Electron.*, vol. 52, no. 1, pp. 206–212, Feb. 2005.
- [84] L. Phan, "Control strategy of a hybrid renewable energy system based on reinforcement learning approach for an isolated microgrid," *Appl. Sci.*, vol. 9, no. 19, p. 4001, Sep. 2019.
- [85] A. Elshurafa, "State-of-charge effects on standalone solar-storage systems in hot climates: A case study in Saudi Arabia," *Sustainability*, vol. 11, no. 12, p. 3471, Jun. 2019.
- [86] A. M. Aly, A. M. Kassem, K. Sayed, and I. Aboelhassan, "Design of microgrid with flywheel energy storage system using HOMER software for case study," in *Proc. Int. Conf. Innov. Trends Comput. Eng. (ITCE)*, Feb. 2019, pp. 485–491.
- [87] S. L. Tesema and G. Bekele, "High wind power penetration large-scale hybrid renewable energy system design for remote off-grid application," *J. Power Energy Eng.*, vol. 7, no. 3, pp. 11–30, 2019.
- [88] H. R. Habib and T. Mahmood, "Optimal planning and design of hybrid energy system for UET Taxila," in *Proc. Int. Conf. Electr. Eng. (ICEE)*, Mar. 2017, pp. 1–9.
- [89] I. Padrón, D. Avila, G. N. Marichal, and J. A. Rodríguez, "Assessment of hybrid renewable energy systems to supplied energy to autonomous desalination systems in two islands of the canary archipelago," *Renew. Sustain. Energy Rev.*, vol. 101, pp. 221–230, Mar. 2019.
- [90] A. J. Babalola and A. D. Yakubu, "Development of an alternative hybrid power system using hybrid micro power optimization model (HOMER)," *Int. J. Advance Ind. Eng.*, vol. 7, no. 1, pp. 1–9, 2019.
- [91] A. B. Awan, "Performance analysis and optimization of a hybrid renewable energy system for sustainable NEOM city in Saudi Arabia," *J. Renew. Sustain. Energy*, vol. 11, no. 2, Mar. 2019, Art. no. 025905.
- [92] S. A. Goudarzi, F. Fazelpour, G. B. Gharehpetian, and M. A. Rosen, "Techno-economic assessment of hybrid renewable resources for a residential building in tehran," *Environ Prog Sustain. Energy*, vol. 38, no. 5, p. 13209, Sep. 2019.
- [93] V. Sohoni, S. Gupta, and R. K. Nema, "Design of wind-PV based hybrid standalone energy systems for three sites in central India," *Trans. Electr. Eng. Electron. Commun.*, vol. 17, no. 1, pp. 24–34, 2019.
- [94] R. Samikannu, V. S. Kumar, B. Diarra, and R. Ravi, "Cost optimization and development of hybrid energy systems for rural areas in ethiopia with a balance of their energy need and resources availability (a case study-on Tuludimtu)," *J. Test. Eval.*, vol. 47, no. 6, Nov. 2019, Art. no. 20180462.
- [95] B. Dursun and E. Aykut, "An investigation on wind/PV/fuel cell/battery hybrid renewable energy system for nursing home in Istanbul," *Proc. Inst. Mech. Eng., A, J. Power Energy*, vol. 233, no. 5, pp. 616–625, Aug. 2019.

- [96] M. Jobayer, S. M. Salimullah, S. Datta, T. Rahman, and M. S. Alam, "Standalone hybrid minigrd for empowering every families in rural areas without dependency to grid electricity," in *Proc. Int. Conf. Sustain. Comput. Sci., Technol. Manage. (SUSCOM)*. Jaipur, India: Amity Univ. Rajasthan, Jun. 2019, pp. 589–593. [Online]. Available: <https://papers.ssrn.com/sol3/results.cfm>
- [97] I. Sofimicari, M. Wazir, B. Mustafa, and F. Obite, "Modelling and analysis of a PV/wind/diesel hybrid standalone microgrid for rural electrification in Nigeria," *Bull. Elect. Eng. Inform.*, vol. 8, no. 4, pp. 1468–1477, 2019.
- [98] H. El-houari, A. Allouhi, S. Rehman, M. S. Buker, T. Kouksou, A. Jamil, and B. El Amrani, "Design, simulation, and economic optimization of an off-grid photovoltaic system for rural electrification," *Energies*, vol. 12, no. 24, p. 4735, Dec. 2019.



**SHAFIQR REHMAN** received the B.S. degree from the Universities of Pretoria, South Africa, in 2012, the M.S. degree from the King Fahd of Petroleum and Minerals (KFUPM), Saudi Arabia, in 1985, and the Ph.D. degree from Aligarh Muslim (AMU), Aligarh, India, in 1981, all in mechanical engineering. He is currently a Research Engineer with the Center for Engineering Research, Research Institute, KFUPM. He has more than 25 years of research experience in surface and upper air meteorology, wind, solar, and geothermal energy resource assessment, wind/PV/diesel hybrid power system design, meteorological data measurements, corrosion management and costing, and global warming issues and trending. He has published more than 250 research papers in refereed ISI journals and conferences and has three U.S. patents to his credit. He has more than 7850 citations as of October 2019 with an H-index of 40. Recently, he was honored with a prestigious national scientific innovation award "Almarai Prize 2017." Earlier, he received Distinguished Researchers Awards, in 2006 and 2012, by KFUPM.



**HABIB UR RAHMAN HABIB** received the B.Sc. degree in electrical engineering and the M.Sc. degree in electrical power engineering from the University of Engineering and Technology Taxila, Pakistan, in 2009 and 2015, respectively. He is currently pursuing the Ph.D. degree with the State Key Laboratory of Advanced Electromagnetic Engineering and Technology, Huazhong University of Science and Technology, Wuhan, China. Since 2009, he has been with the COMSATS Institute of Information Technology, Pakistan, and the Wah Engineering College, University of Wah, Pakistan. He has been a Management Trainee Officer with the Maintenance Department, Dynamic Packaging Pvt. Ltd., Lahore, Pakistan. He is also permanently with the Department of Electrical Engineering, University of Engineering and Technology Taxila, Pakistan. His research interests include electrical planning and estimation, energy resources and planning, modeling and simulation, renewable energy technology and management, smart grid applications in power systems, distributed generation and microgrid, power electronics, power quality, artificial intelligence, fuzzy controllers, algorithm design, and optimization, and model predictive control and its application in power industry.



**SHAORONG WANG** received the B.Sc. degree in electrical engineering from Zhejiang University, Hangzhou, China, in 1984, the M.Sc. degree in electrical engineering from North China Electric Power University, China, in 1990, and the Ph.D. degree from the Huazhong University of Science and Technology, China, in 2004. He is currently a Professor with the School of Electrical and Electronics Engineering, Huazhong University of Science and Technology. His research interests include power system operation and control, power grid planning, active distribution networks, AI and big data applications in power systems, and robotic inspection in power systems.



**MAHMUT SAMI BÜKER** received the master's degree from the KTH Royal Institute of Technology, Sweden, in project management and operational development under mechanical engineering program, and the Ph.D. degree in sustainable energy technologies from the University of Nottingham, U.K. He is currently an Assistant Professor in the field of renewable energy technologies with Konya NEU University. He has worked on a number of projects on solar assisted heating and cooling systems and has strong experimental and simulation skills as well as comprehensive energy analysis techniques through the performance assessment of various renewable energy technologies. He is currently the author or coauthor of over 20 scientific papers particularly in renowned journals. His main interest areas of research are low/zero carbon technologies for buildings, solar thermal and hybrid PV/T systems, solar-assisted heating and cooling applications, thermal comfort, thermal energy storage, enhanced heat transfer, and thermodynamics.



**LUAI M. ALHEMS** received the B.S. and M.S. degrees in mechanical engineering from the King Fahd University of Petroleum and Minerals, Dhahran, Saudi Arabia, in 1994 and 1997, respectively, and the Ph.D. degree in mechanical engineering from Texas A&M University, College Station, Texas, USA, in 2002. He is currently a Professor with the Department of Mechanical Engineering and the Director of the Center for Engineering Research, Research Institute, King Fahd University of Petroleum and Minerals (KFUPM). He has taught and is teaching thermodynamics I, material science and engineering, fluid mechanics, introduction to heat transfer, convection heat transfer, and fatigue and fracture of engineering materials for many years. He has published and presented more than 125 research papers in ISI refereed journals and international conferences. He has eight patents to his name. His research interests include power systems, gas turbine, renewable energy (solar and wind), failure analysis studies, multiphase flow, experimental fluid dynamics, heat transfer and thermodynamics, and convective heat and mass transfer. He has received the Almarai Award, for 2015–2016, in 2015, the Inventors Award in the 18th Gulf Engineering Forum, in March 2015, Best Research Team, and the Energy Engineer Award.



**HASSAN ZUHAI AL GARNI** received the Master of Engineering in electrical and computer engineering and the Ph.D. degree in systems engineering from Concordia University, Canada, in 2013 and 2018, respectively. He is currently an Assistant Professor and the Chairman of the Electrical and Electronics Engineering Technology Department, Jubail Industrial College. His employment experiences include working in Instrumentation and Control at SABIC-SHARQ for five years, and he is teaching at the Jubail Industrial College for 11 years. He published several research articles and conference proceedings in the area of renewable energy. His research interests are in the areas of technical educations, renewable energy (including solar photovoltaic design and optimization and site selection), panel orientation, and tracking systems. He was awarded the Concordia Accelerator Award, in 2018, the Concordia University Conference and Exposition Award, for 2017–2018, and IEEE-SMC student travel grant award.

...